DISSERTATION

QUANTUM CHEMICAL MODELING OF REDOX REACTIVITY, DEGRADATION PATHWAYS AND PERSISTENCE FOR AQUEOUS PHASE CONTAMINANTS

Submitted by

Jens Blotevogel

Department of Soil and Crop Sciences

In partial fulfillment of the requirements

For the Degree of Doctor of Philosophy

Colorado State University

Fort Collins, Colorado

Fall 2010

Doctoral Committee:

Department Head: Gary A. Peterson

Advisor: Thomas Borch

Thomas C. Sale
Kenneth A. Barbarick
Elliot R. Bernstein

ABSTRACT

QUANTUM CHEMICAL MODELING OF REDOX REACTIVITY, DEGRADATION PATHWAYS AND PERSISTENCE FOR AQUEOUS PHASE CONTAMINANTS

Models used to predict the fate of aqueous phase contaminants are often limited by their inability to address the widely varying redox conditions in natural and engineered systems, as well as by their dependence on existing experimental data for structurally similar compounds. Here, a novel approach based on quantum chemical calculations is developed, which can be applied to assess the environmental fate of any contaminant of interest without previous knowledge of the compound. It identifies the thermodynamic conditions necessary for redox-promoted degradation, and predicts degradation pathways as well as contaminant persistence.

Hexamethylphosphoramide (HMPA), a widely used solvent and poorly characterized groundwater contaminant, is used as a test case. The development of an analytical technique based on liquid chromatography / time-of-flight mass spectrometry enables the detection of various degradation products that are reported here for the first time.

The oxidation of HMPA is estimated to require at least iron-reducing conditions at low to neutral pH, and nitrate-reducing conditions at high pH. Furthermore, the transformation of HMPA by permanganate, a common groundwater remediation agent, is

predicted to proceed through sequential *N*-demethylation. Experimental validation confirms the predicted pathways of HMPA oxidation by permanganate to phosphoramide via the formation of less methylated as well as singly and multiply oxygenated reaction intermediates. Pathways predicted to be thermodynamically or kinetically unfavorable are similarly absent in the experimental studies.

Theoretical and experimental investigations, using ^{18}O-labeled water to determine the source of oxygen in the products of HMPA oxidation, reveal a novel mechanism in addition to the one reported in the literature for methyl oxidation. The strategy of calculating Gibbs free energies of activation can be generally used to determine the primary degradation pathway when two or more pathways are thermodynamically favorable. In this study, however, the determined kinetic parameters show that both HMPA oxidation pathways proceed at similar reaction rates.

Hydrolysis of the P-N bond in HMPA is the only thermodynamically favorable reaction that may lead to its degradation under strongly reducing conditions. Through calculation of aqueous Gibbs free energies of activation for all potential reaction mechanisms, it is predicted that HMPA hydrolyzes via an acid-catalyzed A2@P mechanism at pH < 8.2, and an uncatalyzed concerted backside S_N2@P-b mechanism at pH 8.2 - 8.5. The estimated half-lives of thousands to hundreds of thousands of years over the groundwater-typical pH range of 6.0 to 8.5 indicate that HMPA will be persistent in the absence of suitable oxidants. At pH 0, where the hydrolysis reaction is rapid enough to enable measurement, the experimentally determined rate constant and half-life are in excellent agreement with the predicted values.

The newly developed methodology will enable scientists, regulators, and engineers to estimate the favorability of contaminant degradation at a specific field site, suitable approaches to enhance degradation, and the persistence of a contaminant and its reaction intermediates.

ACKNOWLEDGMENTS

I would like to thank my advisors Dr. Thomas Borch and Dr. Tom Sale for their encouragement and the numerous insightful discussions throughout this project. Thanks also to the remaining members of my graduate committee, Dr. Ken Barbarick and Dr. Elliot Bernstein, for their interest in my research project. A special thanks goes to Dr. Dave Gilbert (24 Feb 1962 - 06 May 2008), who paved the road for this project, but left too soon.

My gratitude goes to students, staff, and faculty of the Borch Research Group, the Center for Contaminant Hydrology, and the Center for Bioinformatics at Colorado State University (CSU). My special thanks go to Dr. Yury Desyaterik and Robert Young for their help and discussions on chemical analyses as well as Dr. Arthur Mayeno and Dr. Anthony Rappé for invaluable discussions on computational chemistry.

Primary funding for this work was provided by E.I. du Pont de Nemours and Company. Complementary support was provided by the University Consortium for Field-Focused Groundwater Contamination Research and by the National Science Foundation (NSF) through TeraGrid resources provided by the National Center for Supercomputing Applications (NCSA).

Finally, I am especially grateful to my entire family for their unconditional love and support.

FOR DANIEL & ELIZABETH

TABLE OF CONTENTS

LIST OF TABLES

Page

LIST OF FIGURES

Page

CHAPTER 1

INTRODUCTION

Contaminants in Aqueous Environments

The quality of our water resources is jeopardized by the presence of a vast number of organic and inorganic chemicals that enter the environment through discharge of domestic and industrial wastes, leakages, and accidental spills. Common aqueous phase contaminants include, but are not limited to, halogenated organic compounds, petroleum hydrocarbons, polycyclic aromatic hydrocarbons, explosives, heavy metals, and radionuclides. It is estimated that about 5% of all aquifers in the U.S. are contaminated. However, since these contaminations are often close to or within highly populated areas, their environmental and economical impact is disproportionately high (*1*).

Redox processes play an important part in governing the fate and transport of aqueous phase contaminants. The redox conditions in an aquifer are determined by the presence of electron donors (e.g., organic carbon, sulfides, ferrous iron) and acceptors (e.g., dissolved oxygen, nitrate, ferric iron, sulfate) as well as the pH (Figure 1.1). They control the speciation and mobility of many transition metals, metalloids and radionuclides, as well as the abiotic and biological degradation of organic compounds (*2, 3*). Furthermore, redox conditions do not only determine whether a certain contaminant degradation or immobilization reaction is thermodynamically favorable, but can also

impact degradation rates and pathways. For instance, vinyl chloride is reductively dechlorinated to ethene under reducing conditions, and mineralized to form carbon dioxide under oxidizing conditions (refs (*1*, *4*) and references therein). Thus, the assessment of redox conditions is a prerequisite for understanding contaminant fate and transport at a contaminated site as well as for selecting remediation approaches (*1*, *3*, *5*, *6*).

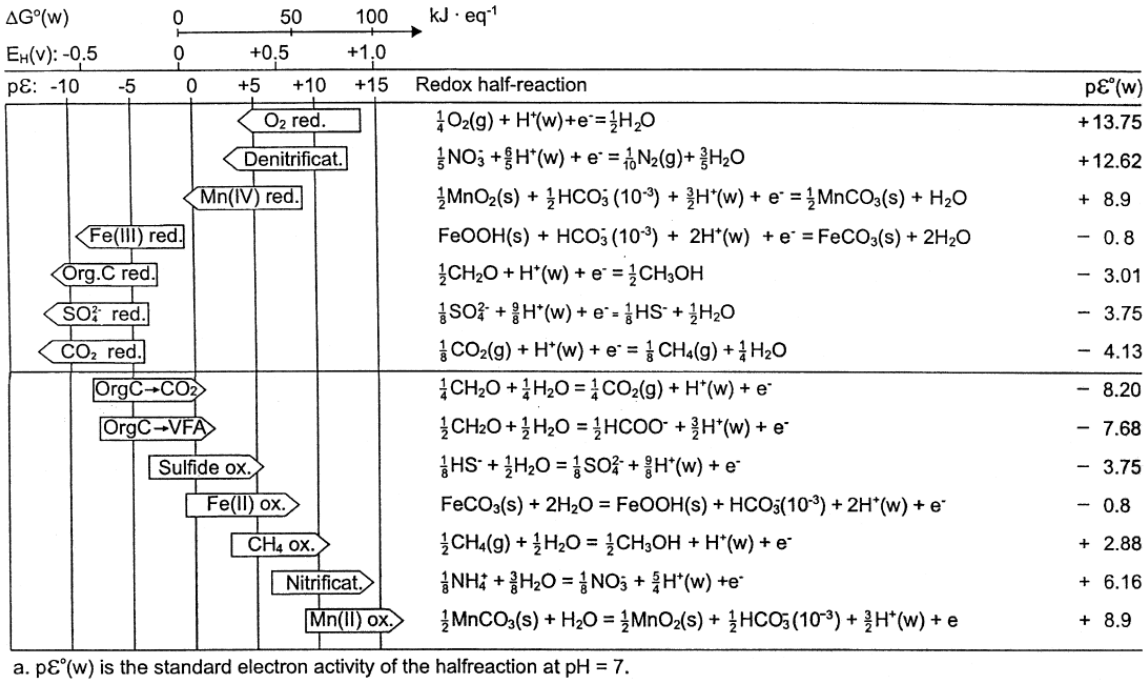

Figure 1.1: Representative redox half reactions for aqueous environments and their standard electron activity at pH 7 ($p\varepsilon^0(w)$). Adapted from refs (*3*, *7*).

Due to the key role of redox conditions in the fate and transport of aqueous phase contaminants, many modern groundwater remediation technologies (as well as some waste and drinking water purification processes) are based on altering these conditions to enhance or enable contaminant degradation or immobilization. For instance, the application of zero-valent metals and reduced organic carbon, such as molasses, ethanol,

and lactate, is used for the reductive degradation of chlorinated solvents and immobilization of chromate (*1, 6, 8*), while dissolved oxygen, nitrate, permanganate, ozone and other strong oxidants are used for contaminant oxidation (*1, 9, 10*).

Only in cases where financial, technological or other site-specific limitations do not allow for an active groundwater remediation, or when remediation technologies cannot reduce contaminant concentrations below the cleanup level(s) with reasonable effort, naturally occurring degradation or immobilization reactions (i.e., natural attenuation) may be taken advantage of. However, since natural attenuation can be a slow process, its efficiency must typically be assessed over the course of many years to verify that this is a viable (passive) remediation strategy at a specific site (*11*).

Contaminant Fate Prediction

As of October 2010, the ACS Chemical Abstracts Service database (*12*) indexes some 45 million commercially available chemicals. Of these, 282,000 were reported to be inventoried or regulated by government bodies. Since the Clean Water Act was passed in 1972, assessment and remediation of contaminated sites has almost exclusively addressed the list of only 126 conventional "priority pollutants" (*13*). In recent years, however, growing concern has arisen over so-called "new and emerging contaminants", such as perfluorinated compounds (*14*), polybrominated diphenyl ethers (PDBEs) (*15*), heterocyclic compounds (*11*), pharmaceuticals and personal care products (PPCPs), steroid hormones, pesticides (*16*), and many others.

For most new and emerging contaminants, properties that govern their fate in both natural environments and engineered remediation systems are unknown. The classical

approach of conducting laboratory studies, however, is highly demanding of time and resources. In order to deal with this large number of potential water contaminants, and at the same time keep assessment cost within a reasonable range, environmental fate models are increasingly used by scientists, engineers, and regulators.

For inorganic compounds, readily applicable software packages, such as PHREEQC (*17*) and MINTEQ2A (*18*), are already available, which predict their speciation and solubility based on thermodynamic equilibrium calculations. For organic compounds, quantitative structure-activity relationships (QSARs) (*19*-*22*) and linear free energy relationships (LFERs) (*23*-*25*) are currently most often applied for environmental fate prediction. Quantitative structure-activity relationships, sometimes also denoted QSPRs (quantitative structure-property relationships), are single or multiple regression analyses that quantitatively relate molecular structure (or descriptors of molecular structure) to certain compound properties, such as biological or chemical reactivity. Linear free energy relationships are also based on regression analysis, but specifically correlate one or more molecular descriptors with a standard Gibbs free energy of reaction (typically through an equilibrium constant) or a Gibbs free energy of activation (typically through a rate constant) (Figure 1.2). For both QSARs and LFERs, molecular descriptors can be of various nature, for instance quantum mechanical, topological, substructural, or physico-chemical (*21, 26*), indicating the inability of any one type of descriptor to accurately describe all features of biological or chemical reactivity.

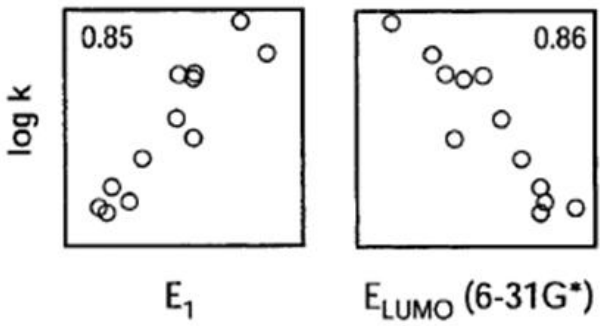

Figure 1.2: Example for a linear free energy relationship based on the correlation of the logarithm of an experimentally determined rate constant (log k) with the quantum chemically calculated one-electron reduction potential (E_1) and the energy of the lowest unoccupied molecular orbital (E_{LUMO}). Numbers indicate the coefficient of determination (R^2). Adapted from ref (*25*).

Usually, training sets of tens to a few thousands of well-characterized substances are used and tested for correlation among an initial set of molecular descriptors. After statistical analysis and identification of the best descriptors (based on the best fit), a linear relationship between the descriptor(s) and the target property is developed (*27*). An appropriate selection of descriptor variables for a QSAR or LFER is crucial: too few descriptors may lead to inaccurate predictions, whereas too many descriptors may compromise the general applicability of the correlation for unknown compounds (*27*).

However, the applicability of QSARs and LFERs suffers from several shortcomings. Many descriptors are not consistent between groups of chemicals, limiting their use to only closely related series of compounds (*28*). Thus, when specific correlations for certain molecular substructures have not been established, these approaches fail to generate a prediction. Also, some descriptors are purely empirical, and their physical sense remains unclear (*29*). Furthermore, due to the need of experimental determination of equilibrium constants, rate constants, and/or molecular descriptors for a large set of different compounds, the development of a QSAR or LFER requires an

extensive experimental effort. Finally, the established relationships are only valid for the specific conditions under which the experimental data were collected, which typically do not cover the widely varying redox and pH settings of natural and engineered environments.

Quantum Chemical Calculations

Through the use of quantum chemical calculations, molecular properties can be determined without any previous knowledge but the elemental composition. These properties include, but are not limited to, molecular structures and energies, bond energies, dipole moments, partial charges, vibrational frequencies, IR and NMR spectra, and thermochemical properties (*30*). Based on these properties, a variety of parameters useful for environmental fate predictions can be derived, such as equilibrium constants, reaction rates, Henry constants, octanol/water partition coefficients, vapor pressure, water solubility, and partial charges (*31-35*). The accuracy of these predictions is virtually only limited by computational capacities. Quantum chemical methods solve the time-independent Schrödinger equation

$$\hat{H}\,\Psi = E\,\Psi$$

where E is the energy of the particle (molecule), Ψ is the (multi-electron) wave function, and $\hat{H}$ is the Hamiltonian operator, which contains contributions from the kinetic energy of electrons and nuclei, as well as the potential energy resulting from Coulombic (electrostatic) attraction between electrons and nuclei, and from Coulombic repulsion due to nucleus-nucleus and electron-electron interactions (*36*). One characteristic difference

among the various quantum chemical methods, commonly referred to as levels of theory, is the calculation of electron correlation, i.e., the electron-electron interactions.

Calculations performed *ab initio* are, as implied by the name, directly derived from first principles without inclusion of experimental parameters. In Hartree-Fock (HF) theory, the simplest but most inaccurate of all *ab initio* methods, electron correlation is only considered through an average, i.e., it assumes that each electron interacts with an average charge distribution created by all other electrons. More accurate treatment of electron correlation is performed by various post-Hartree-Fock methods, such as Møller-Plesset (MP*n*) perturbation theory (especially MP4 and higher), configuration interaction (CI) and coupled cluster (CC) methods (*37*-*39*). These high level calculations can predict energies close to or within chemical accuracy (i.e., ≤1 kcal/mol), but require substantial computational capacities, which currently restricts their applicability to relatively small systems.

In recent years, density functional theory (DFT) has become an attractive alternative due to its practical balance of speed and accuracy (*40*). Whereas *ab initio* methods are wave function-based approaches, DFT uses electron density as the basic variable (*41*, *42*). Electron density is a function of three spatial variables only, independent of molecule size, compared to wave function-based approaches that depend on 3N spatial + N spin = 4N variables, N being the number of electrons. Thus, DFT calculations require substantially less computational capacities than post-Hartree-Fock methods while achieving almost comparable accuracies (*36*). The most popular level of theory, and the functional used in this study, is B3LYP, which is named after its use of Becke's three parameter hybrid exchange functional including the non-local correlation

functional of Lee, Yang and Parr (*43, 44*). Like other DFT functionals, it uses empirical fitting parameters based on experimental data for the calculation of electron correlation (*36*). Consequently, DFT is usually not considered an *ab initio* method.

The molecular orbitals in quantum chemical calculations are approximated by a linear combination of a pre-defined set (i.e., basis set) of atomic orbitals (i.e., basis functions) (*37*). An individual molecular orbital ϕ is defined as

$$\phi = \sum_{i=1}^{N} c_i \chi_i$$

where *N* is the number of atomic orbitals used to construct the molecular orbital, *c* is the molecular orbital expansion coefficient, and χ is the basis function (*30*). The basis functions, also called contracted Gaussians, are formed by a linear combination of primitive Gaussians, which contain the term $e^{-\zeta r^2}$. Here, e^{-r^2} is a Gaussian-type function used to describe the radial decay of the wave function amplitude with increasing distance *r* of the electron from the nucleus, and ζ is the orbital exponent, which is a fixed constant that accounts for how diffuse (large) an orbital is. The construction of each orbital by only one basis function, however, where all orbitals of a given type are identical in size, does not yield an accurate representation of the molecular wave function or electron density (*30*). Consequently, basis sets were introduced where each molecular orbital is formed from a linear combination of two (double-ζ) or more (triple-ζ etc.) sizes of functions for each atomic orbital (*37*). Furthermore, taking into account that changes in the electronic wave function occur in the valence space, so-called split-valence basis sets were created, in which the double-ζ or triple-ζ set of functions is limited to the valence orbitals, while the inert core electrons are still treated with a minimal single-ζ basis set,

thus reducing computational cost (*36*). Popular basis sets are 6-31G and 6-311G: The “6” indicates that the inner-shell orbitals are represented by a single contracted Gaussian that is a linear combination of six primitive Gaussians; the hyphen indicates a split-valence basis set; a double digit number behind the hyphen indicates the use of two basis functions, a triple digit number the use of three basis functions for the valence orbitals; the numbers themselves indicate the number of primitive Gaussians used in the basis functions.

Common additions to the basis set are polarization functions, which add orbitals of higher angular momentum than the valence orbitals occupied in the ground state, i.e., *p*-type orbitals to an *s*-type valence orbital, *d*-type orbitals to *p*-type valence orbitals, and so forth. This allows molecular orbitals to distort and be more asymmetric about their nucleus, which is important for an accurate description of atomic interaction / bonding (*30*). For instance, the notation (3df,p) indicates that three sets of *d*-type (each set having a different orbital exponent ζ) and one set of *f*-type functions are added to each non-hydrogen atom, and one set of *p*-type functions is added to each hydrogen.

Diffuse functions, denoted by “+", can be added to the basis set in order to increase spatial flexibility of the orbitals in systems where electrons are relatively far from the nucleus, such as in anions and highly excited electronic states. A single plus "+" indicates that one *s*-type and three *p*-type diffuse functions are added to non-hydrogen atoms, two plus signs "++" indicate that one *s*-type diffuse function is also added to hydrogen (*45*).

By default, quantum chemical calculations are conducted for atoms or molecules in the gaseous phase. However, solvation effects can substantially alter molecular

geometries and energies, and ultimately thermodynamic and kinetic parameters. The most accurate quantum chemical treatment of solvation is through the explicit inclusion of complete solvation shells, in which the solvent molecules entirely surround the solute species. This approach allows for consideration of short-range solute-solvent interactions such as hydrogen bonding. However, due to the slow decay of electrostatic interactions over distance, several solvation shells are usually necessary for accurate treatment (*46*), which is impractical for even small multi-atomic molecules due to the enormous computational cost. An implicit treatment of solvation effects through the use of continuum solvation models, on the other hand, such as the polarizable continuum model (PCM) (*47*) or the conductor-like screening model (COSMO) (*48*), enables the calculation of solvation free energies under consideration of long-range electrostatic effects. In these models, the solvent is represented as a continuum rather than a cluster of individual solvent molecules. However, vice versa, continuum solvation models do not yield accurate results when the solute experiences strong short-range interaction with the solvent (such as charged species or many transition states). Consequently, mixed explicit and implicit cluster-continuum solvation models have been applied in numerous studies, as well as in this dissertation. The cluster-continuum approach has been shown to yield accurate solvation free energies (refs (*49-52*) and references therein).

Research Objectives

The **overarching goal of this dissertation** was to develop a predictive methodology based on quantum chemical calculations, which can be used to assess the fate of any organic contaminant in an aqueous environment.

The **first objective** was to establish a strategy to estimate the redox reactivity of an aqueous organic contaminant, i.e., its degradability as a function of redox potential and pH. Even though the redox potential is a key parameter in controlling contaminant fate (see above), the prediction of redox reactivity has thus far not been addressed in the various available QSAR software packages. While several quantum chemical studies have focused on the prediction of standard redox potentials of transition state metals (refs (*46, 53, 54*) and references therein), only few have addressed standard redox potentials of organic compounds (*55, 56*). Standard redox potentials, however, are only valid for standard conditions (i.e., pH 0), while the actual redox potential may vary with pH (*6*). Chapter 2 outlines an approach to how the redox potential of an aqueous contaminant can be determined as a function of pH. With this information, it will be possible to predict in which redox zones degradation is favorable, and consequently if natural attenuation processes at a specific field site may lead to contaminant degradation, or which remedial approaches (i.e., application of a certain oxidant or reductant) can be applied to enhance or enable degradation.

The **second objective**, also addressed in Chapter 2, was to predict potential degradation pathways, i.e., which reaction products may be formed under certain redox conditions or with a certain oxidizing/reducing agent, respectively. Here, the common remediation agent permanganate was chosen as test oxidant. The potential degradation pathways are initially determined based on previously reported reaction mechanisms. Subsequently, Gibbs free energies of reaction in aqueous phase (Figure 1.3) are calculated for each individual reaction, enabling the differentiation between reactions that are thermodynamically favorable and unfavorable.

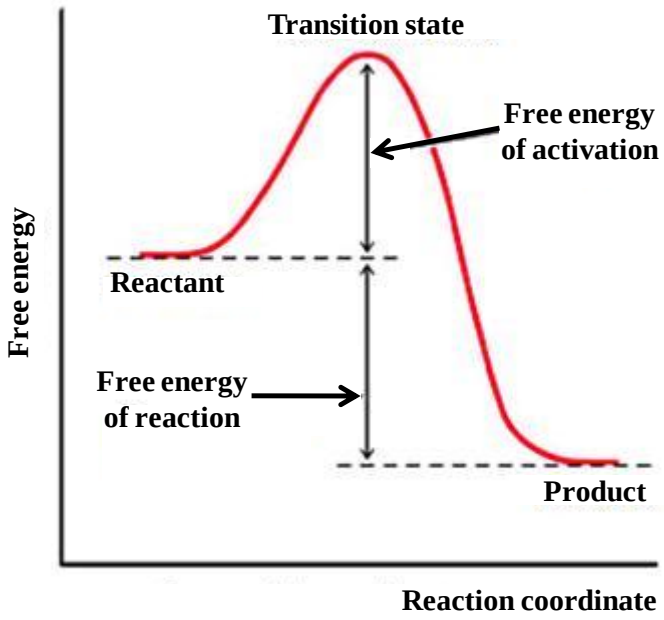

Figure 1.3: Potential energy surface showing the free energy associated with a reactant, transition state, and product.

While thermodynamic parameters can be used to exclude unfavorable pathways, they only indicate that favorable pathways may proceed. Only through determination of kinetic parameters, however, it can be evaluated whether a favorable reaction occurs within a relevant time frame. Thus, the **third objective** of this dissertation was to predict contaminant persistence, briefly addressed in Chapter 2, more detailed in Chapter 3. Here, reaction rate constants and half-lives are calculated based on quantum chemically predicted Gibbs free energies of activation in aqueous phase, which is the difference in free energy between a transition state and the respective reactant(s) (Figure 1.3).

The same strategy, transition state searches and activation energy predictions, can be applied to identify the primary, most likely degradation pathway. This task is important and has been accomplished in several studies to identify the main degradation pathway when two or more pathways are thermodynamically favorable (*34, 57-60*). This

was the **fourth objective** for this dissertation, which is addressed in Chapter 4. Furthermore, through investigations of transition states in combination with intrinsic reaction coordinate (IRC) calculations, which trace the lowest-energy path between two minima on the potential energy surface (i.e., reactants and products), the mechanism(s) for a reaction of interest can be elucidated (*37*). Thus, the **fifth objective** was the determination of aqueous permanganate oxidation mechanisms to validate the potential degradation pathway that was created based on previously reported reaction mechanisms in Chapter 2.

Hexamethylphosphoramide (HMPA, $O=P(N(CH_3)_2)_3$, Figure 1.4) was investigated in this dissertation to develop and test the predictive methodology, as well as to elucidate its environmental fate under natural and engineered conditions. Hexamethylphosphoramide is a water-miscible, colorless liquid with a density of 1.03 g/mL, which has been widely used - although usually in small quantities - as solvent for gases, organic, and organometallic compounds, as polymerization catalyst, stabilizing agent against thermal degradation in polystyrene, UV protectant in polyvinyl and polyolefin resins, de-icing additive for jet fuels, rodenticide, and insect chemosterilant (*61*). It has been detected in groundwater in the U.S. (*62*), and thus raised potential health concerns due to its toxicity and possible carcinogenicity to humans (*63*).

As with many new and emerging contaminants, the environmental fate of HMPA has thus far only been poorly characterized, partly due to the lack of an appropriate analytical method capable of detecting the products of HMPA degradation. The only intermediates from biotic and abiotic oxidation reported prior to this study were the less methylated pentamethylphosphoramide, tetramethylphosphoramide and trimethylphos-

phoramide, as well as the oxygenated formyl-pentamethylphosphoramide and formyl-tetramethylphosphoramide (*64*, *65*). Consequently, a new method based on liquid chromatography coupled with time-of-flight mass spectrometry was developed (Chapter 5), which enabled the detection of HMPA and all of its degradation products. This method was thus applied in all of the validation experiments.

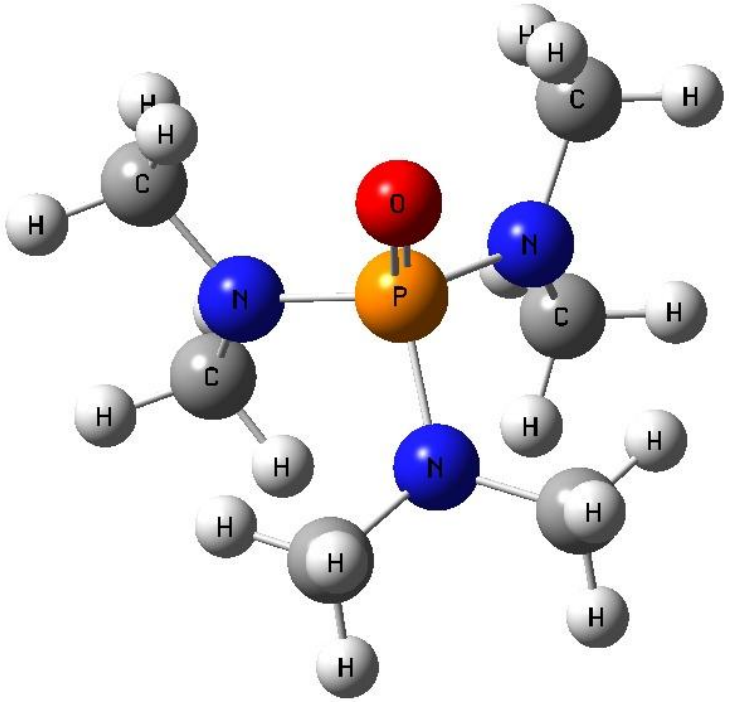

Figure 1.4: 3D molecular structure of hexamethylphosphoramide (HMPA).

Most of the dissertation work is either planned for submission to or already published in peer-reviewed journals. Chapter 2 has been published in the American Chemical Society (ACS) journal of Environmental Science and Technology (Blotevogel et al. 2010, vol. 44, no. 15, pp. 5868-5874). Chapter 3 (Blotevogel et al.) has been submitted (August 19, 2010) to the ACS journal of Environmental Science and Technology for review. Parts of the dissertation have also been presented at several

national and international conferences, i.e., at the 236th and 239th ACS National Meetings in Philadelphia, PA (2008) and San Francisco, CA (2010), the 2nd International Conference on Occurrence, Fate, Effects, and Analysis of Emerging Contaminants in the Environment (EmCon) in Fort Collins, CO (2009), the 2008, 2009, and 2010 Annual Progress Meetings of the University Consortium for Field-Focused Groundwater Contamination Research in Ontario, Canada, and the 2008, 2009, and 2010 American Geophysical Union Hydrology Days in Fort Collins, CO.

References

1. Suthersan, S. S.; Payne, F. C., *In situ Remediation Engineering*. CRC Press: Boca Raton, 2005; p 511.

2. Borch, T.; Kretzschmar, R.; Kappler, A.; Van Cappellen, P.; Ginder-Vogel, M.; Voegelin, A.; Campbell, K., Biogeochemical redox processes and their impact on contaminant dynamics. *Environmental Science & Technology* **2010,** 44, (1), 15-23.

3. Christensen, T. H.; Bjerg, P. L.; Banwart, S. A.; Jakobsen, R.; Heron, G.; Albrechtsen, H. J., Characterization of redox conditions in groundwater contaminant plumes. *Journal of Contaminant Hydrology* **2000,** 45, (3-4), 165-241.

4. Bradley, P. M., Microbial degradation of chloroethenes in groundwater systems. *Hydrogeology Journal* **2000,** 8, (1), 104-111.

5. Ginder-Vogel, M.; Criddle, C. S.; Fendorf, S., Thermodynamic constraints on the oxidation of biogenic UO_2 by Fe(III) (hydr)oxides. *Environmental Science & Technology* **2006,** 40, (11), 3544-3550.

6. Matheson, L. J.; Tratnyek, P. G., Reductive dehalogenation of chlorinated methanes by iron metal. *Environmental Science & Technology* **1994,** 28, (12), 2045-2053.

7. Stumm, W.; Morgan, J. J., *Aquatic Chemistry: Chemical Equilibria and Rates in Natural Waters*. 2nd ed.; John Wiley & Sons, Inc.: New York, NY, 1996; p 1022.

8. Wilkin, R. T.; Su, C. M.; Ford, R. G.; Paul, C. J., Chromium-removal processes during groundwater remediation by a zerovalent iron permeable reactive barrier. *Environmental Science & Technology* **2005,** 39, (12), 4599-4605.

9. Cunningham, J. A.; Rahme, H.; Hopkins, G. D.; Lebron, C.; Reinhard, M., Enhanced *in situ* bioremediation of BTEX contaminated groundwater by combined injection of nitrate and sulfate. *Environmental Science & Technology* **2001,** 35, (8), 1663-1670.

10. Damm, J. H.; Hardacre, C.; Kalin, R. M.; Walsh, K. P., Kinetics of the oxidation of methyl tert-butyl ether (MTBE) by potassium permanganate. *Water Research* **2002,** 36, (14), 3638-3646.

11. Reineke, A. K.; Goen, T.; Preiss, A.; Hollender, J., Quinoline and derivatives at a tar oil contaminated site: Hydroxylated products as indicator for natural attenuation? *Environmental Science & Technology* **2007,** 41, (15), 5314-5322.

12. CAS Database Counter. http://www.cas.org/cgi-bin/cas/regreport.pl (10/12/2010)

13. Daughton, C. G., Non-regulated water contaminants: Emerging research. *Environmental Impact Assessment Review* **2004,** 24, (7-8), 711-732.

14. Fujii, S.; Polprasert, C.; Tanaka, S.; Lien, N. P. H.; Qiu, Y., New POPs in the water environment: distribution, bioaccumulation and treatment of perfluorinated compounds - a review paper. *Journal of Water Supply Research and Technology-Aqua* **2007,** 56, (5), 313-326.

15. Streets, S. S.; Henderson, S. A.; Stoner, A. D.; Carlson, D. L.; Simcik, M. F.; Swackhamer, D. L., Partitioning and bioaccumulation of PBDEs and PCBs in Lake Michigan. *Environmental Science & Technology* **2006,** 40, (23), 7263-7269.

16. Kolpin, D. W.; Furlong, E. T.; Meyer, M. T.; Thurman, E. M.; Zaugg, S. D.; Barber, L. B.; Buxton, H. T., Pharmaceuticals, hormones, and other organic wastewater contaminants in US streams, 1999-2000: A national reconnaissance. *Environmental Science & Technology* **2002,** 36, (6), 1202-1211.

17. Parkhurst, D. L.; Appelo, C. A. J. *User's Guide to PHREEQC (Version 2), A Computer Program for Speciation, Batch-Reaction, One-Dimensional Transport, and Inverse Geochemical Calculations*, US Geological Survey: Denver, CO, 2002.

18. Allison, J. D.; Brown, D. S.; Novo-Gradac, K. J. *MINTEQA2, geochemical assessment model for environmental systems*, Version 3; US Environmental Protection Agency: Washington, DC, 1992.

19. Dimitrov, S.; Breton, R.; MacDonald, D.; Walker, J. D.; Mekenyan, O., Quantitative prediction of biodegradability, metabolite distribution and toxicity of

stable metabolites. *Sar and Qsar in Environmental Research* **2002,** 13, (3-4), 445-455.

20. Hansch, C.; Leo, A., *Exploring QSAR: Fundamentals and Applications in Chemistry and Biology*. American Chemical Society: Washington, DC, 1995; p 557.

21. Karelson, M.; Lobanov, V. S.; Katritzky, A. R., Quantum-chemical descriptors in QSAR/QSPR studies. *Chemical Reviews* **1996,** 96, (3), 1027-1043.

22. Walker, J. D.; Carlsen, L.; Hulzebos, E.; Simon-Hettich, B., Global government applications of analogues, SARs and QSARs to predict aquatic toxicity, chemical or physical properties, environmental fate parameters and health effects of organic chemicals. *Sar and Qsar in Environmental Research* **2002,** 13, (6), 607-616.

23. Hammett, L. P., Some relations between reaction rates and equilibrium constants. *Chemical Reviews* **1935,** 17, (1), 125-136.

24. Hansch, C.; Maloney, P. P.; Fujita, T., Correlation of biological activity of phenoxyacetic acids with Hammett substituent constants and partition coefficients. *Nature* **1962,** 194, (4824), 178-180.

25. Scherer, M. M.; Balko, B. A.; Gallagher, D. A.; Tratnyek, P. G., Correlation analysis of rate constants for dechlorination by zero-valent iron. *Environmental Science & Technology* **1998,** 32, (19), 3026-3033.

26. Benigni, R.; Passerini, L.; Livingstone, D. J.; Johnson, M. A.; Giuliani, A., Infrared spectra information and their correlation with QSAR descriptors. *Journal of Chemical Information and Computer Sciences* **1999,** 39, (3), 558-562.

27. Winkler, D. A., The role of quantitative structure-activity relationships (QSAR) in biomolecular discovery. *Briefings in Bioinformatics* **2002,** 3, (1), 73-86.

28. Burrow, P. D.; Aflatooni, K.; Gallup, G. A., Dechlorination rate constants on iron and the correlation with electron attachment energies. *Environmental Science & Technology* **2000,** 34, (16), 3368-3371.

29. Zevatskii, Y. E.; Samoilov, D. V., Some modern methods for estimation of reactivity of organic compounds. *Russian Journal of Organic Chemistry* **2007,** 43, (4), 483-500.

30. McQuarrie, D. A.; Simon, J. D., *Physical Chemistry: A Molecular Approach*. University Science Books: Sausalito, CA, 1997; p 1270.

31. Barrows, S. E.; Cramer, C. J.; Truhlar, D. G.; Elovitz, M. S.; Weber, E. J., Factors controlling regioselectivity in the reduction of polynitroaromatics in aqueous solution. *Environmental Science & Technology* **1996,** 30, (10), 3028-3038.

32. Bylaska, E. J., Estimating the thermodynamics and kinetics of chlorinated hydrocarbon degradation. *Theoretical Chemistry Accounts* **2006,** 116, (1-3), 281-296.

33. Niederer, C.; Goss, K. U., Effect of *ortho*-chlorine substitution on the partition behavior of chlorophenols. *Chemosphere* **2008,** 71, (4), 697-702.

34. Ozen, A. S.; Aviyente, V.; Klein, R. A., Modeling the oxidative degradation of azo dyes: A density functional theory study. *Journal of Physical Chemistry A* **2003,** 107, (24), 4898-4907.

35. Qasim, M.; Kholod, Y.; Gorb, L.; Magers, D.; Honea, P.; Leszczynski, J., Application of quantum-chemical approximations to environmental problems: Prediction of physical and chemical properties of TNT and related species. *Chemosphere* **2007,** 69, (7), 1144-1150.

36. Koch, W.; Holthausen, M. C., *A Chemist's Guide to Density Functional Theory*. 2nd ed.; Wiley-VCH Verlag GmbH: Weinheim, Germany, 2001; p 300.

37. Foresman, J. B.; Frisch, Æ., *Exploring Chemistry with Electronic Structure Methods*. 2nd ed.; Gaussian: Pittsburgh, PA, 1996; p 302.

38. Møller, C.; Plesset, M. S., Note on an approximation treatment for many-electron systems. *Physical Review* **1934,** 46, (7), 0618-0622.

39. Santiso, E. E.; Gubbins, K. E., Multi-scale molecular modeling of chemical reactivity. *Molecular Simulation* **2004,** 30, (11-12), 699-748.

40. Cartinella, J. L.; Cath, T. Y.; Flynn, M. T.; Miller, G. C.; Hunter, K. W.; Childress, A. E., Removal of Natural Steroid Hormones from Wastewater Using Membrane Contactor Processes. In 2006; Vol. 40, pp 7381-7386.

41. Geerlings, P.; De Proft, F.; Langenaeker, W., Conceptual density functional theory. *Chemical Reviews* **2003,** 103, (5), 1793-1873.

42. Hohenberg, P.; Kohn, W., Inhomogeneous electron gas. *Physical Review B* **1964,** 136, (3B), B864-B871.

43. Becke, A. D., Density-functional thermochemistry. III. The role of exact exchange. *Journal of Chemical Physics* **1993,** 98, (7), 5648-5652.

44. Lee, C. T.; Yang, W. T.; Parr, R. G., Development of the Colle-Salvetti correlation-energy formula into a functional of the electron density. *Physical Review B* **1988,** 37, (2), 785-789.

45. Cramer, C. J., *Essentials of Computational Chemistry: Theories and Models.* John Wiley & Sons, Inc.: New York, NY, 2002; p 542.

46. Uudsemaa, M.; Tamm, T., Density-functional theory calculations of aqueous redox potentials of fourth-period transition metals. *Journal of Physical Chemistry A* **2003,** 107, (46), 9997-10003.

47. Miertus, S.; Scrocco, E.; Tomasi, J., Electrostatic interaction of a solute with a continuum - a direct utilization of ab initio molecular potentials for the prevision of solvent effects. *Chemical Physics* **1981,** 55, (1), 117-129.

48. Klamt, A.; Schuurmann, G., COSMO: A new approach to dielectric screening in solvents with explicit expressions for the screening energy and its gradient. *Journal of the Chemical Society-Perkin Transactions 2* **1993**, (5), 799-805.

49. Bryantsev, V. S.; Diallo, M. S.; Goddard, W. A., Calculation of solvation free energies of charged solutes using mixed cluster/continuum models. *Journal of Physical Chemistry B* **2008,** 112, (32), 9709-9719.

50. Cossi, M.; Barone, V., Solvent effect on vertical electronic transitions by the polarizable continuum model. *Journal of Chemical Physics* **2000,** 112, (5), 2427-2435.

51. Kelly, C. P.; Cramer, C. J.; Truhlar, D. G., SM6: A density functional theory continuum solvation model for calculating aqueous solvation free energies of neutrals, ions, and solute-water clusters. *Journal of Chemical Theory and Computation* **2005,** 1, (6), 1133-1152.

52. Pliego, J. R.; Riveros, J. M., The cluster-continuum model for the calculation of the solvation free energy of ionic species. *Journal of Physical Chemistry A* **2001,** 105, (30), 7241-7247.

53. Li, J.; Fisher, C. L.; Chen, J. L.; Bashford, D.; Noodleman, L., Calculation of redox potentials and pK(a) values of hydrated transition metal cations by a combined density functional and continuum dielectric theory. *Inorganic Chemistry* **1996,** 35, (16), 4694-4702.

54. Roy, L. E.; Jakubikova, E.; Guthrie, M. G.; Batista, E. R., Calculation of one-electron redox potentials revisited. Is it possible to calculate accurate potentials with density functional methods? *Journal of Physical Chemistry A* **2009,** 113, (24), 6745-6750.

55. Namazian, M., Density functional theory response to the calculation of electrode potentials of quinones in non-aqueous solution of acetonitrile. *Journal of Molecular Structure-Theochem* **2003,** 664, 273-278.

56. Namazian, M.; Almodarresieh, H. A.; Noorbala, M. R.; Zare, H. R., DFT calculation of electrode potentials for substituted quinones in aqueous solution. *Chemical Physics Letters* **2004,** 396, (4-6), 424-428.

57. Fueno, H.; Tanaka, K.; Sugawa, S., Theoretical study of the dechlorination reaction pathways of octachlorodibenzo-p-dioxin. *Chemosphere* **2002,** 48, (8), 771-778.

58. Kilic, M.; Kocturk, G.; San, N.; Cinar, Z., A model for prediction of product distributions for the reactions of phenol derivatives with hydroxyl radicals. *Chemosphere* **2007,** 69, (9), 1396-1408.

59. Nonnenberg, C.; van der Donk, W. A.; Zipse, H., Reductive dechlorination of trichloroethylene: A computational study. *Journal of Physical Chemistry A* **2002,** 106, (37), 8708-8715.

60. Zhang, Q. Z.; Qu, X. H.; Wang, W. X., Mechanism of OH-initiated atmospheric photooxidation of dichlorvos: A quantum mechanical study. *Environmental Science & Technology* **2007,** 41, (17), 6109-6116.

61. Lloyd, J. W., Hexamethylphosphoric triamide (HMPA). *American Industrial Hygiene Association Journal* **1975,** 36, (12), 917-919.

62. Campos, D., Field demonstration of UV/H_2O_2 on the treatment of groundwater contaminated with HMPA. In *Chemical Oxidation: Technologies for the Nineties.*, Eckenfelder, W. W.; Bowers, A. R.; Roth, J. A., Eds. Technomic Publishing Company: Lancaster, PA, 1997; Vol. 6, pp 19-26.

63. IARC, *Re-evaluation of Some Organic Chemicals, Hydrazine, and Hydrogen Peroxide. IARC Monographs on the Evaluation of Carcinogenic Risk of Chemicals to Humans, Vol. 71*; International Agency for Research on Cancer: Lyon, France, 1999; p 1589.

64. Jones, A. R.; Jackson, H., Metabolism of hexamethylphosphoramide and related compounds. *Biochemical Pharmacology* **1968,** 17, (11), 2247-2252.

65. Terry, P. H.; Borkovec, A. B., Insect chemosterilants. 4. Oxidation of hexamethylphosphoric triamide and synthesis of *N*-formylphosphoramides. *Journal of Medicinal Chemistry* **1968,** 11, (5), 958-961.

CHAPTER 2

QUANTUM CHEMICAL PREDICTION OF REDOX REACTIVITY AND DEGRADATION PATHWAYS FOR AQUEOUS PHASE CONTAMINANTS: AN EXAMPLE WITH HMPA

Introduction

Due to the vast number of anthropogenic chemicals in the environment and their potential adverse health effects, environmental fate predictions have become an indispensable component of risk assessment today (*1*). Furthermore, theoretical models that predict unknown physicochemical properties or biogeochemical reactivity are used to pre-assess newly developed compounds in order to identify environmental effects prior to large-scale production and commercialization (*2*). Currently, standard risk assessment strategies most frequently involve predictions based on quantitative structure-activity relationships (QSARs) (*3*). These approaches are attractive since they generate results with minimal computational costs once the relationship and descriptor values have been determined. However, the utility of QSARs is constrained as they rely on experimental databases and are often only valid for narrow ranges of conditions that do not necessarily cover the widely varying redox settings of natural and engineered environments.

Thermodynamic properties ultimately govern the persistence or degradability of a compound in the environment. For many contaminants of concern, however, information

on Gibbs free energies of formation or reaction in aqueous phase is unavailable, leading researchers to estimate fundamental thermodynamic properties (*4, 5*) to assess the favorability of transformations or to predict degradation pathways (*6-8*). In recent years, increases in computational speed have enabled thermodynamic predictions based on quantum chemical calculations for molecules or systems comprising up to a few hundred atoms (9). These approaches allow for accurate investigation of chemicals without any previous knowledge on the substance. Furthermore, quantum chemical models can be used to generate kinetic information, such as activation energies and reaction rates (*10, 11*). This strategy has been widely applied to identify reaction mechanisms and primary degradation pathways when multiple pathways are possible (*12-16*).

The fate of a contaminant in groundwater, however, will also depend on the redox conditions in an aquifer (*17, 18*). Consequently, in many *in situ* remedial approaches, the redox conditions are manipulated by the delivery of strong oxidants or reductants in order to enable or enhance the degradation of redox-sensitive contaminants. For inorganic compounds, readily applicable thermodynamic equilibrium models are already available (ref (*19*) and references therein). Strategies to assess the redox reactivity of organic contaminants, on the other hand, are very limited. Several quantum chemical methods used for calculation of standard redox potentials have been developed (ref (*20*) and references therein). One of the most popular approaches is the application of the Born-Haber cycle, in which the free energy of a half reaction is determined from the free energy of reaction in gas phase and solvation free energies of the oxidized and reduced species (*21*). This approach, however, requires the inclusion of at least two explicit hydration shells to yield accurate predictions, which substantially increases the

computational cost (*22*). Namazian and co-workers (*23, 24*) calculated standard redox potentials for organic compounds based on the quantum chemically-predicted free energy of reaction and a known experimental redox potential for one of the constituent half reactions, thus eliminating the need of explicit solvation by using less costly implicit solvation models. However, no attempts have so far been made to include the influence of pH on redox reactivity in predictive models and use this information to elucidate the conditions necessary for contaminant degradation.

Here, a novel quantum chemical approach to predict the fate of aqueous phase contaminants in natural and engineered environments is presented. The calculations are based on density functional theory (DFT) which allows for a practical balance between accuracy and computational efficiency, compared to the accurate but more expensive post-Hartree Fock *ab initio* methods (*25*). The specific objectives of this work are to predict chemical reactivity under different redox conditions, potential degradation pathways, and contaminant persistence.

Hexamethylphosphoramide (HMPA), a water-miscible, colorless liquid which is widely used as solvent for polymers and organo-metallic compounds (*26*), is used as a test compound for development and validation of the predictive methodology. Hexamethylphosphoramide has been detected in groundwater in the US (*27*) and thus represents a contaminant of potential concern. It has been shown to induce nasal tumors in rats and mutagenic effects in fruit flies (*28*). Pentamethylphosphoramide (PMPA), tetramethylphosphoramide (TetMPA), and trimethylphosphoramide (TriMPA) have been detected as metabolites in the same two species (*29*). Terry and Bořkovec investigated the oxidation of HMPA by permanganate and H_2O_2 and identified formylated reaction

intermediates in addition to PMPA (*30*). In these studies, the generation of a hydroxymethyl intermediate was suggested, but not verified due to the lack of appropriate analytical techniques. No further information about the environmental fate of HMPA has been reported. The consequence of our limited knowledge regarding HMPA, as with innumerable other anthropogenic compounds, is a need to develop advanced tools to assess contaminant fate under natural and engineered conditions.

Computational Details

Quantum chemical calculations were conducted to predict thermodynamic and kinetic parameters for HMPA fate prediction. All calculations were performed using the Gaussian 03 program package without symmetry constraints and with default settings unless otherwise noted. Standard Gibbs free energies of reaction in aqueous phase ($\Delta_r G^0_{(aq)}$) were determined at the restricted B3LYP level of theory with the 6-311++G(d,p) basis set for the elements P, O, N, C, and H, as well as the effective core potential (ECP)-type basis set LANL2DZ for Mn. For the MnO_4^- / $HMnO_4^{2-}$ redox couple, one explicit water molecule was found to stabilize the ground state structures and was thus included in the calculations. Inclusion of additional explicit water molecules did not change the free energies of reaction. For the MnO_4^- / MnO_3^- redox couple, explicit solvation had no effect on the free energies of reaction and was thus not considered. The integral equation formalism polarizable continuum model (IEFPCM) was used to account for implicit solvation effects on aqueous species (*31*). Due to the use of UA0 cavity radii, the thermal correction to Gibbs free energy including the zero-point correction from a frequency analysis was added to the total free energy in solution. All aqueous phase free

energies were converted to standard state conditions by adding a free-energy change of $RT\ ln(24.5)$ = +7.9 kJ/mol due to the concentration change from gas to aqueous phase. Free energies of reaction at pH 7 were determined via $\Delta_r G'^{0}_{(aq)} = \Delta_r G^{0}_{(aq)} + RT\ ln\ Q$, where Q is the reaction quotient. Potential energy minima were verified by frequency calculations (i.e., no imaginary frequencies). Conformational analyses of the potential energy surfaces were not performed.

Transition state (TS) structures were first optimized at the unrestricted B3LYP level of theory with a 6-31G(d) basis set on C, H, N, and O and a 6-31G(2d) basis set on P, and verified by both intrinsic reaction coordinate (IRC) and frequency calculations (i.e., exactly one imaginary frequency). Explicit water molecules were then sequentially added to the TS optimizations until the determined free energies of activation stabilized. Due to the well-documented convergence problems that plague polarizable continuum models (PCM) (*32, 33*) as well as the observation that the effects of *implicit* solvation only negligibly change the molecular properties found in gas phase (*32, 34*), TS optimizations, frequency and IRC calculations were initially performed without the use of IEFPCM. Only the lowest-energy TS structure for each reaction mechanism including explicit solvation was then optimized at the unrestricted B3LYP level of theory with a 6-31+G(d) basis set on C, H, N, and O and a 6-31+G(2d) basis set on P, and verified by both frequency (at 22 °C) and IRC calculations. Subsequently, single point energy calculations on the optimized TS structures were performed at the B3LYP/6-311++G(3df,3pd) level of theory in combination with IEFPCM.

The reaction half-life ($t_{1/2}$) was calculated from the Gibbs free energy of activation in aqueous phase ($\Delta^{\ddagger}G_{(aq)}$) at 22 °C (same temperature as the experimental system) via transition state theory (*35*):

$$t_{1/2} = \frac{ln(2)}{k} = \frac{ln\,(2)}{\left[\kappa\left(\frac{k_B T}{h}\right) exp\left(\frac{-\Delta^{\ddagger}G_{(aq)}}{RT}\right)\right]}$$

where k is the first-order rate constant, k_B is the Boltzmann constant, T is the temperature in Kelvin, h is Planck's constant, R is the universal gas constant, and κ is the transmission coefficient which accounts for quantum mechanical tunneling effects:

$$\kappa = 1 + \frac{1}{24}\left(\frac{1.44\,\nu_i}{T}\right)^2$$

where ν_i is the magnitude of the imaginary frequency (cm^{-1}) corresponding to the reaction coordinate at the transition state.

Experimental Section

HMPA Oxidation Experiments

Oxidation of HMPA by permanganate was investigated experimentally to test the quantum chemical predictions. In a 1-L Pyrex media glass bottle, an 800 mL solution containing 0.25 mM HMPA (99%, MP Biomedicals) and 6 mM $KMnO_4$ was prepared in 30 mM phosphate buffer at pH 7.0. A parallel control experiment was set up in the absence of $KMnO_4$. The bottles were sealed with PTFE-faced silicone septa and stirred on a magnetic stir plate (240 rpm) at ambient temperature (22 ºC). For liquid chromatography - (electrospray ionization) - time of flight - mass spectrometry (LC/TOF-MS) analyses (see Analytical Methods below), samples (0.2 mL) were quenched by

adding 1.8 mL of 3 mM $Na_2S_2O_3$ and filtered (0.2 µm, nylon). Storage of quenched and filtered samples at ambient temperature over a period of one week revealed that all oxidation reactions were halted. Samples (3 mL) for formaldehyde analysis were quenched with 80 µL of 1 M $Na_2S_2O_3$ and filtered (as above). Formaldehyde was derivatized with 2,4-dinitrophenylhydrazine dissolved in acetonitrile and phosphoric acid at pH 4, and extracted with chloroform. For total nitrogen analyses, 10-mL samples were quenched with 300 µL of 1 M $Na_2S_2O_3$ and filtered (as above). For carbinolamides ($HOCH_2NRP$), a rapid (non-oxidative) decomposition was observed after quenching. Thus, due to the high sampling frequency, the oxidation experiments were performed one at a time to allow for immediate analyses. This experiment was conducted three times, verifying the reproducibility of the observations made. The analytical results will be presented in another paper.

HMPA Hydrolysis Experiments

To investigate the reactivity of HMPA in the absence of a strong oxidant, phosphate buffered (30 mM; pH 7.0) DI water (800 mL) in 1-L Pyrex media glass bottles sealed with a PTFE-faced silicone septum were prepared in triplicate and autoclaved. Hexamethylphosphoramide was injected to yield a final concentration of 0.25 mM. The reaction bottles were stored in the dark without agitation at ambient temperature (22 ºC). 150-µL samples were diluted 1:10 with DI water and analyzed monthly by LC/TOF-MS.

Analytical Methods

Hexamethylphosphoramide and its phosphoramide-containing transformation products were analyzed with an Agilent 1100 Series liquid chromatograph equipped with

a 150 mm × 2.1 mm XTerra phenyl column, 3.5 µm particle size (Waters) in combination with an Agilent G3250AA MSD TOF system (LC/MS-TOF). The injection volume was 10 µL and the flow rate was 0.5 mL/min. During the first three hours of the HMPA oxidation experiment (i.e., while HMPA was detectable) and for the HMPA hydrolysis experiment, separation was carried out isocratically with 0.01% formic acid in water / acetonitrile (98:2). For the samples obtained three hours after initiation of the HMPA oxidation experiment, chromatographic separation was carried out isocratically with 0.01% formic acid in water. The capillary and fragmentation voltages were 2.8 kV and 140 V, respectively. The mass analyzer was calibrated from *m/z* 90 to 600 in positive ionization mode. For the detection of carboxylic acids, samples were analyzed in negative ionization mode, using the same parameters, except for capillary voltage (2.0 kV). Besides HMPA, reference standards were only available for PMPA, TetMPA, and TriMPA (all custom synthesized and generously provided by DuPont, 97% purity). The limits of detection (LOD) were 0.039 µM, 0.070 µM, 0.17 µM, and 0.18 µM, respectively.

Oxidation-reduction potential (ORP) and pH were measured with a UP-25 pH/mV/Ion Meter (Denver Instruments). Total nitrogen was quantified with a TNM-1 Total Nitrogen Measuring Unit connected to a TOC-V CSH Total Organic Carbon Analyzer (both Shimadzu). Formaldehyde analyses were carried out on a 5890 Series II gas chromatograph (Hewlett Packard) equipped with a flame ionization detector, using a method modified from Dalene et al. (*36*). The LOD for formaldehyde was 0.27 µM.

Results

Prediction of Contaminant Reactivity Under Different Redox Conditions

To identify the thermodynamic conditions favoring HMPA oxidation, stability lines were determined, based on quantum chemically-calculated free energies of reaction, and superimposed onto stability (Pourbaix) diagrams (Figure 2.1). Initial oxidation of HMPA can occur at the methyl substituent, to give hydroxymethyl-pentamethyl-phosphoramide (HM-PMPA, compound 4 in Figure 2.2), and at the nitrogen atom, to form HMPA *N*-oxide (compound 2 in Figure 2.2), as previously described (*29*).

Gibbs free energies for oxidation or reduction half reactions, however, cannot be calculated directly due to the presence of protons and free electrons in the formal half-reaction equations. Thus, the Gibbs free energy of reaction is calculated first for HMPA oxidation by any chosen oxidant, for which its reduction half-reaction is known, here hydrogen peroxide. The detailed calculation of the stability lines is presented here for the oxidation of HMPA to HM-PMPA as an example:

$$\text{HMPA} + H_2O_2 = \text{HM-PMPA} + H_2O \qquad \mathbf{\Delta_r G^0_{(aq)} = -268\ kJ/mol}$$

The known half reaction for H_2O_2 reduction (*37*)

$$H_2O_2 + 2\ H^+ + 2\ e^- = 2\ H_2O \qquad \mathbf{\Delta_r G^0_{(aq)} = -342\ kJ/mol}$$

is then subtracted:

$$\text{HMPA} + H_2O_2 = \text{HM-PMPA} + H_2O \qquad \mathbf{\Delta_r G^0_{(aq)} = -268\ kJ/mol}$$

$$-\quad H_2O_2 + 2\ H^+ + 2\ e^- = 2\ H_2O \qquad \mathbf{\Delta_r G^0_{(aq)} = -342\ kJ/mol}$$

$$\text{HMPA} - 2\ H^+ - 2\ e^- = \text{HM-PMPA} - H_2O \qquad \mathbf{\Delta_r G^0_{(aq)} = +74\ kJ/mol}$$

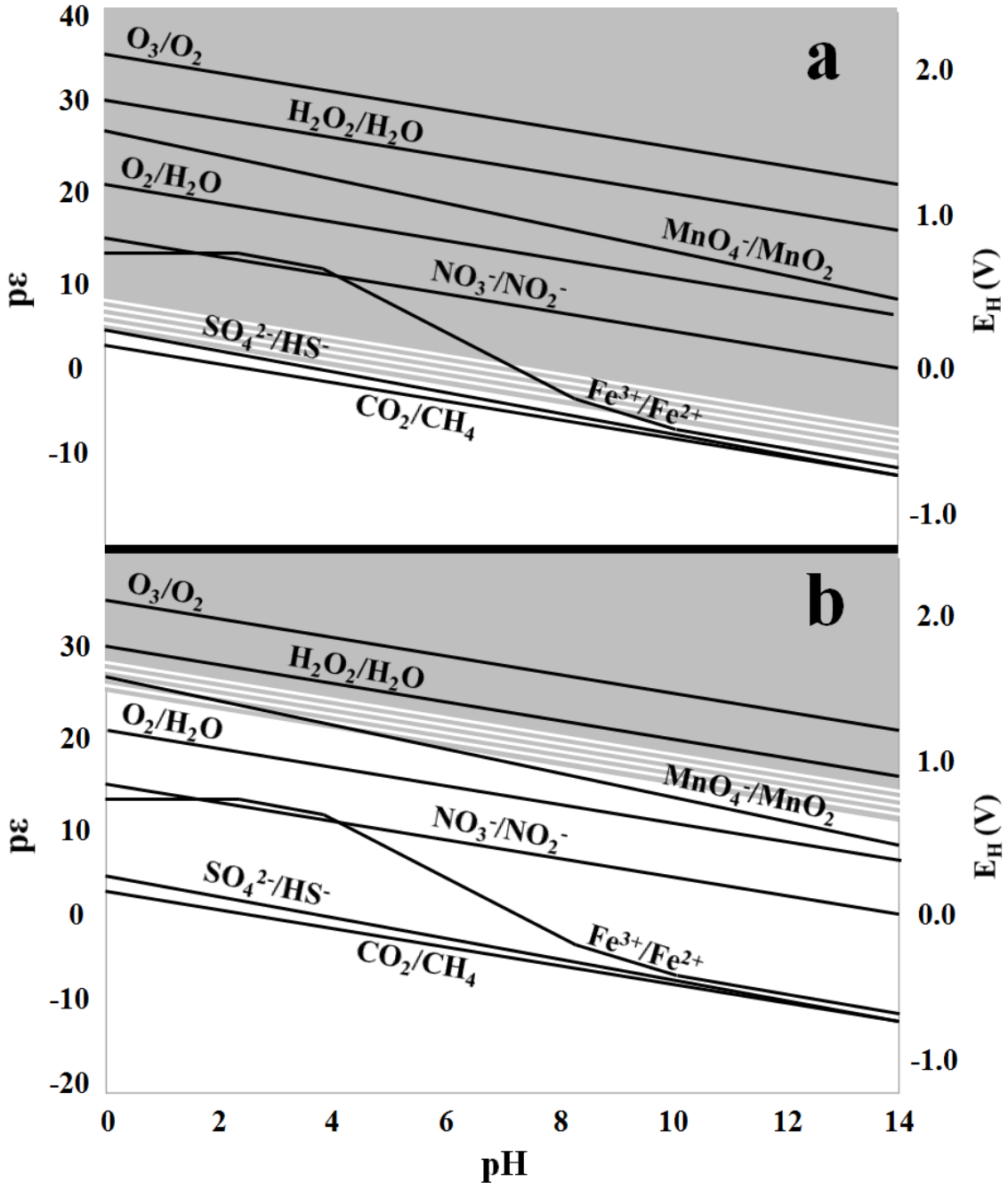

Figure 2.1: (a) Stability diagram for the HMPA / hydroxymethyl-PMPA redox couple. (b) Stability diagram for the HMPA / HMPA *N*-oxide redox couple. HMPA oxidation is unfavorable under conditions represented by white fields and favorable under conditions represented by gray fields. The gray-white hatched areas separating the stability fields reflect uncertainty associated with the estimated error range of the prediction (±0.1 V). All stability lines were adapted from (37) and represent standard conditions except [Fe] = 10^{-5} M and $[C]_{inorg} = 10^{-3}$ M for the iron redox couple.

Rearrangement and inversion yield:

$$HM\text{-}PMPA + 2\ H^+ + 2\ e^- = HMPA + H_2O \qquad \mathbf{\Delta_r G^0_{(aq)} = -74\ kJ/mol}$$

The equilibrium constant K is calculated from:

$$\log K = -\Delta_r G^0_{(aq)} / 2.3RT = 13.0$$

The stability line is the determined via:

$$\log K = \log(HMPA) - \log(HM\text{-}PMPA) + 2\ pH + 2\ p\varepsilon$$

At equilibrium, the activities of HMPA and HM-PMPA are equal and cancel out. Solving for the electron activity pε yields:

$$p\varepsilon = 1/2 \log K - pH = 6.5 - pH$$

For the HMPA / HMPA *N*-oxide redox couple, for which a Gibbs free energy of reaction for oxidation by H_2O_2 of -31 kJ/mol was predicted, the same strategy yields the following stability line:

$$p\varepsilon = 1/2 \log K - pH = 27.3 - pH$$

These two equations describe the centerlines of the gray-white hatched areas in Figure 2.1 that separate favorable and unfavorable conditions for HMPA oxidation.

The stability diagrams reveal that HMPA oxidation to HM-PMPA (Figure 2.1a) is favorable in the presence of strong oxidants typically used for *in situ* groundwater remediation. The process is also favorable under naturally occurring aerobic and nitrate-reducing conditions. Under iron-reducing conditions, oxidation to HM-PMPA is favorable only at neutral and lower pH values, depending on the total Fe and carbonate concentrations (here: 10^{-5} M and 10^{-3} M, respectively). Under sulfate-reducing and methanogenic conditions, this reaction is thermodynamically unfavorable. For the

oxidation to HMPA *N*-oxide (Figure 2.1b), only very strong oxidants, such as H_2O_2 and ozone, may lead to transformation.

Prediction of Potential Contaminant Degradation Pathways

Based on the results of the stability diagrams, the common remediation agent permanganate (MnO_4^-) was chosen as the model oxidant with which to further investigate potential HMPA degradation pathways and products. A hypothetical degradation pathway was created based on expert knowledge (Figure 2.2), and the thermodynamic favorability of possible oxidation reactions as well as redox-independent decomposition and hydrolysis reactions was calculated, as described in the Computational Details section. The determined aqueous free energies of reaction at neutral pH predict that HMPA can be oxidized at the methyl substituent to form HM-PMPA via hydride abstraction by MnO_4^-, in accordance with the reported mechanism of alkyl substituent oxidation by permanganate (*38*), where the oxygen in the hydroxymethyl substituent stems from the solvent water. Furthermore, the calculations indicate that hydrolysis of HMPA to tetramethylphosphoric diamide (compound 1 in Figure 2.2) and dimethylamine is thermodynamically favorable, whereas oxidation at the nitrogen atom to form HMPA *N*-oxide is unfavorable, in agreement with the predicted stability diagram (Figure 1b).

For the transformation of HM-PMPA, three reactions were calculated to be favorable, as indicated by negative free energies of reaction: oxidation to dihydroxy-methyl-TetMPA (compound 9 in Figure 2.2), oxidation to formyl-PMPA (compound 5 in Figure 2.2) via hydride abstraction from the deprotonated alkoxide (*39*), and decomposition to formaldehyde and PMPA (compound 7 in Figure 2.2). However, the combination of two HM-PMPA molecules to form the condensation product *N*,*N*'''-

methylenebis[pentamethylphosphoramide] (compound 10 in Figure 2.2), formaldehyde, and water, as previously observed during distillation of HM-PMPA (*40*), was calculated to be unfavorable under standard conditions in water at neutral pH.

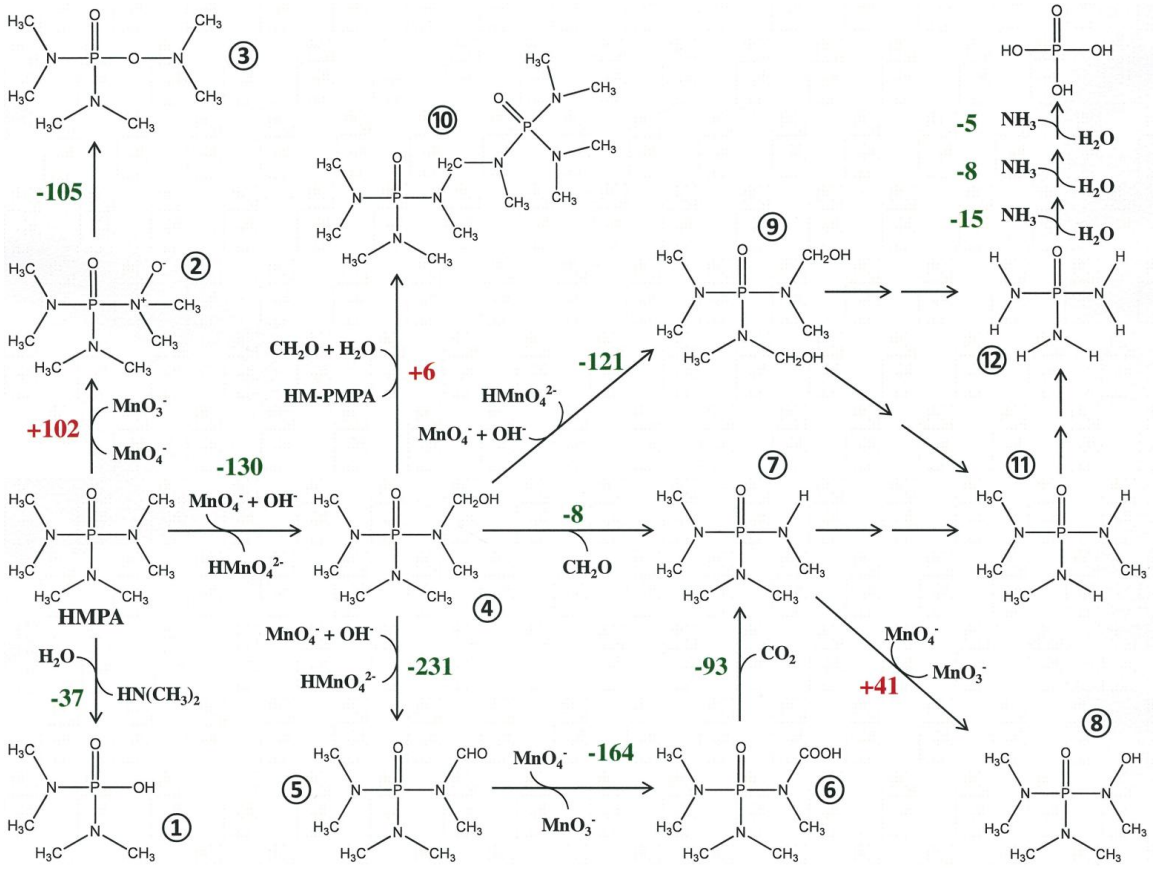

Figure 2.2: Potential degradation pathway for HMPA in permanganate-containing solution showing the predicted aqueous free energies of reaction (kJ/mol) at pH 7. Free energies are marked (-) green for favorable and (+) red for unfavorable transformations.

For formyl-PMPA, oxidation to carboxyl-PMPA (compound 6 in Figure 2.2) with subsequent decarboxylation to PMPA was calculated to be favorable. The oxidation mechanism for the formyl substituent leading to the formation of a carboxylic acid was assumed to proceed via oxygen transfer from MnO_4^- to yield MnO_3^- as previously shown

for the oxidation of various aldehydes using ^{18}O-labelled permanganate (*41, 42*). Oxidation of formyl-PMPA to formyl-hydroxymethyl-TetMPA was also calculated to be exergonic ($\Delta_r G'^0_{(aq)}$ = -130 kJ/mol; not shown in Figure 2.2 for simplicity).

Oxidation at the demethylated nitrogen atom is unfavorable for PMPA; rather, PMPA is oxidized to hydroxymethyl-TetMPA ($\Delta_r G'^0_{(aq)}$ = -128 kJ/mol; not shown in Figure 2.2), analogous to HMPA oxidation by permanganate.

Thus, the overall transformation of HMPA in permanganate-containing solution is predicted to proceed through oxidative *N*-demethylation via the formation of less methylated intermediates, such as PMPA, TetMPA (compound 11 in Figure 2.2), TriMPA and so forth, as well as singly-, doubly-, and possibly more highly-oxygenated phosphoramide-based compounds to eventually yield phosphoramide (compound 12 in Figure 2.2). Subsequently, phosphoramide may hydrolyze through three sequential deamination steps, leading to the formation of *o*-phosphate and ammonia. Phosphoramide hydrolysis has been reported to occur under all pH conditions (*43*).

Experimental Validation

Qualitative LC/MS-TOF analysis of samples from the HMPA oxidation experiment confirmed the predictions made based on the free energy calculations. None of the thermodynamically unfavorable transformation products were detected. Aside from the non-oxygenated intermediates such as PMPA, TetMPA, and TriMPA, a variety of oxygenated compounds were observed (Table 2.1). These included mono-, di-, and tri-hydroxymethyl and/or formyl PMPA, TetMPA and TriMPA, as well as minor amounts of carboxyl-PMPA over the course of 46 hours. The chromatographic peak areas revealed

that none of these intermediates were accumulating. Analysis for phosphoramide, at day 14 post-reaction start, revealed its presence.

Table 2.1: LC/MS-TOF data for HMPA and its major transformation products detected during the 46-hour permanganate oxidation experiment.

Compound (*Number in Figure 2*)	**Retention time (min)**	**Base peak**	**Base peak formula**	**Observed *m/z***	**Theoretical *m/z***	**Error (ppm)**
			ESI positive			
HMPA	11.3[a]	$[M+H]^+$	$C_6H_{19}N_3OP^+$	180.1294	180.1267	15.0
formyl-PMPA (*5*)	4.1[a]; 10.1[b]	$[M+H]^+$	$C_6H_{17}N_3O_2P^+$	194.1082	194.1060	11.3
HM-PMPA (*4*)	3.9[a]; 9.1[b]	$[M+H]^+$-H_2O	$C_6H_{17}N_3OP^+$	178.1131	178.1111	11.2
PMPA (*7*)	3.3[a]; 7.0[b]	$[M+H]^+$	$C_5H_{17}N_3OP^+$	166.1131	166.1111	12.0
diformyl-TetMPA	2.3[a]; 3.6[b]	$[M+H]^+$	$C_6H_{15}N_3O_3P^+$	208.0849	208.0852	-1.4
formyl-HM-TetMPA	2.0[a]; 3.3[b]	$[M+H]^+$-H_2O	$C_6H_{15}N_3O_2P^+$	192.0902	192.0903	-0.5
formyl-TetMPA	3.1[b]	$[M+H]^+$	$C_5H_{15}N_3O_2P^+$	180.0909	180.0903	3.3
diHM-TetMPA (*9*)	1.9[a]; 2.9[b]	$[M+H]^+$-H_2O	$C_6H_{17}N_3O_2P^+$	194.1086	194.1060	13.4
HM-TetMPA	2.6[b]	$[M+H]^+$-H_2O	$C_5H_{15}N_3OP^+$	164.0980	164.0954	15.8
TetMPA (*11*)	1.7[a]; 2.4[b]	$[M+H]^+$	$C_4H_{15}N_3OP^+$	152.0974	152.0954	13.1
formyl-diHM-TriMPA	1.5[b]	$[M+H]^+$-H_2O	$C_6H_{15}N_3O_3P^+$	208.0854	208.0852	1.0
formyl-HM-TriMPA	1.5[b]	$[M+H]^+$-H_2O	$C_5H_{13}N_3O_2P^+$	178.0750	178.0746	2.2
formyl-TriMPA	1.4[b]	$[M+H]^+$	$C_4H_{13}N_3O_2P^+$	166.0759	166.0746	7.8
TriMPA	1.3[b]	$[M+H]^+$	$C_3H_{13}N_3OP^+$	138.0794	138.0797	-2.2
			ESI negative			
carboxyl-PMPA (*6*)	4.1[a]	$[M-H]^-$-CO_2	$C_5H_{15}N_3OP^-$	164.0911	164.0954	-26.2

[a] mobile phase 0.01% HCOOH in water / ACN (98:2); [b] mobile phase 0.01% HCOOH in water

Quantitative analysis of HMPA, PMPA, TetMPA, and TriMPA, the four compounds where references were available, demonstrated that HMPA is rapidly oxidized by permanganate, becoming undetectable after 3 hours of reaction. The non-oxygenated intermediates PMPA, TetMPA, and TriMPA were all detected, however, at

molar concentrations less than 3% of the initial 0.25 mM HMPA concentration at all time points sampled. Thus, compounds oxygenated at one or more methyl substituents comprised the majority of the oxidation products during the initial 46 hours of HMPA degradation. Analysis of total nitrogen in the aqueous phase revealed that volatilization and sorption were negligible. Both the pH (7.0) and the ORP (0.63 V) remained constant throughout the experiment.

Formaldehyde was also detected (at concentrations below 10 μM), indicating that the decomposition of hydroxymethyl-containing intermediates (Figure 2.2) was indeed occurring.

In the control experiments without permanganate, HMPA concentrations remained constant, and neither phosphoramide-containing reaction intermediates nor formaldehyde were detected. This stability was further confirmed by the HMPA hydrolysis experiments, where no transformation was observed over the course of six months (see Experimental Section).

Prediction of Contaminant Persistence

To predict the persistence of HMPA in the absence of a strong oxidant, the rate of HMPA hydrolysis was estimated by computationally determining transition states and identifying the lowest energy TS, which likely corresponds to the kinetically most favorable pathway. Four potential mechanisms were considered, each of which had previously been proposed for hydrolysis of tetracoordinate phosphorus compounds: a stepwise dissociative mechanism (elimination-addition) with a tricoordinate intermediate, a stepwise associative mechanism (addition-elimination) with a pentacoordinate intermediate, and concerted backside and frontside mechanisms with a single

pentacoordinate transition state (*44*, *45*). At pH 7, the transition state with the lowest energy corresponded to the acid-catalyzed concerted backside nucleophilic attack at phosphorus (S_N2@P) mechanism, in agreement with previous experimental findings for phosphorus amides (*43*, *44*). A minimum of five explicit water molecules was required in the transition state optimizations before the activation energies stabilized. Based on the calculated free energy of activation of 97 kJ/mol at 22 °C under standard conditions (i.e., pH 0), a half-life of 12,300 years for HMPA hydrolysis at neutral pH is predicted.

Discussion

The redox conditions of an aquifer play a crucial role in the environmental fate of contaminants as the thermodynamic driving force behind their transformation into harmful or innocuous products (*17*). Thus, the prediction of redox reactivity is extremely valuable. For standard conditions, redox potentials have previously been predicted to within 0.3 V using quantum chemical methods (*20*, *22*, *23*). Here, a quantum chemical approach to estimate the pH-dependence of redox reactivity is described (Figure 2.1), based on calculations for the respective contaminant and known half reactions for electron acceptors and donors typically occurring in aqueous environments. This approach circumvents the consideration of explicit solvation effects, allowing for substantially faster computations compared to other approaches (see the Introduction) (*20*, *22*). The accuracy of the calculated B3LYP reaction energies is estimated to be within 10 - 20 kJ/mol (*46*), corresponding to a redox potential of approximately 0.05 - 0.1 V for a half-reaction involving two electrons. Each stability line is only valid for the respective redox couple and is independent of the reaction mechanism. To determine the

pε/pH conditions necessary for complete mineralization, one diagram for every redox couple within the degradation pathway, or at least for the redox reaction with the highest free energy, must be generated. In the case of HMPA, this is the initial oxidation of the methyl substituent, as the oxidation reactions of the alcoholic and aldehydic substituents have lower free energies of reaction and thus may proceed at lower redox potentials. Moreover, the diagrams in Figure 1 were calculated for standard conditions (i.e., 1 M concentrations for all species at 25 ºC), which are not representative of typical conditions in aqueous environments. However, the true concentrations of both contaminants and electron acceptors or donors at a particular field site can be taken into account by simply adding the well-known term *RT ln Q* to the standard free energies. A specific temperature can also easily be incorporated in the quantum chemical calculations. This is important for the assessment of redox reactivity, especially when two stability lines are closely spaced.

The prediction of potential degradation pathways initially requires expert knowledge. All possible transformations must be identified so that favorable reaction products are not overlooked. Subsequently, the calculation of aqueous free energies of reaction at, for example, groundwater-typical pH values, can be used to exclude thermodynamically unfavorable reactions, such as HMPA oxidation at the nitrogen atom by permanganate. Again, care must be taken since standard conditions do not accurately characterize contaminated field sites, where the parent compound is initially the predominant species. For reactions with slightly positive free energies, the concentrations of all species participating in the reaction need to be considered via addition of *RT ln Q*. For instance, the formation of *N*,*N*'''-methylenebis[pentamethylphosphoramide] from

HM-PMPA ($\Delta_r G'^0_{(aq)}$ = +6 kJ/mol) can become favorable when HM-PMPA is present in excess. In addition, the estimated error of 10 - 20 kJ/mol for the B3LYP reaction energies prevents reliable exclusion of this reaction. In this specific case, however, the condensation product *N*,*N*"'-methylenebis[pentamethylphosphoramide] was not detected in our system, as expected, due to the different experimental conditions (*40*).

The predictions of both redox reactivity (Figure 2.1) and potential degradation pathways (Figure 2.2) are based solely on thermodynamic calculations. Kinetic constraints, however, are not considered; therefore, reactions calculated to be thermodynamically favorable may still not proceed on a practical time scale due to high activation barriers. For example, although hydrolysis of HMPA is thermodynamically favorable ($\Delta_r G'^0_{(aq)}$ = -37 kJ/mol), the calculated half-life of 12,300 years indicates persistence in water at neutral pH in the absence of a suitable oxidant. Acidic or basic conditions, however, would alter the degradation kinetics.

It is noted that activation barriers calculated via the popular B3LYP functional are typically underestimated (*47*). Other DFT methods, such as MPWB1K (*47*) or BB1K (*48*), may yield more accurate predictions for thermochemical kinetics. A potential underestimation of activation barriers corresponds to an underestimation of reaction half-lives, and would thus imply that a contaminant is even more persistent than predicted.

When calculating free energies of activation in aqueous phase, consideration of all possible reaction mechanisms (or, alternatively, thorough scans of the potential energy surface), as well as inclusion of explicit water molecules, are of paramount importance. If the lowest-energy transition state is not correctly identified, reaction half-lives will be overestimated. Unlike activation energies, free energies of reaction can be accurately

computed using less costly implicit solvation models (*33*). These account for long-range bulk solvent-solute interactions such as electrostatic effects, but not for short-range effects such as hydrogen bonding (*31, 32, 49*), which may be important in TS calculations.

Conclusion

The degradation of HMPA requires the presence of suitable oxidants, as hydrolysis is hindered by a high activation barrier at neutral pH. HMPA is rapidly oxidized to phosphoramide by the common remediation agent permanganate via sequential *N*-demethylation. Subsequently, phosphoramide hydrolyzes to ammonia and *o*-phosphate (*43*). Using LC/MS-TOF, it was demonstrated for the first time that HMPA oxidation by permanganate does proceed through the formation of hydroxymethylated compounds. Furthermore, a carboxylated intermediate was detected, which had not been observed previously by Terry and Bořkovec (*30*). The application of stronger oxidants such as ozone may, however, favor a different degradation pathway, such as oxidation at the nitrogen atom, producing HMPA *N*-oxide and its rearrangement product ((bis(dimethylamino)phosphinyl)-oxy)dimethylamine (compound 3 in Figure 2) (*50*). In conclusion, based on the quantum chemical predictions, HMPA-contaminated water can be successfully remediated through the application of permanganate without accumulation of persistent reaction intermediates.

The quantum chemical methodology presented here can be used by scientists and engineers to predict the fate of both organic and inorganic contaminants as a function of redox potential and pH in aqueous phases such as groundwater. This novel method

overcomes many limitations of standard QSAR approaches. The quantum chemical determination of stability lines can serve as a powerful screening tool to assess whether the natural conditions at a specific field site favor contaminant transformation. This determination can also identify the type of redox-active remediation agents that can be used to enhance or enable degradation. The calculation of aqueous free energies of reaction allows for the identification of potential degradation products, and the exclusion of unfavorable transformation pathways. Finally, kinetics and therefore the persistence of a contaminant and its degradation products can also be estimated, along with primary degradation pathways, based on calculated activation energies. The prediction of primary degradation pathways is part of our ongoing studies.

References

1. Cronin, M. T. D.; Walker, J. D.; Jaworska, J. S.; Comber, M. H. I.; Watts, C. D.; Worth, A. P., Use of QSARs in international decision-making frameworks to predict ecologic effects and environmental fate of chemical substances. *Environmental Health Perspectives* **2003,** 111, (10), 1376-1390.

2. Bennett, E. R.; Clausen, J.; Linkov, E.; Linkov, I., Predicting physical properties of emerging compounds with limited physical and chemical data: QSAR model uncertainty and applicability to military munitions. *Chemosphere* **2009,** 77, (10), 1412-1418.

3. Boethling, R. S.; Mackay, D., *Handbook of Property Estimation Methods for Chemicals: Environmental and Health Sciences*. CRC Press: Boca Raton, FL, 2000; p 481.

4. Dolfing, J.; Harrison, B. K., Gibbs free-energy of formation of halogenated aromatic compounds and their potential role as electron acceptors in anaerobic environments. *Environmental Science & Technology* **1992,** 26, (11), 2213-2218.

5. Holmes, D. A.; Harrison, B. K.; Dolfing, J., Estimation of Gibbs free energies of formation for polychlorinated biphenyls. *Environmental Science & Technology* **1993,** 27, (4), 725-731.

6. Beurskens, J. E. M.; Dekker, C. G. C.; Vandenheuvel, H.; Swart, M.; Dewolf, J., Dechlorination of chlorinated benzenes by an anaerobic microbial consortium that selectively mediates the thermodynamic most favorable reactions. *Environmental Science & Technology* **1994,** 28, (4), 701-706.

7. Huang, C. L.; Harrison, B. K.; Madura, J.; Dolfing, J., Gibbs free energies of formation of PCDDs: Evaluation of estimation methods and application for predicting dehalogenation pathways. *Environmental Toxicology and Chemistry* **1996,** 15, (6), 824-836.

8. Woods, S. L.; Trobaugh, D. J.; Carter, K. J., Polychlorinated biphenyl reductive dechlorination by vitamin B-12s: Thermodynamics and regiospecificity. *Environmental Science & Technology* **1999,** 33, (6), 857-863.

9. Siegbahn, P. E. M., The performance of hybrid DFT for mechanisms involving transition metal complexes in enzymes. *Journal of Biological Inorganic Chemistry* **2006,** 11, (6), 695-701.

10. Lei, W. F.; Zhang, R. Y.; McGivern, W. S.; Derecskei-Kovacs, A.; North, S. W., Theoretical study of OH-O_2-isoprene peroxy radicals. *Journal of Physical Chemistry A* **2001,** 105, (2), 471-477.

11. Zhang, Q. Z.; Li, S. Q.; Qu, X. H.; Shi, X. Y.; Wang, W. X., A quantum mechanical study on the formation of PCDD/Fs from 2-chlorophenol as precursor. *Environmental Science & Technology* **2008,** 42, (19), 7301-7308.

12. Fueno, H.; Tanaka, K.; Sugawa, S., Theoretical study of the dechlorination reaction pathways of octachlorodibenzo-p-dioxin. *Chemosphere* **2002,** 48, (8), 771-778.

13. Kilic, M.; Kocturk, G.; San, N.; Cinar, Z., A model for prediction of product distributions for the reactions of phenol derivatives with hydroxyl radicals. *Chemosphere* **2007,** 69, (9), 1396-1408.

14. Nonnenberg, C.; van der Donk, W. A.; Zipse, H., Reductive dechlorination of trichloroethylene: A computational study. *Journal of Physical Chemistry A* **2002,** 106, (37), 8708-8715.

15. Ozen, A. S.; Aviyente, V.; Klein, R. A., Modeling the oxidative degradation of azo dyes: A density functional theory study. *Journal of Physical Chemistry A* **2003,** 107, (24), 4898-4907.

16. Zhang, Q. Z.; Qu, X. H.; Wang, W. X., Mechanism of OH-initiated atmospheric photooxidation of dichlorvos: A quantum mechanical study. *Environmental Science & Technology* **2007,** 41, (17), 6109-6116.

17. Borch, T.; Kretzschmar, R.; Kappler, A.; Van Cappellen, P.; Ginder-Vogel, M.; Voegelin, A.; Campbell, K., Biogeochemical redox processes and their impact on

contaminant dynamics. *Environmental Science & Technology* **2010,** 44, (1), 15-23.

18. Christensen, T. H.; Bjerg, P. L.; Banwart, S. A.; Jakobsen, R.; Heron, G.; Albrechtsen, H. J., Characterization of redox conditions in groundwater contaminant plumes. *Journal of Contaminant Hydrology* **2000,** 45, (3-4), 165-241.

19. Meeussen, J. C. L., ORCHESTRA: An object-oriented framework for implementing chemical equilibrium models. *Environmental Science & Technology* **2003,** 37, (6), 1175-1182.

20. Roy, L. E.; Jakubikova, E.; Guthrie, M. G.; Batista, E. R., Calculation of one-electron redox potentials revisited. Is it possible to calculate accurate potentials with density functional methods? *Journal of Physical Chemistry A* **2009,** 113, (24), 6745-6750.

21. Li, J.; Fisher, C. L.; Chen, J. L.; Bashford, D.; Noodleman, L., Calculation of redox potentials and pK(a) values of hydrated transition metal cations by a combined density functional and continuum dielectric theory. *Inorganic Chemistry* **1996,** 35, (16), 4694-4702.

22. Uudsemaa, M.; Tamm, T., Density-functional theory calculations of aqueous redox potentials of fourth-period transition metals. *Journal of Physical Chemistry A* **2003,** 107, (46), 9997-10003.

23. Namazian, M.; Almodarresieh, H. A.; Noorbala, M. R.; Zare, H. R., DFT calculation of electrode potentials for substituted quinones in aqueous solution. *Chemical Physics Letters* **2004,** 396, (4-6), 424-428.

24. Namazian, M.; Norouzi, P.; Ranjbar, R., Prediction of electrode potentials of some quinone derivatives in acetonitrile. *Journal of Molecular Structure-Theochem* **2003,** 625, 235-241.

25. Ess, D. H.; Houk, K. N., Activation energies of pericyclic reactions: Performance of DFT, MP2, and CBS-QB3 methods for the prediction of activation barriers and reaction energetics of 1,3-dipolar cycloadditions, and revised activation enthalpies for a standard set of hydrocarbon pericyclic reactions. *Journal of Physical Chemistry A* **2005,** 109, (42), 9542-9553.

26. Lloyd, J. W., Hexamethylphosphoric triamide (HMPA). *American Industrial Hygiene Association Journal* **1975,** 36, (12), 917-919.

27. Campos, D., Field demonstration of UV/H_2O_2 on the treatment of groundwater contaminated with HMPA. In *Chemical Oxidation: Technologies for the Nineties.*, Eckenfelder, W. W.; Bowers, A. R.; Roth, J. A., Eds. Technomic Publishing Company: Lancaster, PA, 1997; Vol. 6, pp 19-26.

28. Zijlstra, J. A.; Brussee, J.; Vandergen, A.; Vogel, E. W., Importance of multiple hydroxylated metabolites in hexamethylphosphoramide (HMPA)-mediated mutagenesis in *Drosophila melanogaster*. *Mutation Research* **1989,** 212, (2), 193-211.

29. Jones, A. R.; Jackson, H., Metabolism of hexamethylphosphoramide and related compounds. *Biochemical Pharmacology* **1968,** 17, (11), 2247-2252.

30. Terry, P. H.; Borkovec, A. B., Insect chemosterilants. 4. Oxidation of hexamethylphosphoric triamide and synthesis of *N*-formylphosphoramides. *Journal of Medicinal Chemistry* **1968,** 11, (5), 958-961.

31. Cances, E.; Mennucci, B.; Tomasi, J., A new integral equation formalism for the polarizable continuum model: Theoretical background and applications to isotropic and anisotropic dielectrics. *Journal of Chemical Physics* **1997,** 107, (8), 3032-3041.

32. Barone, V.; Cossi, M.; Tomasi, J., A new definition of cavities for the computation of solvation free energies by the polarizable continuum model. *Journal of Chemical Physics* **1997,** 107, (8), 3210-3221.

33. Stare, J.; Henson, N. J.; Eckert, J., Mechanistic aspects of propene epoxidation by hydrogen peroxide. Catalytic role of water molecules, external electric field, and zeolite framework of TS-1. *Journal of Chemical Information and Modeling* **2009,** 49, (4), 833-846.

34. Nguyen, M. T.; Raspoet, G., The hydration mechanism of ketone: 15 years later. *Canadian Journal of Chemistry-Revue Canadienne De Chimie* **1999,** 77, (5-6), 817-829.

35. Raman, S.; Ashcraft, R. W.; Vial, M.; Klasky, M. L., Oxidation of hydroxylamine by nitrous and nitric acids. Model development from first principle SCRF calculations. *Journal of Physical Chemistry A* **2005,** 109, (38), 8526-8536.

36. Dalene, M.; Persson, P.; Skarping, G., Determination of formaldehyde in air by chemisorption on glass filters impregnated with 2,4-dinitrophenylhydrazine using gas chromatography with thermionic specific detection. *Journal of Chromatography* **1992,** 626, (2), 284-288.

37. Stumm, W.; Morgan, J. J., *Aquatic Chemistry: Chemical Equilibria and Rates in Natural Waters*. 2nd ed.; John Wiley & Sons, Inc.: New York, NY, 1996; p 1022.

38. Gardner, K. A.; Mayer, J. M., Understanding C-H bond oxidations: $H^{\bullet}$ and H^{-} transfer in the oxidation of toluene by permanganate. *Science* **1995,** 269, (5232), 1849-1851.

39. Fatiadi, A. J., The classical permanganate ion - Still a novel oxidant in organic chemistry. *Synthesis-Stuttgart* **1987**, (2), 85-127.

40. Terry, P. H.; Borkovec, A. B., Insect chemosterilants. IX. *N*-(hydroxymethyl)-*N*,*N'*,*N'*,*N''*,*N''*-pentamethylphosphoric triamide. *Journal of Medicinal Chemistry* **1970,** 13, (4), 782-783.

41. Jaky, M.; Szammer, J., Oxidation of aldehydes with permanganate in acidic and alkaline media. *Journal of Physical Organic Chemistry* **1997,** 10, (6), 420-426.

42. Wiberg, K. B.; Stewart, R., The mechanisms of permanganate oxidation. I. The oxidation of some aromatic aldehydes. *Journal of the American Chemical Society* **1955,** 77, (7), 1786-1795.

43. Richter, S.; Topelmann, W.; Lehmann, H. A., Hydrolysis of phosphoric acid amides. *Zeitschrift Fur Anorganische Und Allgemeine Chemie* **1976,** 424, (2), 133-143.

44. Rahil, J.; Haake, P., Reactivity and mechanism of hydrolysis of phosphonamides. *Journal of the American Chemical Society* **1981,** 103, (7), 1723-1734.

45. van Bochove, M. A.; Swart, M.; Bickelhaupt, F. M., Nucleophilic substitution at phosphorus centers (S_N2@P). *Chemphyschem* **2007,** 8, (17), 2452-2463.

46. Noodleman, L.; Lovell, T.; Han, W. G.; Li, J.; Himo, F., Quantum chemical studies of intermediates and reaction pathways in selected enzymes and catalytic synthetic systems. *Chemical Reviews* **2004,** 104, (2), 459-508.

47. Zhao, Y.; Truhlar, D. G., Hybrid meta density functional theory methods for thermochemistry, thermochemical kinetics, and noncovalent interactions: The MPW1B95 and MPWB1K models and comparative assessments for hydrogen bonding and van der Waals interactions. *Journal of Physical Chemistry A* **2004,** 108, (33), 6908-6918.

48. Zhao, Y.; Lynch, B. J.; Truhlar, D. G., Development and assessment of a new hybrid density functional model for thermochemical kinetics. *Journal of Physical Chemistry A* **2004,** 108, (14), 2715-2719.

49. Tomasi, J.; Mennucci, B.; Cammi, R., Quantum mechanical continuum solvation models. *Chemical Reviews* **2005,** 105, (8), 2999-3093.

50. Holden, I.; Segall, Y.; Kimmel, E. C.; Casida, J. E., Peracid-mediated *N*-oxidation and rearrangement of dimethylphosphoramides - Plausible model for oxidative bioactivation of the carcinogen hexamethylphosphoramide (HMPA). *Tetrahedron Letters* **1982,** 23, (49), 5107-5110.

CHAPTER 3

PREDICTION OF CONTAMINANT PERSISTENCE IN AQUEOUS PHASE: A QUANTUM CHEMICAL APPROACH

Introduction

Through inadvertent releases of chemicals, surface waters and groundwaters have become contaminated with a wide range of organic compounds, such as chlorinated solvents (*1*), complex mixtures of hydrocarbons (*2*), nitroaromatic compounds (*3*), pesticides, personal care products, pharmaceuticals, steroid hormones (*4*), and numerous other, often termed "new and emerging" contaminants (*5*). Due to financial, technological, or other site-specific limitations, these contaminations cannot always be actively remediated, leaving natural attenuation (NA) as the only process that may lead to contaminant removal. Unfortunately, many of these compounds and their degradation products are poorly characterized with respect to their environmental fate, or exhibit substantially different reactivity under different field conditions. Thus, to verify that monitored natural attenuation (MNA) is a viable (passive) remediation strategy at a specific site, contaminant mass loss, electron acceptor or donor consumption, and formation of degradation products must be assessed (*2*). Depending on physicochemical and other properties that influence contaminant persistence as well as site-specific

biogeochemical conditions (*6*), however, NA processes may require long periods (years or decades) to achieve consequential contaminant losses.

An alternative to time-consuming experimental studies of the ever-increasing number of environmental contaminants, computational tools have been developed that can help assess their degradability and/or persistence. Currently, applied models for fate prediction are predominantly based on quantitative structure-activity relationships (QSARs) (*7*). However, QSAR-based predictions often fail when sufficient experimental data from structurally similar compounds are unavailable. Here, a strategy is applied to estimate contaminant persistence based on quantum chemical calculations of transformation kinetics, which can be used for any type of contaminant or reaction of interest, even for those lacking data on physicochemical properties or degradability. The underlying rationale for this strategy is the concept that the Gibbs free energy of activation, which can be determined from the difference in Gibbs free energy between transition state(s) and reactant(s), governs reaction rates according to transition state theory: the higher the free energy of activation, the lower the reaction rate (constant), and the longer the reaction half-life. Thus, once the major reaction pathway(s) have been determined and the reaction rate constant(s) (or half-lives) calculated, the persistence of a contaminant can be assessed.

As test case for the prediction of contaminant persistence, hexamethyl-phosphoramide (HMPA, Figure 3.1), an extensively used solvent and groundwater contaminant (*8*), is investigated here. Previous experimental studies have shown that HMPA-contaminated groundwater can be remediated through the application of permanganate, Fenton's reagent, or a combined UV/H_2O_2 process (see Chapter 2 and ref

(*8*)). However, quantum chemical calculations indicated that HMPA oxidation is thermodynamically unfavorable below -30 mV at neutral pH. In the absence of suitable oxidants, hydrolysis of the P-N bond was predicted to be the only favorable reaction that may lead to its degradation ($\Delta_r G'^{0}_{(aq)}$ = -37 kJ/mol) (see Chapter 2). In the same study, however, no hydrolysis of HMPA was experimentally observed over the course of six months at pH 7.

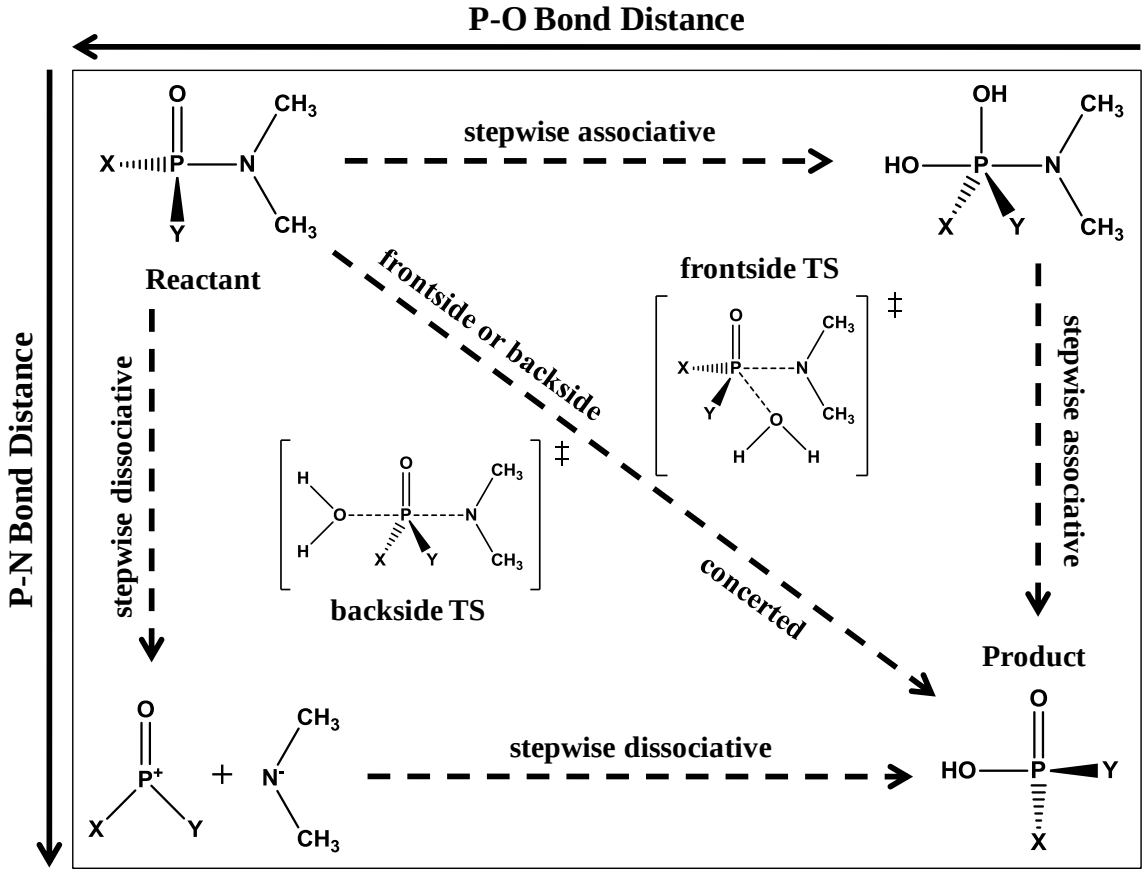

Figure 3.1: Conceptual potential energy surface and potential mechanisms of P-N bond hydrolysis, indicating changes in P-O and P-N bond distances during reaction. X and Y are arbitrary substituents (for HMPA, X = Y = $N(CH_3)_2$); chirality of the product is dependent on actual mechanism. TS = transition state.

Transformation of a reactant to its product(s) may occur via more than just one transition state, i.e., a single product may arise via different reaction mechanisms. Consequently, all plausible reaction mechanisms should be investigated to maximize prediction accuracy. Mechanisms can be determined based on potential energy surface scans, expert knowledge, and/or literature studies. The reaction path(s) with the lowest free energy of activation govern(s) the total reaction rate. For P-N bond hydrolysis in tetracoordinate phosphorus compounds like HMPA, four general mechanisms have previously been reported to be theoretically possible (Figure 3.1) (*9*): (1) a stepwise associative mechanism (addition-elimination, $S_N2I@P$) with a pentacoordinate intermediate, (2) a stepwise dissociative mechanism (elimination-addition, $S_N1@P$) with a tricoordinate intermediate, (3) a concerted frontside mechanism ($S_N2@P$-f), and (4) a concerted backside mechanism ($S_N2@P$-b), with the latter two having a pentacoordinate transition state. In addition, the reaction can be catalyzed by protons at low pH (e.g., A2@P mechanism) and by hydroxide ions at high pH.

Acid-catalyzed hydrolysis of phosphoric triamide (three P-N bonds), as well as many other tetracoordinate phosphorus amides, such as phosphorodiamidates (one P-O and two P-N bonds), phosphonamides (one P-C and two P-N bonds), and phosphinamides (one P-N and two P-C bonds), was suggested to proceed via an A2@P mechanism, i.e., initial protonation of the nitrogen with a subsequent concerted $S_N2@P$ reaction (Scheme 3.1) (*9*-*13*):

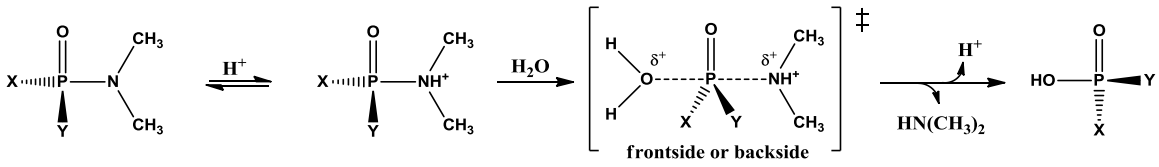

Scheme 3.1

The activation of the P-N bond through protonation greatly increases hydrolysis rates as it makes the nitrogen-containing substituent a better leaving group, which is reflected by a first order dependence of the rate constant on proton activity (*14*). Whereas acid-catalyzed hydrolysis can be the predominant mechanism for tetracoordinate phosphorus amides at near-neutral pH, the base-catalyzed mechanism was shown to contribute to the total rate of hydrolysis in phosphoramide only at pH values greater than 9 (*13*), and was thus not investigated here. The mechanism for uncatalyzed P-N bond hydrolysis in phosphoramide compounds like HMPA, however, has not yet been elucidated due to the slow reaction rates at neutral pH (*12*), which impede experimental investigations.

In this Chapter, the mechanisms of P-N bond hydrolysis in HMPA are investigated, Gibbs free energies of activation are calculated, and reaction rate constants and half-lives are estimated as a function of pH, using density functional theory (DFT) and a cluster-continuum solvation model (*15*). The objective of this study is to assess the persistence of aqueous HMPA in the absence of suitable oxidants over the groundwater-typical pH range of 6.0 to 8.5.

Computational Details

Quantum chemical calculations were conducted to investigate the mechanisms and kinetics of HMPA hydrolysis. All calculations were performed via Gaussian 03 using the B3LYP functional without symmetry constraints and default settings unless noted otherwise. Potential energy minima for reactants and intermediates were verified by frequency calculations (i.e., no imaginary frequencies). First-order saddle points

(transition states) were verified by both frequency (i.e., exactly one imaginary frequency) and intrinsic reaction coordinate (IRC) calculations.

To account for solvation effects on reaction mechanisms and rates, a cluster-continuum solvation model (*16*) was applied. In the cluster-continuum approach, a (limited) number of explicit solvent molecules are placed around the reactant(s) and studied using an implicit continuum solvation model. Initially, the ideal number of explicit solvent molecules (*16*) was determined for each of the potential hydrolysis mechanisms. For this task, reactant, intermediate (INT) and transition state (TS) structures were optimized in the gas phase. Explicit water molecules were then sequentially added until the determined free energies stabilized. For the $S_N2I@P$, $S_N1@P$, and $S_N2@P$-f mechanisms, the 6-31+G(d) basis set was used on all elements. For the $S_N2@P$-b and A2@P mechanisms, however, the transition states could only be located when a second d-orbital was used for phosphorus. These transition states were initially optimized using the 6-31G(d) basis set on C, H, N, and O as well as the 6-31G(2d) basis set on P.

After determination of the ideal number of explicit water molecules, all respective lowest-energy ground and transition states including explicit solvation were optimized at the B3LYP/6-31+G(d) level of theory (6-31+G(2d) on P) with the integral equation formalism polarizable continuum model (IEFPCM) (*17*). Subsequently, single-point energy calculations were performed on the optimized geometries at the B3LYP/6-311++G(3df,3pd) level of theory in combination with IEFPCM.

Due to convergence problems (*18, 19*) that occurred during one of the IEFPCM model calculations using Gaussian 03, the newer Gaussian 09 was used to optimize the

ground state structure of the S_N2@P-b mechanism, which included six explicit water molecules. For this calculation, the default Gaussian 09 IEFPCM settings were replaced by Gaussian 03 default IEFPCM settings. A subsequent frequency analysis of the optimized structure in Gaussian 03 showed no imaginary frequencies.

The Gibbs free energies of reaction, $\Delta_r G_{(aq)}$, and the Gibbs free energies of activation, $\Delta^{\ddagger} G_{(aq)}$, in aqueous phase at 22 °C (same temperature as our experimental system) were calculated from the total free energies in solution and the thermal corrections to Gibbs free energy from a frequency analysis at 295.15 K. Pseudo-first-order rate constants (k_i, with i = 1, 2) were calculated via transition state theory:

$$k_i = \kappa \left(\frac{k_B T}{h}\right) exp\left(\frac{-\Delta^{\ddagger} G_{(aq)}}{RT}\right)$$

where κ is the transmission coefficient (see Chapter 2), k_B is the Boltzmann constant, T is the temperature, h is Planck's constant, and R is the universal gas constant. For uncatalyzed hydrolysis, the predicted rate constant k_1 is with respect to the activity of HMPA (i.e., $r = k_1 \{HMPA\}$, where r is the hydrolysis rate), and for acid-catalyzed hydrolysis, the predicted rate constant k_2 is with respect to the activity of the protonated species HMPA-H^+ (i.e., $r = k_2 \{HMPA\text{-}H^+\}$).

A total pseudo-first-order rate constant k_{hyd} for HMPA hydrolysis, where r_{tot} is the total reaction rate and the total HMPA activity $\{HMPA_{tot}\} = \{HMPA\} + \{HMPA\text{-}H^+\}$, is defined in the rate equation:

$$r_{tot} = k_{hyd} \{HMPA_{tot}) = k_1 \{HMPA\} + k_2 \{HMPA\text{-}H^+\}$$

The activity of the protonated species depends on its acidity constant K_a and the proton activity:

$$\{HMPA - H^+\} = \frac{\{HMPA\}\{H^+\}}{K_a}$$

Substitution and rearrangement then yield the equation that was used to calculate k_{hyd} from the quantum chemically predicted k_1 and k_2:

$$k_{hyd} = \left[\frac{k_1 K_a + k_2\{H^+\}}{K_a + \{H^+\}}\right]$$

Pseudo-first-order reaction half-lives $t_{1/2}$ were calculated via:

$$t_{1/2} = \frac{ln2}{k_{hyd}}$$

Experimental Section

To experimentally determine k_{hyd}, the hydrolysis of HMPA over time was measured. Triplicates of DI water (100 mL) were adjusted to pH 0 with HCl (37 %) in 250-mL Pyrex media glass bottles sealed with PTFE-faced silicone septa. The pH was measured with a UP-25 pH/mV/Ion Meter (Denver Instruments). Hexamethylphosphoramide (40 µL, 99% purity, MP Biomedicals) was added and the reaction bottles were stored in the dark without agitation at 22 ºC. Samples for analysis (15µL) were diluted 1:100 with a NaOH solution of pH 12, resulting in a pH of 7, at which HMPA hydrolysis was shown to be negligible over a period of at least six months (see Chapter 2). The samples were analyzed with an Agilent 1100 Series liquid chromatograph equipped with a 150 mm × 2.1 mm XTerra Phenyl column, 3.5 µm particle size (Waters), in combination with an Agilent G3250AA MSD TOF system (LC/MS-TOF). Separation was carried out isocratically with 0.01% formic acid / acetonitrile (98:2) as described in Chapter 2.

Results

To predict the reaction rates and half-lives for HMPA hydrolysis over the groundwater-typical pH range of 6.0 to 8.5, the potential reaction mechanisms outlined in the Introduction were investigated computationally.

Associative Stepwise Mechanism

In the first transition state (TS1, $\Delta^{\ddagger}G_{(aq)}$ = 189 kJ/mol, Figure 3.2) of the $S_N2I@P$ mechanism (Figure 3.1), the attacking nucleophile H_2O transfers a proton to the oxygen that is double-bonded to the central phosphorus atom, while the remaining hydroxyl group forms a new covalent bond with phosphorus. For the formed pentacoordinate intermediate (INT, $\Delta_rG_{(aq)}$ = 182 kJ/mol, Figure 3.2), a pseudorotation mechanism, as reported previously for some lower molecular weight phosphorus compounds (*20*), could not be found, possibly due to steric hindrance imposed by the bulky dimethylamine substituents. Rather, direct proton transfer proceeds through a second TS (TS2, $\Delta^{\ddagger}G_{(aq)}$ = 212 kJ/mol, Figure 3.2), forming tetramethylphosphoric diamide as the product.

Dissociative Stepwise Mechanism

The heterolytic dissociation of the P-N bond (to form the ionic intermediate; Figure 3.1) is predicted to have a $\Delta_rG_{(aq)}$ of +215 kJ/mol in aqueous phase. Considering that the free energy of the transition state connecting the reactant with the intermediate must be even higher than that of the intermediate, implying that the free energy of activation is >215 kJ/mol and thus significantly greater than that of all the other mechanisms considered (cf. Figure 3.2), the $S_N1@P$ mechanism was ruled out without further determination of the transition states.

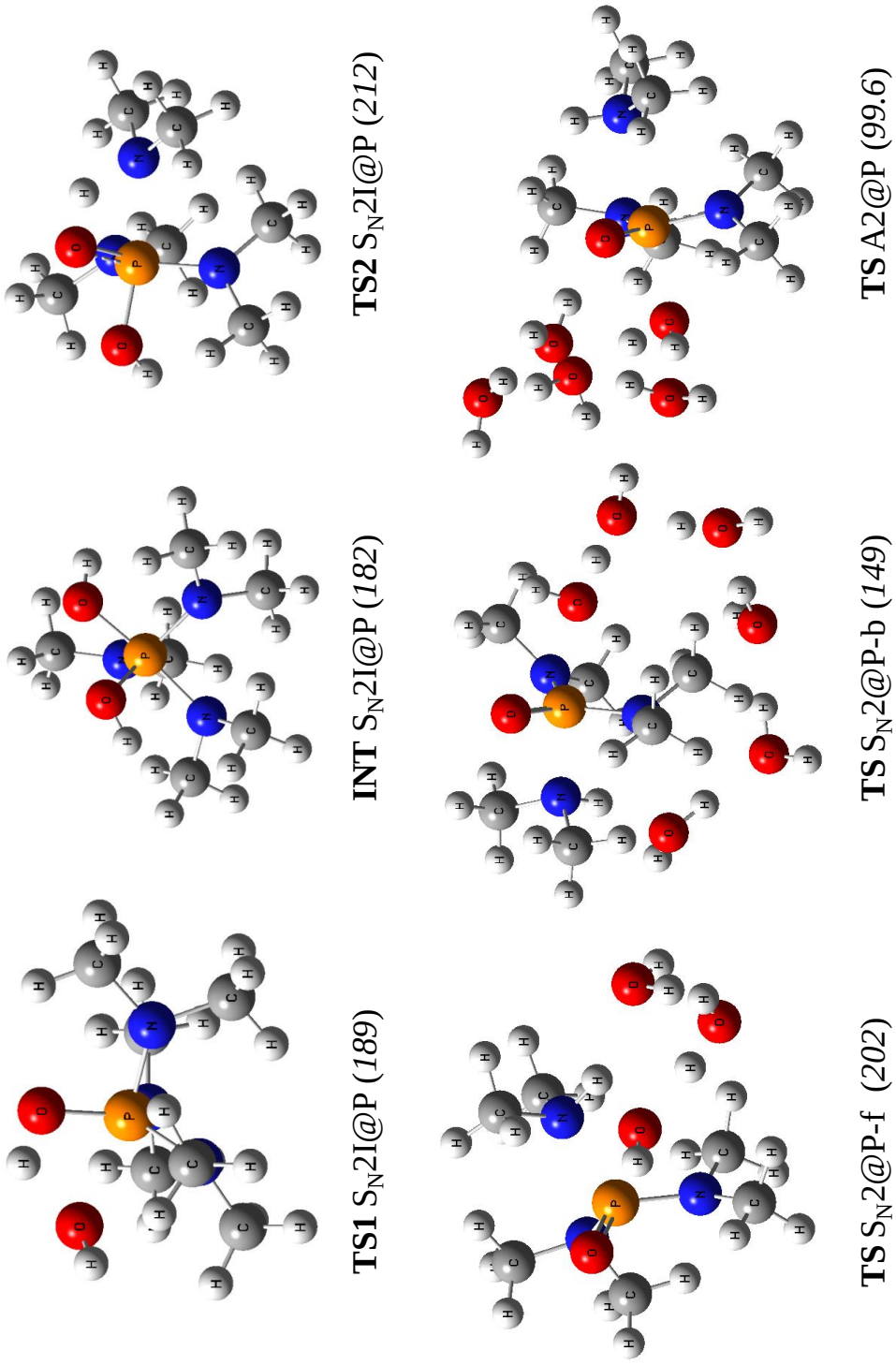

Figure 3.2: Optimized geometries of stationary points for HMPA hydrolysis in aqueous phase. Values in parentheses are Gibbs free energies of activation (for transition states) and reaction (for the intermediate) in aqueous phase at 22 °C (kJ/mol).

Concerted Frontside Mechanism

In the S_N2@P-f transition state ($\Delta^{\ddagger}G_{(aq)}$ = 202 kJ/mol, Figure 3.2), the attacking water molecule transfers a proton to the nitrogen atom within the leaving dimethylamine. The P-N bond lengthens from 1.70 Å in the ground state to 1.93 Å in the transition state, while the resulting hydroxide ion approaches the phosphorus to subsequently form a covalent P-O bond. A concerted proton relay transfer mechanism, in which the proton on the nitrogen stems from a different water cluster molecule than the attacking nucleophile H_2O molecule, could not be located due to steric hindrance by the methyl substituents.

Concerted Backside Mechanism

In the S_N2@P-b mechanism (Figure 3.1), H_2O attacks the phosphorus on one side to form a P-OH bond, requiring proton transfer to remove the excess proton. On the opposite side of the phosphorus, the leaving dimethylamine substituent is a potent proton acceptor. To avoid unrealistic (destabilizing) charge separation in the transition state and enable proton transfer through the solvent water between the phosphorus-attacking water molecule and the leaving dimethylamine substituent, model systems containing at least five explicit water molecules were created and evaluated. Five was the minimum number of water molecules to allow the solvent cluster to span the HMPA molecule. In the lowest-energy conformation of the backside transition state (Figure 3.2: S_N2@P-b), which included six explicit water molecules, the P-N bond distance is 0.07 Å longer (i.e., a total distance of 2.00 Å) compared to the frontside attack. The free energy of activation in aqueous phase for the S_N2@P-b mechanism (149 kJ/mol) was determined to be 53 kJ/mol lower than for the frontside mechanism.

Acid-Catalyzed Concerted Backside Mechanism

For the hydrolysis of the protonated species, it was inferred that the backside mechanism is the kinetically most favorable mechanism, based on the substantially lower activation barrier of the backside over the frontside S_N2@P mechanism for the uncatalyzed P-N bond hydrolysis, and the assumption that the steric effects are similar for both uncatalyzed and acid-catalyzed hydrolysis. Thus, only the backside A2@P mechanism was investigated to elucidate acid-catalyzed P-N bond hydrolysis.

In the ground state of the *N*-protonated HMPA species, the P-N bond distance is 0.14 Å longer than in the unprotonated species (i.e., 1.85 Å vs. 1.71 Å). In the transition state (Figure 3.2: A2@P), which is stabilized by four additional explicit water molecules, the P-N bond distance is 0.47 Å longer than in the uncatalyzed S_N2@P-b mechanism (i.e., 2.47 Å). The free energy of activation in aqueous phase for acid-catalyzed P-N bond hydrolysis (99.6 kJ/mol) is 50 kJ/mol lower than for the uncatalyzed mechanism.

Prediction of Reaction Rate and Half-Life at 22 °C

P-N bond hydrolysis of the uncatalyzed HMPA molecule is independent of the pH, which is reflected by a straight line with a slope of zero when the pseudo-first-order rate constant k_1 is plotted against the pH (Figure 3.3). For acid-catalyzed P-N bond hydrolysis, k_2 depends on both the pH and the acidity constant K_a of HMPA, as described in the Computational Details section. Since an experimental pK_a (with $pK_a = -\log K_a$) is unavailable, we estimated it to be -0.38 using SPARC (*21*). The plot of $\log k_2$ vs. pH yields a straight line with a slope of -1, indicative of the first-order dependence of acid-catalyzed P-N bond hydrolysis on pH (*14*). This A2@P mechanism dominates P-N bond hydrolysis at pH values < 8.2. The uncatalyzed S_N2@P-b mechanism only predominates

at pH > 8.2, and becomes a noticeable contributor to the total rate constant k_{hyd} only at pH values greater than ca. 7.

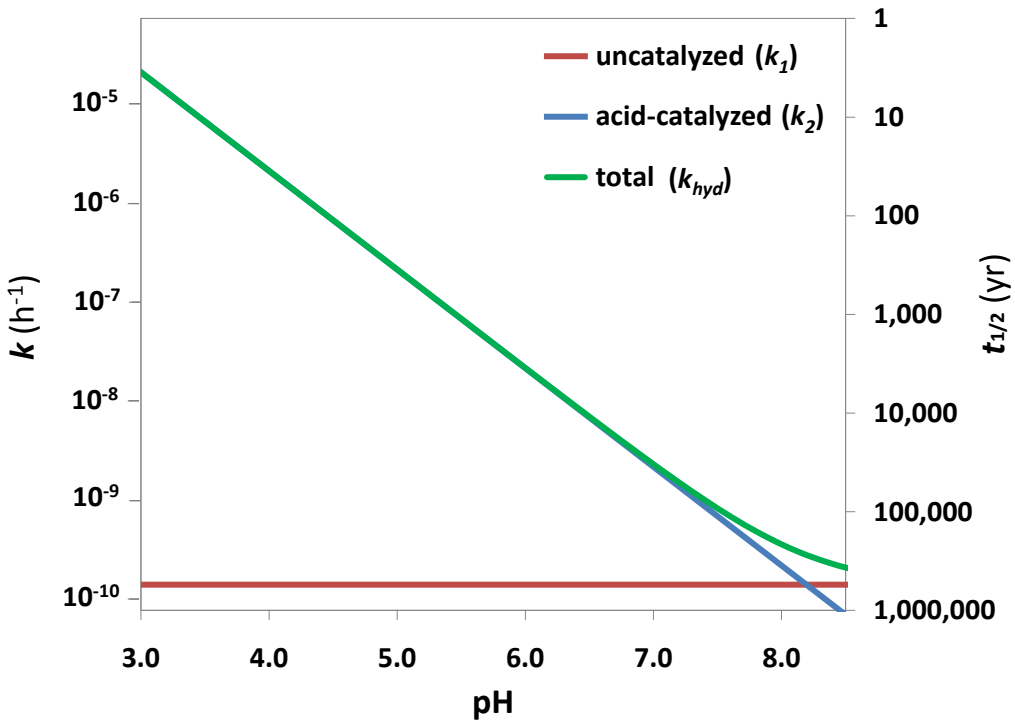

Figure 3.3: Predicted pseudo-first-order rate constants and half-lives at 22 °C for uncatalyzed, acid-catalyzed, and total P-N bond hydrolysis of HMPA.

Moreover, Figure 3.3 indicates that the predicted half-life of P-N bond hydrolysis is 3,500 years at pH 6, 33,000 years at pH 7, and 370,000 years at pH 8.5. An increase in proton activity substantially decreases half-lives to time periods of less than one year at pH < 2.5. At pH 0, the rate constant of HMPA hydrolysis is predicted to be 0.0159 h^{-1}, corresponding to a half-life of 43.5 hours.

Experimental Validation at 22 °C

To validate the theoretical prediction, the hydrolysis rate and half-life of HMPA were measured at pH 0, at which the reaction was sufficiently rapid to enable experimental determination. The total pseudo-first-order rate constant k_{hyd} was found to be 0.00839 h^{-1} (Figure 3.4), corresponding to a half-life of 82.6 hours. Tetramethylphosphoric diamide was observed as the only product of HMPA degradation, confirming that P-N bond hydrolysis was the only reaction leading to its degradation. The mass-to-charge ratio (*m/z*) for the base peak $[M+H]^+$ of tetramethylphosphoric diamide with the molecular formula $PO_2N_2C_4H_{14}^+$ was measured to be 153.0787, with an error of -3.9 ppm with respect to the theoretical *m/z* of 153.0793.

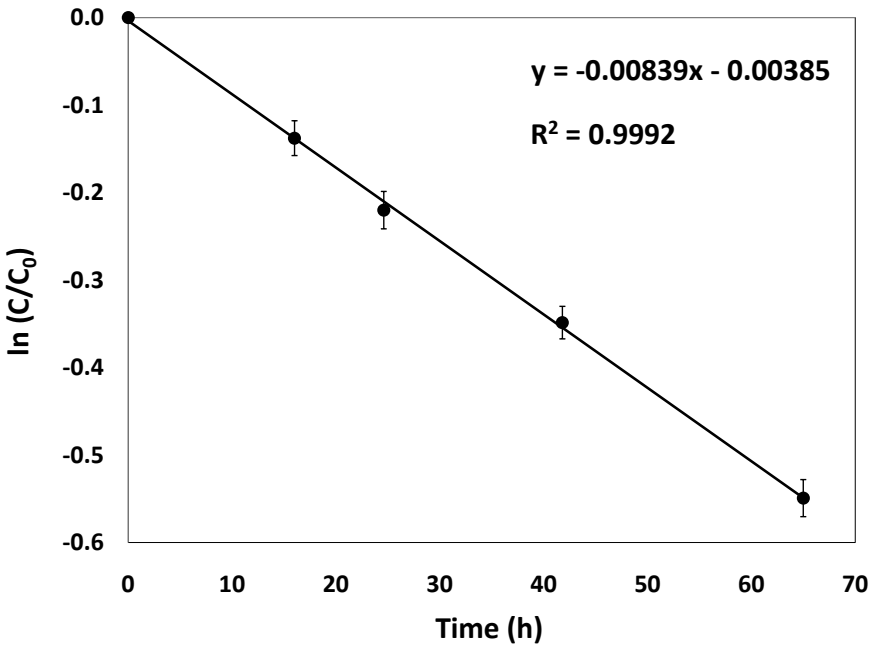

Figure 3.4: Kinetic plot for HMPA hydrolysis at pH 0 and 22 °C.

In a parallel study at pH 7, which can be regarded as control for this experiment, neither hydrolysis nor any other reaction of HMPA were observed over a period of 6 months (see Chapter 2).

Discussion

To estimate reaction rate constants and half-lives, and ultimately to predict the persistence of HMPA in the absence of suitable oxidants, the potential P-N bond hydrolysis mechanisms and their free energies of activation in aqueous phase were computationally evaluated and compared.

The dissociative stepwise S_N1@P mechanism showed the highest free energy, indicating that it does not significantly contribute to the total rate of hydrolysis. This mechanism has previously been proposed for P-N bond hydrolysis in phosphoramidates with two P-O bonds, resulting in the formation of a metaphosphate intermediate (PO_3^-) (*10, 22*). However, it has never been suggested to occur in tetracoordinate phosphorus amides with two or more P-N bonds. The associative stepwise S_N2I@P mechanism (assumed to be predominant in phosphinamides under base-catalyzed conditions (*12*)) and the frontside concerted S_N2@P-f mechanism are kinetically more favorable than the S_N1@P mechanism, but they are still negligible based on the calculated free energies of activation (>200 kJ/mol).

In previous experimental studies, the S_N2@P mechanism, or the corresponding acid-catalyzed A2@P mechanism, respectively, was proposed to be favored for tetracoordinate phosphorus amides that are structurally similar to HMPA, including phosphoramide (*9-13*). The calculations conducted here support this hypothesis for P-N

bond hydrolysis of HMPA. However, it is specifically the backside concerted S_N2@P-b mechanism that is the main pathway for hydrolysis, as it is predicted to be 53 kJ/mol lower in free energy of activation compared to the frontside mechanism. This difference corresponds to a difference in reaction rate of almost ten orders of magnitude, indicating that virtually no other mechanism than the concerted backside S_N2@P-b contributes to the uncatalyzed hydrolysis of the P-N bond, given that all realistic pathways have been examined and that the calculations are relatively accurate.

The acid-catalyzed A2@P mechanism, however, is the kinetically most favorable P-N bond hydrolysis mechanism for HMPA at pH values lower than 8.2. Despite the fact that only a minuscule amount of HMPA molecules is protonated at near-neutral pH (the pK_a was estimated to be -0.38), this mechanism is still favored due to a free energy of activation that is 47 kJ/mol lower than for the uncatalyzed mechanism (for 1 M HMPA or HMPA-H^+, respectively). The estimated crossing point for acid-catalyzed and uncatalyzed hydrolysis at pH 8.2 and 22 °C is comparable to the ones determined experimentally for phosphoramide of 8.30 at 30 °C and 8.46 at 15 °C (*13*).

It is noted that there likely exists a base-catalyzed mechanism for HMPA hydrolysis as well. For phosphoramide, it was shown that base catalysis predominated at pH values of > 9.7 at 15 °C and > 9.0 at 30 °C (*13*). However, as groundwater pH is typically in the range of 6.0 - 8.5, the base-catalyzed mechanism was not investigated here.

The experimental measurement of HMPA hydrolysis at pH 0 revealed that, for the A2@P mechanism, the computationally calculated reaction rate constant was overestimated and thus the half-life was underestimated by factor of 1.9. Consequently,

HMPA is slightly more persistent than predicted by the methods used in this study. Three potential sources of error for this prediction are: First, the B3LYP functional is known to systematically underestimate activation barriers (*23*), resulting in an overestimation of the reaction rate (constant). Especially when relatively small basis sets are used, errors on the order of 20 kJ/mol have been reported (*23*, *24*). Here, a single-point energy calculation with a large basis set (6-311++G(3df,3pd)) was added, which is a computationally efficient approach to increase the accuracy of the predicted energies (*25*). Second, the cluster-continuum solvation model may introduce an error in solvation energies due to an arbitrary orientation of the water molecules in the incomplete first solvation shell (*26, 27*). This problem can be mitigated through the use of one or more full solvation shells (*26*), which, however, is computationally very expensive when large molecules are investigated. When an incomplete first solvation shell is used, it was generally found that more accurate solvation energies are obtained when the explicit water molecules are similarly oriented around the same functional group(s) in both ground and transition state complexes. Third, the pK_a for protonation of the nitrogen within the HMPA molecule of -0.38 had to be estimated using SPARC. This negative value appears to be within a reasonable range though, since comparable (i.e., slightly negative) pK_a values have been measured previously for dimethylamine substituents of structurally similar phosphinamides (*28*). In a rigorous test estimating 4,338 ionization constants, SPARC has been shown to predict pK_a values with a root mean square deviation of 0.36 units for amino reaction centers (*21*).

It is noted that reaction rates are very sensitive with respect to changes in activation barriers, as well as changes in pK_a for pH-dependent reactions. A difference in

free energy of activation of only 5.65 kJ/mol (at 22 °C), or a difference in pK_a of one unit for reactions with first-order dependence on proton activity, will change both reaction rate constant and half-life by one order of magnitude. A factor of 1.9, as observed in this prediction, corresponds to an error in free energy of activation of only 1.58 kJ/mol or an error in pK_a of 0.36. Thus, the predictive strategy applied here yields an estimation that is in excellent agreement with the experimental result, even though some of the introduced errors might have compensated each other.

Conclusion

In the absence of suitable oxidants, where P-N bond hydrolysis is the only thermodynamically favorable degradation reaction, HMPA is persistent over the groundwater-typical pH spectrum of 6.0 - 8.5. Hexamethylphosphoramide contains three P-N bonds that must be hydrolyzed to form the mineralization product *o*-phosphate as well as dimethylamine, which has been shown to be biodegradable under aerobic to methanogenic conditions (*29*). However, predicted half-lives for the first hydrolysis step range from thousands to hundreds of thousands years at near-neutral pH. This hydrolysis is substantially slower than for phosphoramide, the product of HMPA oxidation by permanganate, for which a half-life at pH 7 and 22 °C of 15 days can be derived from the kinetic parameters provided in ref (*13*). This rate is in agreement with experimental observations, which have shown that an increase in substituent size decreases P-N bond hydrolysis rates (*11, 14*). Therefore, natural attenuation (NA) processes are not effective for HMPA degradation under mildly to strongly reducing conditions at contaminated field sites. Only a substantial decrease in pH to values around 2-3 (or even lower at lower

water temperatures) leads to appreciable reaction rates. However, acidification is not an option for *in situ* remediation due to adverse effects, such as ecosystem harm and heavy metal mobilization. Remediation by strong oxidants remains as viable strategy for HMPA-contaminated field sites (see Chapter 2 and ref (*8*)).

The results of this study illustrate that quantum chemical calculations can be successfully applied to predict contaminant persistence. Here, DFT calculations were applied in combination with a cluster-continuum model to account for solvent effects, which has been shown to yield satisfactory solvation energies (*16, 19, 30*). However, it is re-emphasized that reaction rate (constant) and half-life predictions are very sensitive to errors in the calculation of Gibbs free energies of activation, such that the application of high levels of theory for the computation would be ideal, e.g., use of the computationally very expensive coupled cluster or configuration interaction methods (*24, 31*). Nevertheless, the predictive strategy presented here is a valuable approach that can in general be applied to both redox- and non-redox-dependent degradation reactions without previous knowledge of a contaminant, especially when appropriate QSARs are unavailable or reaction rates are too slow to enable experimental measurement.

References

1. Hunkeler, D.; Aravena, R.; Butler, B. J., Monitoring microbial dechlorination of tetrachloroethene (PCE) in groundwater using compound-specific stable carbon isotope ratios: Microcosm and field studies. *Environmental Science & Technology* **1999,** 33, (16), 2733-2738.

2. Reineke, A. K.; Goen, T.; Preiss, A.; Hollender, J., Quinoline and derivatives at a tar oil contaminated site: Hydroxylated products as indicator for natural attenuation? *Environmental Science & Technology* **2007,** 41, (15), 5314-5322.

3. Borch, T.; Inskeep, W. P.; Harwood, J. A.; Gerlach, R., Impact of ferrihydrite and anthraquinone-2,6-disulfonate on the reductive transformation of 2,4,6-trinitrotoluene by a gram-positive fermenting bacterium. *Environmental Science & Technology* **2005,** 39, (18), 7126-7133.

4. Kolpin, D. W.; Furlong, E. T.; Meyer, M. T.; Thurman, E. M.; Zaugg, S. D.; Barber, L. B.; Buxton, H. T., Pharmaceuticals, hormones, and other organic wastewater contaminants in US streams, 1999-2000: A national reconnaissance. *Environmental Science & Technology* **2002,** 36, (6), 1202-1211.

5. Richardson, S. D., Water analysis: Emerging contaminants and current issues. *Analytical Chemistry* **2009,** 81, (12), 4645-4677.

6. Borch, T.; Kretzschmar, R.; Kappler, A.; Van Cappellen, P.; Ginder-Vogel, M.; Voegelin, A.; Campbell, K., Biogeochemical redox processes and their impact on contaminant dynamics. *Environmental Science & Technology* **2010,** 44, (1), 15-23.

7. Boethling, R. S.; Mackay, D., *Handbook of Property Estimation Methods for Chemicals: Environmental and Health Sciences*. CRC Press: Boca Raton, FL, 2000; p 481.

8. Campos, D., Field demonstration of UV/H_2O_2 on the treatment of groundwater contaminated with HMPA. In *Chemical Oxidation: Technologies for the Nineties.*, Eckenfelder, W. W.; Bowers, A. R.; Roth, J. A., Eds. Technomic Publishing Company: Lancaster, PA, 1997; Vol. 6, pp 19-26.

9. Rahil, J.; Haake, P., Reactivity and mechanism of hydrolysis of phosphonamides. *Journal of the American Chemical Society* **1981,** 103, (7), 1723-1734.

10. Chanley, J. D.; Feageson, E., A study of hydrolysis of phosphoramides. II. Solvolysis of phosphoramidic acid and comparison with phosphate esters. *Journal of the American Chemical Society* **1963,** 85, (8), 1181-1190.

11. Garrison, A. W.; Boozer, C. E., The acid-catalyzed hydrolysis of a series of phosphoramidates. *Journal of the American Chemical Society* **1968,** 90, (13), 3486-3494.

12. Koizumi, T.; Haake, P., Acid-catalyzed and alkaline hydrolyses of phosphinamides. The lability of phosphorus-nitrogen bonds in acid and mechanisms of reaction. *Journal of the American Chemical Society* **1973,** 95, (24), 8073-8079.

13. Richter, S.; Topelmann, W.; Lehmann, H. A., Hydrolysis of phosphoric acid amides. *Zeitschrift Fur Anorganische Und Allgemeine Chemie* **1976,** 424, (2), 133-143.

14. Haake, P.; Koizumi, T., Hydrolysis of phosphinamides and nature of P-N bond. *Tetrahedron Letters* **1970**, (55), 4845-4848.

15. Pliego, J. R.; Riveros, J. M., The cluster-continuum model for the calculation of the solvation free energy of ionic species. *Journal of Physical Chemistry A* **2001,** 105, (30), 7241-7247.

16. Pliego, J. R., Basic hydrolysis of formamide in aqueous solution: a reliable theoretical calculation of the activation free energy using the cluster-continuum model. *Chemical Physics* **2004,** 306, (1-3), 273-280.

17. Cances, E.; Mennucci, B.; Tomasi, J., A new integral equation formalism for the polarizable continuum model: Theoretical background and applications to isotropic and anisotropic dielectrics. *Journal of Chemical Physics* **1997,** 107, (8), 3032-3041.

18. Barone, V.; Cossi, M.; Tomasi, J., A new definition of cavities for the computation of solvation free energies by the polarizable continuum model. *Journal of Chemical Physics* **1997,** 107, (8), 3210-3221.

19. Stare, J.; Henson, N. J.; Eckert, J., Mechanistic aspects of propene epoxidation by hydrogen peroxide. Catalytic role of water molecules, external electric field, and zeolite framework of TS-1. *Journal of Chemical Information and Modeling* **2009,** 49, (4), 833-846.

20. Chang, N. Y.; Lim, C., Factors governing the enhanced reactivity of five-membered cyclic phosphate esters. *Journal of the American Chemical Society* **1998,** 120, (9), 2156-2167.

21. Hilal, S. H.; Karickhoff, S. W.; Carreira, L. A., A rigorous test for SPARC's chemical reactivity models: Estimation of more than 4300 ionization pK_as. *Quantitative Structure-Activity Relationships* **1995,** 14, (4), 348-355.

22. Haake, P.; Allen, G. W., Studies on phosphorylation by phosphoroguanidinates. Mechanism of action of creatine: ATP transphosphorylase (creatine kinase). *Proceedings of the National Academy of Sciences of the United States of America* **1971,** 68, (11), 2691-2693.

23. Zhao, Y.; Truhlar, D. G., Hybrid meta density functional theory methods for thermochemistry, thermochemical kinetics, and noncovalent interactions: The MPW1B95 and MPWB1K models and comparative assessments for hydrogen bonding and van der Waals interactions. *Journal of Physical Chemistry A* **2004,** 108, (33), 6908-6918.

24. Zhang, Q.; Bell, R.; Truong, T. N., *Ab initio* and density functional theory studies of proton transfer reactions in multiple hydrogen bond systems. *Journal of Physical Chemistry* **1995,** 99, (2), 592-599.

25. Paul, K. W.; Kubicki, J. D.; Sparks, D. L., Quantum chemical calculations of sulfate adsorption at the Al- and Fe-(hydr)oxide-H_2O interface - Estimation of Gibbs free energies. *Environmental Science & Technology* **2006,** 40, (24), 7717-7724.

26. Bryantsev, V. S.; Diallo, M. S.; Goddard, W. A., Computational study of copper(II) complexation and hydrolysis in aqueous solutions using mixed cluster/continuum models. *Journal of Physical Chemistry A* **2009,** 113, (34), 9559-9567.

27. Kamerlin, S. C. L.; Haranczyk, M.; Warshel, A., Are mixed explicit/implicit solvation models reliable for studying phosphate hydrolysis? A comparative study of continuum, explicit and mixed solvation models. *Chemphyschem* **2009,** 10, (7), 1125-1134.

28. Haake, P.; Koizumi, T., Basicity of phosphinamides and site of protonation. *Tetrahedron Letters* **1970**, (55), 4849-4850.

29. van Agteren, M. H.; Keuning, S.; Janssen, D. B., *Handbook on Biodegradation and Biological Treatment of Hazardous Organic Compounds*. Kluwer Academic Publishers: Norwell, MA, 1998; p 495.

30. Nguyen, M. T.; Raspoet, G.; Vanquickenborne, L. G., Necessity to consider a three-water chain in modelling the hydration of ketene imines and carbodiimides. *Journal of the Chemical Society-Perkin Transactions 2* **1999**, (4), 813-820.

31. Niu, S. Q.; Hall, M. B., Comparison of Hartree-Fock, density functional, Moller-Plesset perturbation, coupled cluster, and configuration interaction methods for the migratory insertion of nitric oxide into a cobalt-carbon bond. *Journal of Physical Chemistry A* **1997,** 101, (7), 1360-1365.

CHAPTER 4

NOVEL C-H BOND OXIDATION MECHANISM BY AQUEOUS PHASE PERMANGANATE

Introduction

The oxidation of the C-H bond is one of the most important reactions in both biological (i.e., substrate oxidation) and chemical systems (i.e., fine chemical synthesis) (*1*, *2*). One oxidant capable of C-H bond oxidation is the permanganate ion (MnO_4^-), which has been widely used for over a century (*3*) as reagent for the synthesis of organic compounds (*4*) as well as for drinking water, waste water, and groundwater treatment (*5*). The mechanism of C-H bond oxidation by permanganate has been mostly studied in non-aqueous phase due to the low aqueous solubility of many alkylated chemicals of interest, such as aliphatic and alkylaromatic hydrocarbons. In numerous studies, alkylated compounds were shown to be oxidized to the corresponding aldehydes and carboxylic acids (refs (*4*, *6*) and references therein). It was proposed that, after hydrogen ($H^\bullet$) abstraction by permanganate (*3*), the radical ion pair $HMnO_4^{\bullet-}$ / $R\text{-}CH_2^\bullet$ collapses through an oxygen-rebound mechanism to form an alkyl-manganate-ester (i.e., a C-O-Mn bond) (*7*). The fate of this ester, i.e., its decomposition to form the final oxygenated product, was not elucidated.

In aqueous phase, Gardner & Mayer (*3*) observed that the concentration of dissolved oxygen had no effect on the rate of toluene oxidation by permanganate. Since molecular oxygen is a radical scavenger, they concluded that the methyl substituent in toluene is not oxidized through a radical pathway, but "most likely" through hydride (H^-) abstraction by permanganate and concurrent stabilization of the carbocation by a molecule of the solvent water to form an alcoholic species (Scheme 4.1), even though benzaldehyde and benzoic acid, but not benzyl alcohol were detected by HPLC analysis.

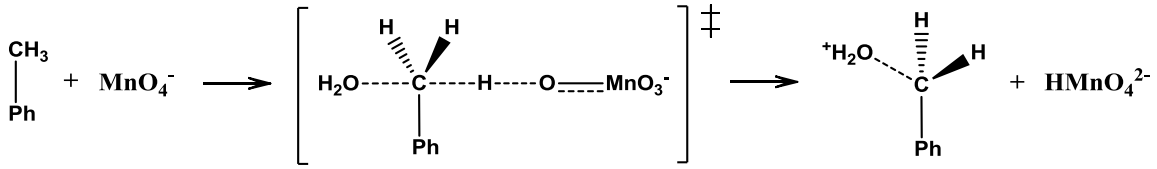

Scheme 4.1

For the groundwater contaminant hexamethylphosphoramide (HMPA), it was previously predicted based on thermodynamic calculations, that its oxidation by aqueous permanganate proceeds through the initial formation of an alcoholic substituent, which is then oxidized to an aldehydic substituent (see Chapter 2). The potential degradation pathway for the thermodynamic investigations had been generated based on the C-H bond oxidation mechanism proposed by Gardner & Mayer (*3*) as well as the report by Terry & Bořkovec (*8*), who detected formyl-pentamethylphosphoramide (formyl-PMPA) from the oxidation of HMPA by aqueous permanganate, and speculated that hydroxymethyl-pentamethylphosphoramide (HM-PMPA) was the precursor. This was supported by the experimental detection of HM-PMPA via LC/ESI-TOF-MS (see Chapter 2). However, the oxygenated reaction intermediates were not quantified due to the lack of reference compounds, and the mechanism of HMPA oxidation by aqueous permanganate was not

further investigated. Thus, the first objective of this study is to elucidate the mechanism of C-H bond oxidation in HMPA by aqueous permanganate through transition state searches to validate the degradation pathway generated based on expert knowledge.

The second objective is to perform a proof-of-principle experiment to show that Gibbs free energies of activation, which can be calculated from free energies of the transition states and reactant(s), can be used to predict the most likely degradation pathway. This is an important task when the formation of two or more degradation products is thermodynamically favorable (*9-13*). In this case, it is the lowest activation barrier(s) that will determine the primary degradation pathway.

Experimental Section

HMPA Oxidation Experiment in Unlabeled and ^{18}O-labeled Water

Initially, the oxidation of HMPA by permanganate was investigated in 30 mM phosphate-buffered DI water at pH 7.0 and 22 °C containing 0.25 mM HMPA (99.1%, MP Biomedicals) and 6 mM $KMnO_4$ (certified ACS). The details of this experiment are presented in Chapter 2.

To determine the source of oxygen in the HMPA oxidation products, 1 mL of $H_2{}^{18}O$ (97.2%, Cambridge Isotope Laboratories) was transferred into an HPLC vial. $KMn^{16}O_4$ and HMPA were subsequently added to yield final concentrations of 60 mM and 2.5 mM, respectively. Thus, for both compounds, the final concentrations were 10 times higher than in the initial HMPA oxidation experiment using unlabeled water. Preliminary experiments had shown that, in this concentration range, HMPA oxidation by permanganate follows pseudo-first-order kinetics, however, with respect to MnO_4^-,

despite the fact that it was present in 24-fold molar excess compared to HMPA. The reaction vial was stored non-agitated in the dark at 22 °C.

For liquid chromatography / electrospray ionization - time-of-flight - mass spectrometry (LC/ESI-TOF-MS) analyses (see Analytical Methods below), samples (15 µL) were quenched by adding 1.485 mL of 5 mM $Na_2S_2O_3$ and filtered (0.2 µm, nylon).

Analytical Methods

Hexamethylphosphoramide and its phosphoramide-containing transformation products were analyzed with an Agilent 1100 Series liquid chromatograph equipped with a 150 mm × 2.1 mm XTerra phenyl column, 3.5 µm particle size (Waters) coupled to an Agilent G3250AA MSD TOF system with an electrospray ionization (ESI) source (LC/ESI-TOF-MS). Separation was carried out isocratically with 0.01% formic acid in water / acetonitrile (98:2). Details of the method are described in Chapter 2.

For HMPA and PMPA (97%, custom-synthesized and generously provided by DuPont), a ten-point calibration curve was generated. For HM-PMPA and formyl-PMPA, however, no reference standards were available. Since HM-PMPA has been shown to decompose to PMPA and formaldehyde in a non-redox-dependent reaction (see Chapter 2), triplicates of the reactive solution from the HMPA oxidation experiment in phosphate-buffered, unlabeled DI water (100 mL) were set up. At one hour post-reaction start, the entire batches were quenched by adding each 0.5 mL of 1M $Na_2S_2O_3$, and filtered (0.2 µm, nylon). Since, under these conditions, PMPA is exclusively formed from the decomposition of HM-PMPA, the decrease in total peak area for HM-PMPA during 30.5 hours of non-agitated storage in the dark at 22 °C was calibrated against the increase in the total peak area of PMPA.

Formyl-PMPA was quantified based on the samples taken 15 minutes post-reaction start in the HMPA oxidation experiment in unlabeled DI water. At 15 minutes post-reaction start, only HMPA, HM-PMPA, and formyl-PMPA were detectable in the aqueous samples. Measurements of total nitrogen in solution had revealed that there were no sorption or volatilization losses from the reactive aqueous solution (see Chapter 2). It was assumed that the sum of molar concentrations of HMPA, HM-PMPA, and formyl-PMPA at 15 minutes post-reaction start equalled the initial molar HMPA concentration before oxidation was started. Thus, the total peak area of formyl-PMPA was calibrated against the difference between initial HMPA concentration and the sum of HMPA and HM-PMPA concentrations after 15 minutes of oxidation.

The concentrations of ^{16}O- and ^{18}O-formyl-PMPA were quantified based on their relative peak area (*PA*) ratio, determined from their respective base peak contributions, in combination with the total formyl-PMPA concentration, i.e.:

$$[^{16}\mathrm{O}-\mathrm{formyl}-\mathrm{PMPA}] = \frac{PA(^{16}\mathrm{O})}{PA(^{16}\mathrm{O}) + PA(^{18}\mathrm{O})}[\mathrm{formyl}-\mathrm{PMPA}]_{\mathrm{total}}$$

and vice versa for ^{18}O-formyl-PMPA.

Determination of Pseudo-first-order Oxidation Rate Constants

For HMPA, a pseudo-first-order rate constant k_{obs} can be readily obtained from its disappearance over time. Hydroxymethyl-pentamethylphosphoramide and formyl-PMPA, however, are produced and degraded at the same time. Thus, to determine k_{obs} for those two compounds, an analytical iterative solution for networks of irreversible (pseudo-)first-order reactions (*14*) was applied and implemented in Mathcad (Version 14.0.0.163, PTC). This algorithm involves the solution of a coefficient matrix, in which

the individual k_{obs} for all reactions within the network are the coefficients, for the direct calculation of species concentrations at any time of interest. The matrix coefficients were manually iterated and fit to the experimental data, until the pooled unweighted non-linear R^2 as well as the non-linear R^2 for each individual compound, which were based upon the use of the total corrected sum of squares, were maximized.

Gibbs free energies of activation in aqueous phase ($\Delta^{\ddagger}G_{(aq)}$) were then determined from the matrix coefficients, i.e., the determined k_{obs} values, based on transition state theory:

$$\Delta^{\ddagger}G_{(aq)} = -RT\ ln\left(\frac{k_{obs}h}{k_BT}\right)$$

where R is the universal gas constant, T is the temperature in Kelvin, h is Planck's constant, and k_B is the Boltzmann constant.

Computational Details

Quantum chemical calculations via Gaussian 03 were conducted to investigate the mechanisms of C-H bond oxidation by permanganate in both methane and HMPA. The exception was the oxidation of HMPA leading to formation of the methyl-manganate-ester, for which Gaussian 09 was used. All calculations were performed without symmetry constraints at the B3LYP level of theory with different basis sets for P, O, N, C, and H as specified in the text, as well as the ECP-type LANL2DZ basis set for Mn and K in all calculations. Potential energy minima for ground states were verified by frequency calculations (i.e., no imaginary frequencies). First-order saddle points for transition states were verified by both frequency (i.e., exactly one imaginary frequency)

and intrinsic reaction coordinate (IRC) calculations. The integral equation formalism polarizable continuum model (IEFPCM) (*15*) was used to account for implicit solvation effects.

Results

HMPA Oxidation Experiment in Unlabeled Water

Based on the assumption that all HMPA is initially oxidized to the corresponding alcohol, the kinetic model (i.e., the coefficient matrix) was initially set up to determine the pseudo-first-order rate constants (i.e., k_{12}, k_{23}, k_{24}, and k_{34}) presented in Scheme 4.2. Since HM-PMPA and formyl-PMPA were the only oxygenated intermediates that could be quantified, the network was simplified by lumping all species but HMPA, HM-PMPA, and formyl-PMPA into the "Rest". The lumped "Rest" was quantified by subtracting the sum of the molar concentration of the three species (i.e., HMPA, HM-PMPA, and formyl-PMPA) at any sample time from the initial molar HMPA concentration. This assumption appeared reasonable since previous measurements of total nitrogen in solution had revealed that there were no sorption or volatilization losses from the reactive aqueous solution.

Figure 4.1 shows that, based on the assumption that all HMPA is initially oxidized to the corresponding alcohol, the experimental data could not be fit by the pseudo-first-order kinetic model, as indicated by a pooled unweighted non-linear R^2 of 0.4417 as well as low non-linear R^2 values for all species but HMPA.

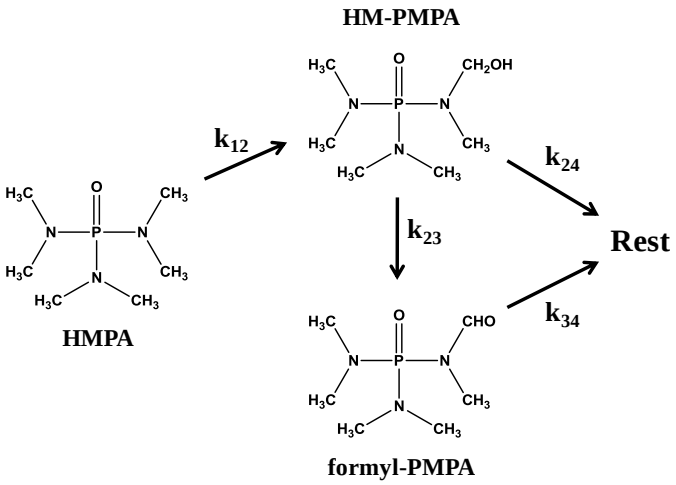

Scheme 4.2

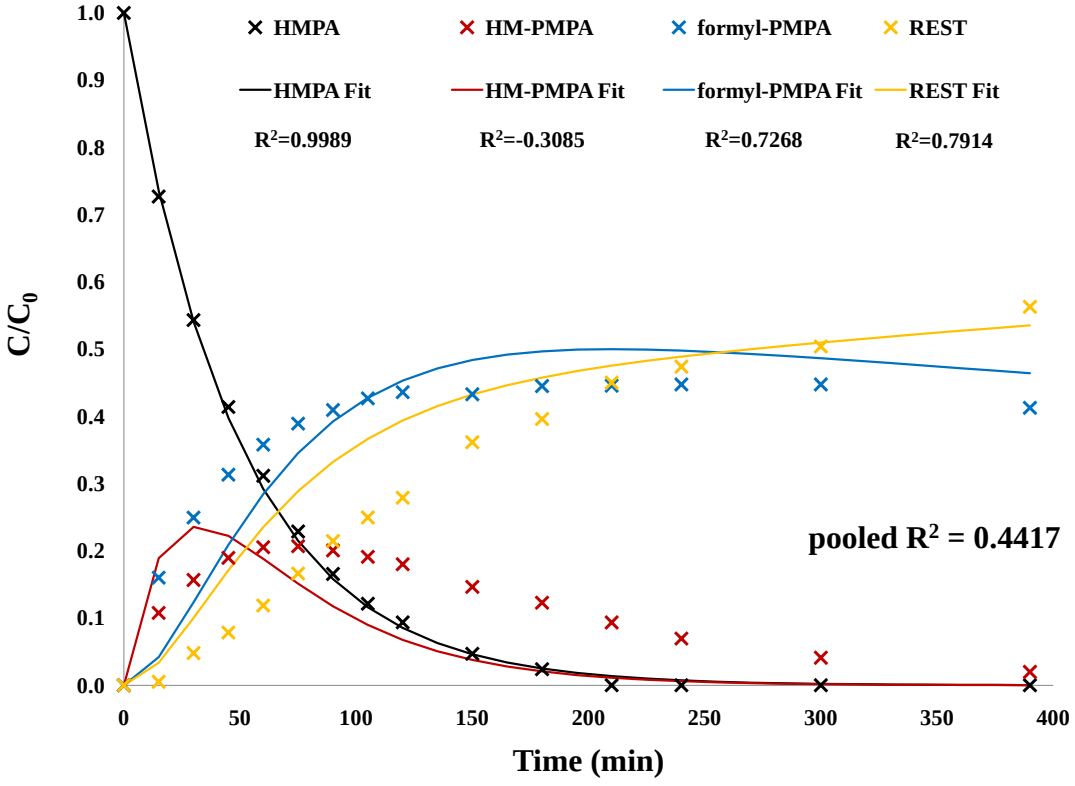

Figure 4.1: Pseudo-first-order fit for the HMPA oxidation experiment in unlabeled water, assuming that all HMPA is initially oxidized to the corresponding alcohol HM-PMPA.

HMPA Oxidation Experiment in ^{18}O-labeled Water

To test the hypothesis that HMPA can be oxidized directly to its corresponding aldehyde (i.e., formyl-PMPA) by permanganate, as suggested for C-H bond oxidations in non-aqueous phase (*4*, *7*), the HMPA oxidation experiment was conducted in ^{18}O-labeled water to enable identification of the source of oxygen in formyl-PMPA. Theoretical calculations indicated that this reaction is thermodynamically favorable ($\Delta_r G'^0_{(aq)}$ = -226 kJ/mol, calculated at the B3LYP/6-311++G(d,p) level of theory). If formyl-PMPA is produced from HM-PMPA, the oxygen will stem from the solvent water according to the mechanism proposed by Gardner & Mayer (*3*), and will thus include an ^{18}O isotope (see Scheme 4.1). However, if formyl-PMPA is produced by direct oxygen transfer from (the unlabeled) permanganate, it will not possess an ^{18}O isotope. Table 4.1 shows the TOF-MS characteristics for the detected HM-PMPA and formyl-PMPA species.

Table 4.1: TOF-MS characteristics of the key products from HMPA oxidation by aqueous permanganate.

Compound	Molecular ion peak	Molecular ion peak formula	Observed *m/z*	Theoretical *m/z*	Error (ppm)
^{18}O-HM-PMPA	$[M+Na]^+$	$C_6H_{18}N_3Na^{16}O^{18}OP^+$	220.1077	220.1071	2.7
^{16}O-formyl-PMPA	$[M+H]^+$	$C_6H_{17}N_3{}^{16}O_2P^+$	194.1053	194.1053	0.0
^{18}O-formyl-PMPA	$[M+H]^+$	$C_6H_{17}N_3{}^{16}O^{18}OP^+$	196.1095	196.1095	0.0

Three compounds were identified by their accurate masses. The presence of ^{16}O-formyl-PMPA clearly indicates that the oxygen in this species stems from the ^{16}O-permanganate, not from the solvent water. ^{18}O-formyl-PMPA is the expected oxidation product from ^{18}O-HM-PMPA, which was also detected, however, only as a sodiated

molecular ion peak since the protonated species loses water during electrospray ionization (see Chapter 2) and thus its characteristic oxygen molecule. In direct injection mode, a peak with the nominal mass of 218 was also observed, which could not be assigned to a single species, but likely included contributions from sodiated ^{18}O-formyl-PMPA, potassiated HMPA, and potentially ^{16}O-HM-PMPA. The formation of ^{16}O-HM-PMPA was not expected based on the report of Gardner & Mayer (*3*). However, the chromatograms revealed that HM-PMPA indeed contributed to the *m/z* 218 peak. The exact mass of 218.0989, however, showed an error of 4.0 mDa (18.3 ppm) compared to the theoretical mass for ^{16}O-HM-PMPA (218.1029), thus substantially higher than for the other identified products (Table 4.1). Nevertheless, the observed mass could not be fit to any other phosphoramide-based structure.

The kinetic model was set up as shown in Scheme 4.3, allowing for direct HMPA oxidation to formyl-PMPA.

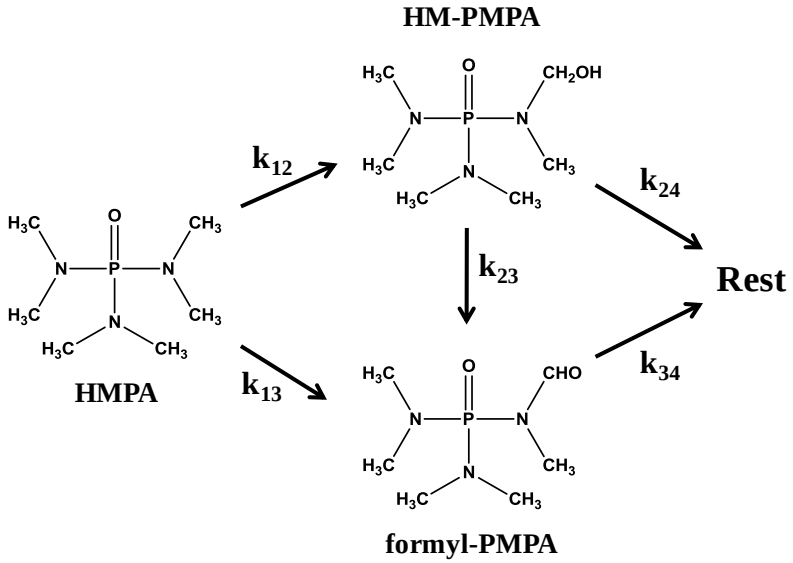

Scheme 4.3

The results of the HMPA oxidation experiment in ^{18}O-labeled water and the pseudo-first-order model are shown in Figure 4.2. Allowing for direct oxidation of HMPA to formyl-PMPA in addition to oxidation to HM-PMPA, an excellent fit with a pooled unweighted non-linear R^2 of 0.9939 is obtained. Furthermore, the individual non-linear R^2 values for the five species are all >0.98.

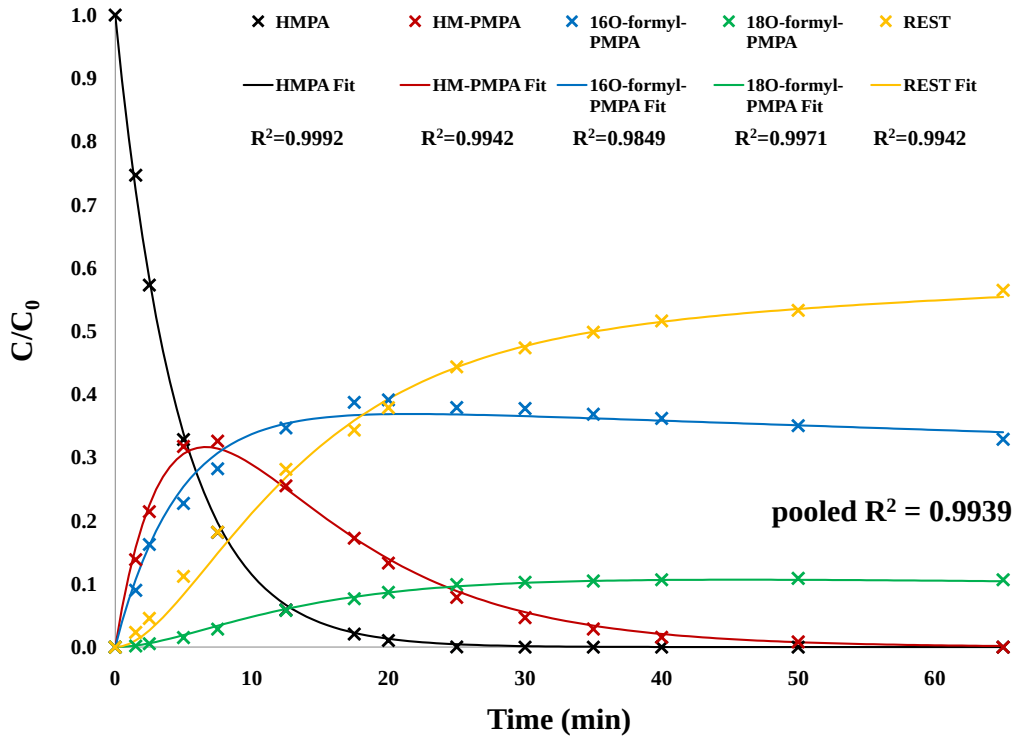

Figure 4.2: Pseudo-first-order fit for the HMPA oxidation experiment in ^{18}O-labeled water, accounting for HMPA oxidation to both HM-PMPA and formyl-PMPA by permanganate in aqueous solution.

In Figure 4.3, the determined pseudo-first-order reaction rate constants and the corresponding Gibbs free energies of activation in aqueous phase for the oxidation of HMPA to HM-PMPA and formyl-PMPA and the oxidation of HM-PMPA to formyl-PMPA are presented.

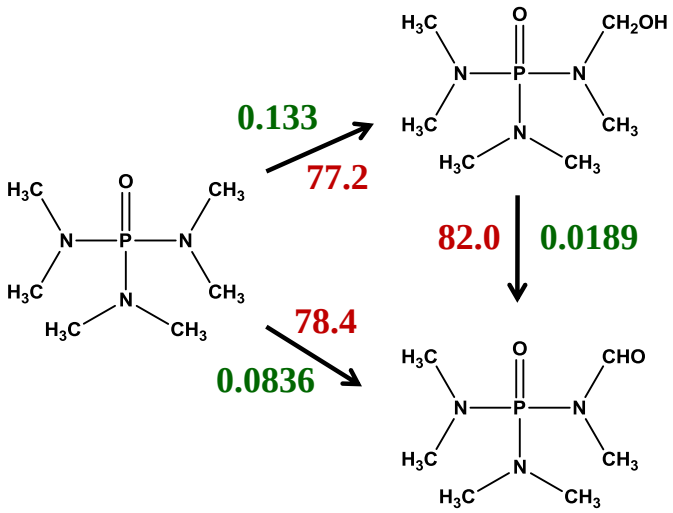

Figure 4.3: Pseudo-first-order rate constants (shown in green, min^{-1}) and Gibbs free energies of activation in aqueous phase (shown in red, kJ/mol) for oxidation by permanganate in aqueous solution at 22 °C.

Theoretical Investigation of Methane Oxidation by Aqueous Permanganate

To further investigate the potential mechanisms of C-H bond oxidation by permanganate in aqueous phase, initial test calculations were performed using methane. For the mechanism leading to alcohol (i.e., methanol) formation, OH^- was used as oxygen donor instead of H_2O to avoid inclusion of multiple explicit water molecules that are necessary to solvate the free excess proton (see Scheme 4.1). Figure 4.4 shows the two transition states found for methane oxidation to methanol by aqueous permanganate: a backside mechanism, in which permanganate and OH^- attack the carbon atom from opposite sides, and a frontside mechanism, in which permanganate and OH^- attack from the same side. The calculated Gibbs free energies of activation indicate that the backside mechanism is kinetically more favorable by 29.3 kJ/mol. The absolute energies of 97.8 or 127.1 kJ/mol are likely inaccurate due to the lack of explicit solvation.

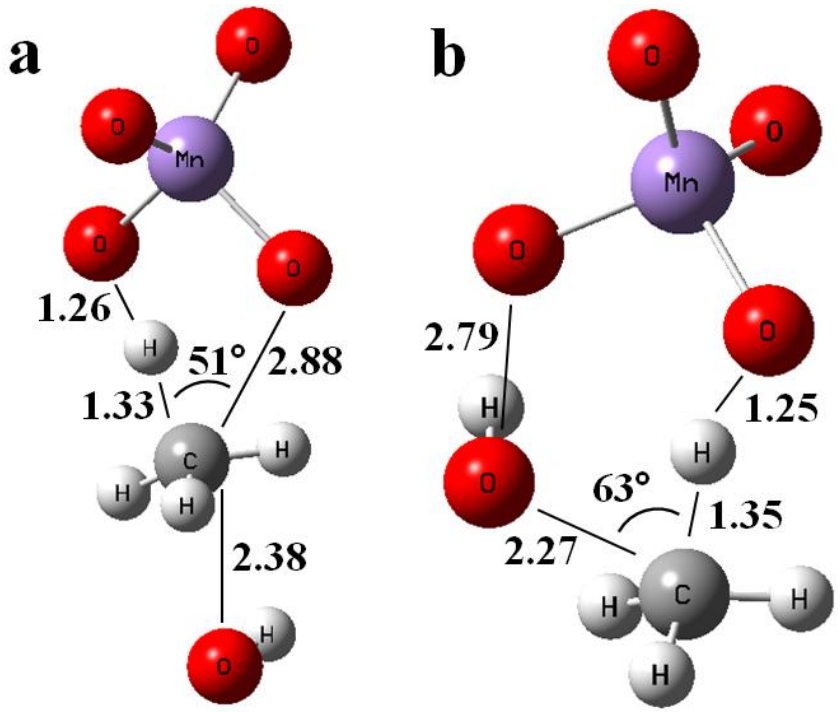

Figure 4.4: Transition states for methane oxidation by aqueous permanganate leading to the formation of methanol, determined at the B3LYP/6-31G level of theory (LANL2DZ for Mn) including IEFPCM. (a) shows the backside, (b) the frontside mechanism. Relevant bond angles and distances (Å) are indicated.

In Figure 4.5a, the transition state for oxidation from methane to a methyl-manganate-ester by aqueous permanganate is shown. A substantial difference in the geometry compared to the backside mechanism leading to methanol formation (Figure 4.4a) is the shorter C-O bond distance of 2.26 Å compared to 2.88 Å, indicating a stronger interaction between the two atoms. In fact, the IRC of the transition state in Figure 4.5a, which traces the path of a chemical reaction, suggests that these two atoms form a C-O bond subsequent to hydride abstraction (Figure 4.5b). The Gibbs free energy of the transition state is 1.7 kJ/mol lower than the frontside mechanism for methanol formation, but 27.6 kJ/mol higher than the backside mechanism.

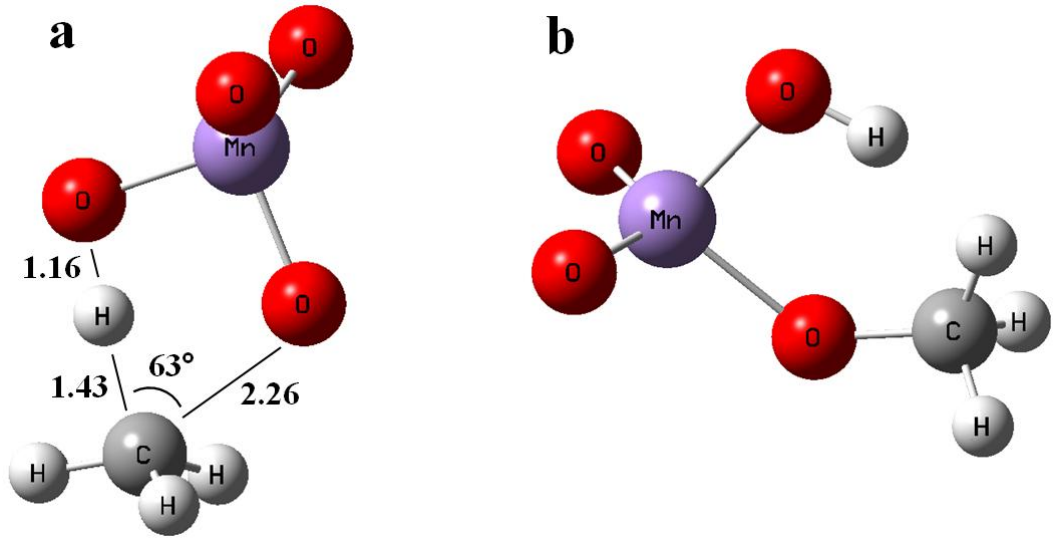

Figure 4.5: (a) Transition state for methane oxidation by aqueous permanganate leading to the formation of formaldehyde, determined at the B3LYP/6-31G level of theory (LANL2DZ for Mn) including IEFPCM. Relevant bond angles and distances (Å) are indicated. (b) Molecular structure of the forming methyl-manganate-ester as indicated by an IRC calculation. The geometry is taken from the IRC calculation and was not optimized to a ground state.

Theoretical Investigation of HMPA Oxidation by Aqueous Permanganate. The oxidation of HMPA to HM-PMPA by permanganate has thus far only been investigated with Gaussian 03. Convergence problems with IEFPCM have impeded consideration of implicit solvation effects. Consequently, the reaction mechanisms were investigated in the gas phase.

Figure 4.6 shows the transition state for backside HMPA oxidation to HM-PMPA by permanganate, including OH^- and one explicit water molecule. It is noted that, since the backside mechanism involves attack of two species (i.e., permanganate and OH^- or water, respectively) from opposite sites at the methyl substituent, it can only proceed at a limited number of sites due to steric hindrance by the bulky dimethylamino substituents.

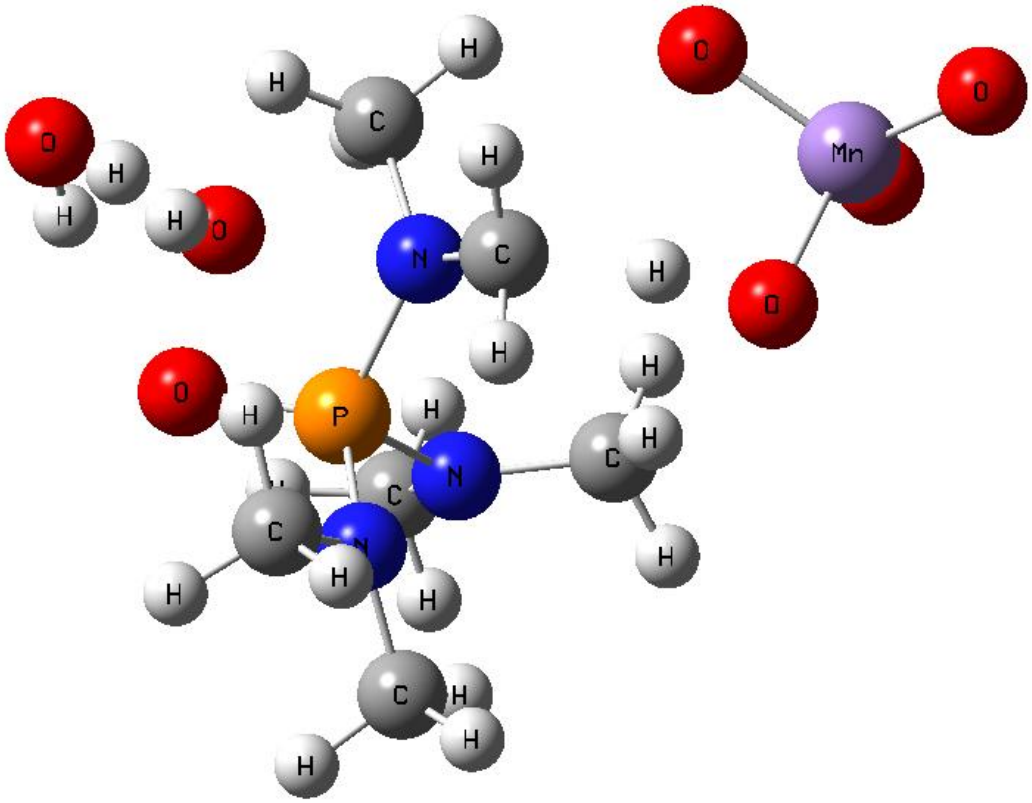

Figure 4.6: Transition state for backside HMPA oxidation to HM-PMPA by permanganate in the gas phase, determined at the B3LYP/6-31G level of theory (LANL2DZ for Mn).

Figure 4.7 shows the transition state for frontside HMPA oxidation to HM-PMPA by permanganate. In the gas phase, the frontside mechanism is 83 kJ/mol kinetically less favorable than the backside mechanism.

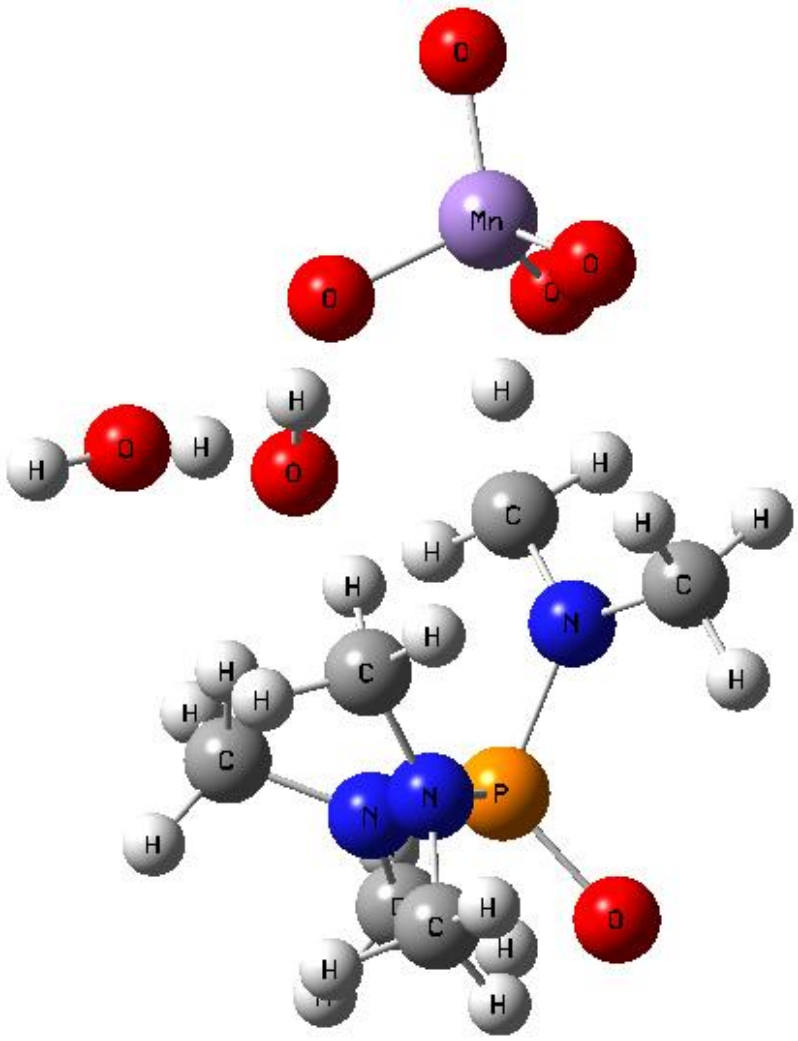

Figure 4.7: Transition state for frontside HMPA oxidation to HM-PMPA by permanganate in the gas phase, determined at the B3LYP/6-31G level of theory (LANL2DZ for Mn).

For the methyl oxidation mechanism leading to the formation of a methyl-manganate-ester, initial calculations with Gaussian 03 had indicated that a minimum of four explicit water molecules were necessary until the solvation free energies stabilized. Furthermore, a potassium cation was included in the calculation to balance the negative charge on the permanganate ion. Figure 4.8 shows the transition state, which was determined using Gaussian 09, since convergence problems with IEFPCM in Gaussian 03

impeded the optimization of the corresponding ground state reactant complex. The Gibbs free energy of activation in aqueous phase was predicted to be 72.0 kJ/mol at the B3LYP/6-31+G(d) level of theory (LANL2DZ for Mn and K).

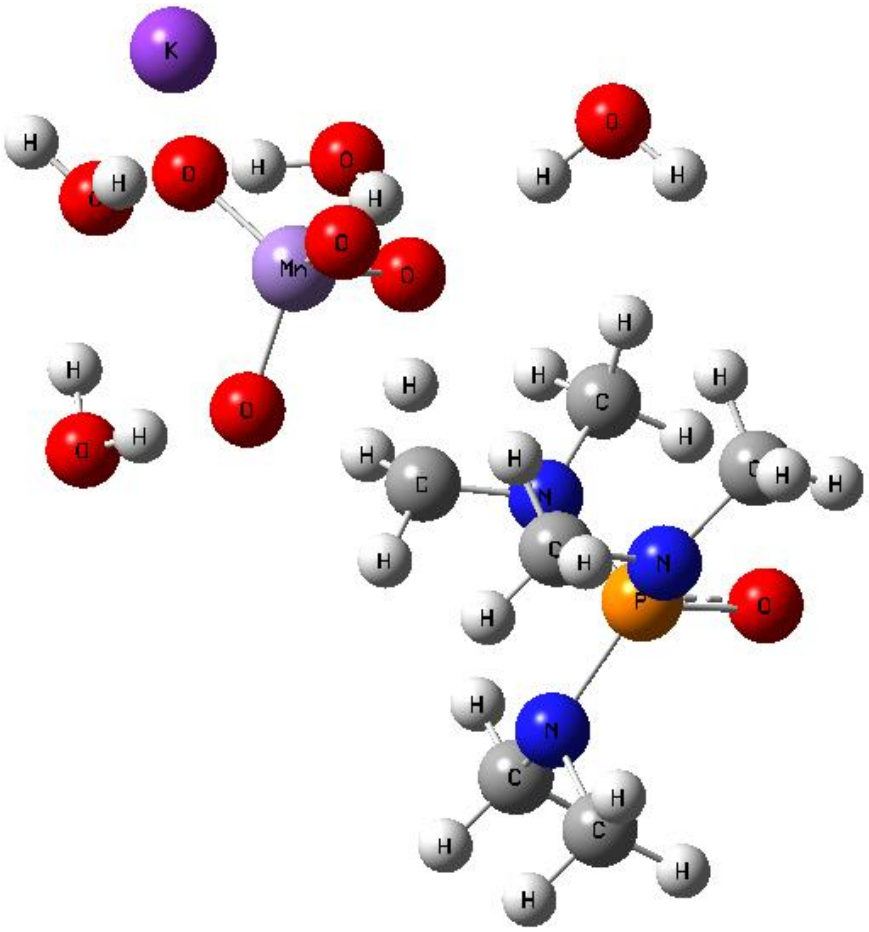

Figure 4.8: Transition state for HMPA oxidation by aqueous permanganate in aqueous phase leading to the formation of a methyl-manganate-ester, determined at the B3LYP/6-31+G(d) level of theory (LANL2DZ for Mn and K).

Discussion

Thus far, it has been assumed that, in aqueous phase, C-H bonds are oxidized by permanganate via hydride abstraction and concurrent stabilization of the carbocation through the solvent water, forming an alcohol (Scheme 4.1) (*3*). The detection of ^{18}O-

HM-PMPA from the oxidation of HMPA in ^{18}O-labeled water confirms this assumption. However, the experimental data could not be fitted with a pseudo-first-order kinetic model, which exclusively allowed this reaction mechanism for HMPA oxidation. Yet, it was confirmed that the (overall) degradation kinetics of HMPA do follow pseudo-first-order behavior when HMPA was allowed to be oxidized directly to an aldehyde by aqueous permanganate. In addition, an excellent experimental fit was achieved, and the presence of ^{16}O-formyl-PMPA unambiguously proves that permanganate is the oxygen donor.

Before this novel oxidation mechanism is discussed, it has to be noted that this mechanism does not necessarily have to proceed, or be kinetically favorable, respectively, in all types of alkyl compounds. For instance, the theoretical investigations of methane oxidation by aqueous permanganate showed that the backside mechanism of methanol formation is kinetically more favorable than both frontside mechanism and the mechanism leading to methyl-manganate-ester formation, which have roughly the same free energy of activation. Based on the preliminary results for HMPA oxidation by aqueous permanganate, however, it appears that the backside mechanism might be sterically hindered in this molecule, which in turn may make the other two mechanisms kinetically more favorable. For toluene, however, the compound investigated by Gardner & Mayer (*3*), these steric constraints do not exist.

The goodness of the kinetic model fit as well as the IRC calculation for the respective transition state (Figure 4.5) indicate that the initial step of the novel oxidation mechanism involves hydride abstraction by permanganate with subsequent formation of a methyl-manganate-ester, as proposed by Strassner & Houk (*7*) for permanganate

oxidation of alkanes in non-aqueous media. The predicted free energy of activation of 72 kJ/mol for this reaction, compared to a free energy of activation of 78.4 kJ/mol from the kinetic fit for the entire reaction from HMPA to formyl-PMPA (Figure 4.3), suggests that the initial formation of the ester is the rate-limiting step. Supporting evidence for this suggestion is the fact that (1) this two-step reaction reveals pseudo-first-order behavior, such that one step (here: the second) must be substantially faster and (2) no methyl-manganate-ester was observed by TOF-MS analysis, neither in positive nor in negative ionization mode. A mechanism for alkyl-manganate-ester decomposition has not been found or reported yet. It appears likely that this second step is a decomposition of the ester through Mn-O bond breaking and deprotonation (Scheme 4.4), according to the decomposition of a permanganate ester that has been proposed to form during aldehyde oxidation to a carboxylic acid by permanganate (*16-18*).

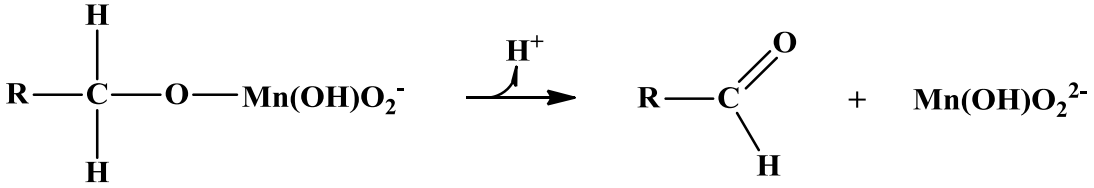

Scheme 4.4

The kinetic model system does not consider any other potential oxidation mechanism than the two discussed. However, the observed molecular peak with the nominal mass of 218 suggests that ^{16}O-HM-PMPA was also formed, even though the accurate mass reveals a substantial error that was not found for the other analytes. At this point, it cannot be excluded that ^{16}O-HM-PMPA was formed in the electrospray ionization process, where unlabeled water from the quenching solution and mobile phase as well as dissolved O_2 are potential oxygen sources. However, ^{16}O was also detected in

both diHM-PMPA and HM-PMPA dimers, both of which only lose one water and thus still incorporate one characteristic hydroxyl group. The presence of ^{16}O-HM-PMPA would indicate that there is at least one more mechanism in which permanganate transfers oxygen to the methyl substituent, however, forming an alcoholic and not an aldehydic substituent.

Two oxygen transfer mechanisms appear possible based on proposed mechanisms for alkyl substituent oxidation by other strong oxidants. In the first potential mechanism, the methyl-manganate-ester does not decompose to form an aldehyde, but hydrolyzes to form an alcohol (Scheme 4.5), according to the suggestion for C-H bond oxidation by ruthenium tetraoxide (RuO_4) (*19*).

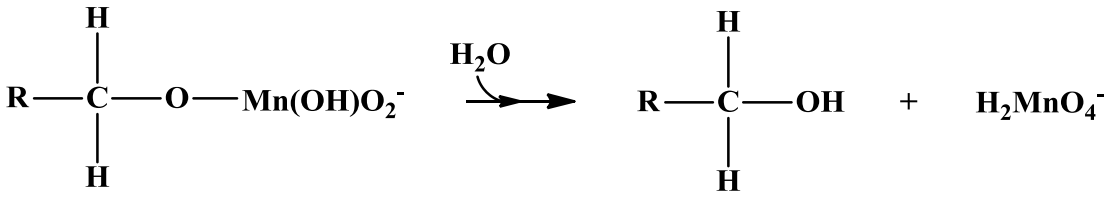

Scheme 4.5

In the second potential mechanism, the C-H bond is directly oxidized by oxygen insertion (Scheme 4.6), according to the suggestion for C-H bond oxidation by dioxiranes (*20, 21*).

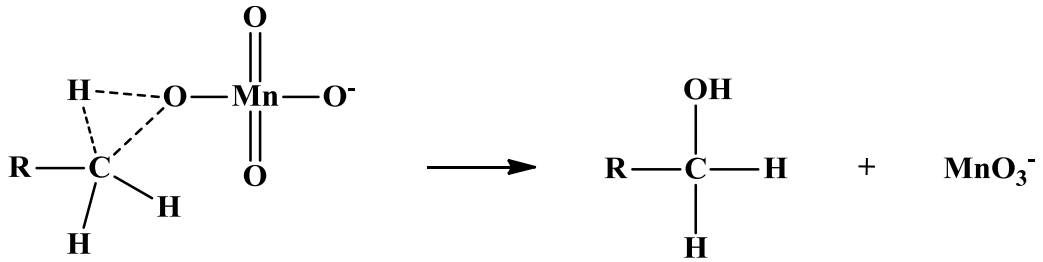

Scheme 4.6

Any additional mechanism of HM-PMPA formation, however, would contradict the kinetic model, since an equal or better fit under the two boundary conditions, i.e., (1) the total concentrations of HM-PMPA and formyl-PMPA must not change, and (2) the ratio of $^{16}O/^{18}O$ in formyl-PMPA must not change, is not possible. Thus, if there was an additional mechanism of HM-PMPA formation, there would also have to be an error in the two assumptions on which the model is based.

The first assumption lies in the indirect calibration of formyl-PMPA (see the Experimental Section). However, if the actual formyl-PMPA concentrations were substantially lower due to an error in the calibration, this would have to be compensated by correspondingly higher concentrations of the remaining species that were lumped into the "Rest". Consequently, HM-PMPA and/or formyl-PMPA would have to be degraded faster, which would in turn change their slopes in the kinetic model, thus only deteriorating their kinetic fit.

The second assumption is that the kinetic model is only true for pseudo-first-order reaction kinetics. This, however, seems to be a reasonable assumption since HMPA was experimentally observed to show overall pseudo-first-order kinetics under the applied conditions, where the reaction rate is independent of the HMPA concentration. This entails the oxidation of HMPA to ^{18}O-HM-PMPA as well as the oxidation of HM-PMPA to formyl-PMPA (at constant pH) to be pseudo-first-order (*3*, *16*). Finally, both experimental observations and theoretical considerations indicated that the two-step oxidation mechanism leading from HMPA directly to the aldehyde appears to have one substantially slower, rate-limiting step. Consequently, it can also be assumed that this reaction largely follows pseudo-first-order reaction kinetics.

Conclusion

The oxidation of the C-H bond in HMPA by aqueous permanganate does not only proceed through hydride abstraction with concurrent oxygen transfer by the solvent water, but also through a novel mechanism that involves oxygen transfer by permanganate. The theoretical investigations indicate that this novel mechanism may proceed by an oxygen rebound mechanism as suggested previously for C-H bond oxidation in non-aqueous phase, i.e., through the formation of a methyl-manganate-ester after hydride abstraction. The fate of this ester remains to be determined. However, the kinetic model fit of the experimental data imply that formyl-PMPA is directly produced from HMPA, circumventing the formation of HM-PMPA in this mechanism. Furthermore, TOF-MS analyses of the oxidation products suggest that a third mechanism may exist, in which oxygen transfer from permanganate leads to the formation of HM-PMPA. The relatively high error in the measured *m/z*, the uncertainty if this product is formed during oxidation or in the electrospray process, and the contradiction to the kinetic model fit, however, question this potential mechanism.

The findings of this study have general implications for chemical synthesis applications, in which aqueous phase C-H bond oxidation leading directly to the formation of a C=O bond has thus far not been exploited. Yet, oxidation of the relatively inert alkanes at transition metal centers is one of the most widely applied and one of the most economically valuable reactions performed in fine chemical synthesis (*1*). Furthermore, this novel mechanism has not yet been considered in groundwater remediation applications, where permanganate is a commonly used oxidant (*5*). While biological HMPA oxidation processes are assumed to proceed exclusively through the

formation of the mutagenic HM-PMPA (*8, 22, 23*), the application of permanganate can at least partially circumvent its production through direct oxidation of HMPA to formyl-PMPA. Formyl-PMPA also possesses mutagenic potential, however, substantially lower than HM-PMPA (*23*). Moreover, formyl-PMPA is not a formaldehyde generator unlike HM-PMPA, which can decompose to form the known human carcinogen formaldehyde (see Chapter 2 and ref (*24*)).

However, further research is necessary to elucidate the mechanisms of C-H bond oxidation in HMPA by permanganate in aqueous phase. Especially the question whether some of the HM-PMPA is formed through oxygen transfer by permanganate or potentially within the electrospray ionization process can be clarified experimentally, for instance, by repeating / reversing the oxidation experiment using ^{18}O-labeled permanganate in $H_2{}^{16}O$. In addition, quantum chemical investigations of the potential oxidation mechanisms can provide evidence through the prediction of Gibbs free energies of activation in aqueous phase, excluding the ones that are kinetically unfavorable. The latter task has thus far been impeded by convergence problems with the IEFPCM implicit solvation model in Gaussian 03, which, however, have been successfully addressed in the new Gaussian 09 version. Especially the question whether ^{18}O-HM-PMPA is produced via a backside or frontside mechanism can only be determined theoretically, but may have important implications for varying C-H bond oxidation mechanisms in dependence on substrate structure.

With respect to the first objective of this study, it can be concluded that the generation of potential degradation pathways based on expert knowledge is biased, and that the exclusive reliance on reported reaction mechanisms may lead to neglect of

degradation pathways. Rather, an appropriate pathway prediction should include mechanistic investigations, which can be achieved through potential energy surface scans and transition state searches.

The second objective, the (proof-of-principle) prediction of the primary degradation pathway (i.e., HMPA to HM-PMPA versus HMPA to formyl-PMPA), could not be finalized here, again, due to convergence problems of IEFPCM in Gaussian 03. However, the experimentally determined Gibbs free energies of activation in aqueous phase for these two reactions reveal a difference of only 1.2 kJ/mol, substantially lower than the error of ca. 10 - 20 kJ/mol that can be expected with this level of theory (*25*), and even within the error range of highest-level post-Hartree-Fock methods such as coupled cluster (CC) or configuration interaction (CI) calculations (*26, 27*). Thus, for this specific test system of HMPA oxidation by aqueous permanganate, even the most accurate quantum chemical calculation could only predict that the two C-H bond oxidation reactions proceed at similar rates.

References

1. Labinger, J. A.; Bercaw, J. E., Understanding and exploiting C-H bond activation. *Nature* **2002,** 417, (6888), 507-514.

2. Stone, K. L.; Borovik, A. S., Lessons from nature: Unraveling biological C-H bond activation. *Current Opinion in Chemical Biology* **2009,** 13, (1), 114-118.

3. Gardner, K. A.; Mayer, J. M., Understanding C-H bond oxidations: $H^{\bullet}$ and H^{-} transfer in the oxidation of toluene by permanganate. *Science* **1995,** 269, (5232), 1849-1851.

4. Fatiadi, A. J., The classical permanganate ion - Still a novel oxidant in organic chemistry. *Synthesis-Stuttgart* **1987**, (2), 85-127.

5. Schnarr, M.; Truax, C.; Farquhar, G.; Hood, E.; Gonullu, T.; Stickney, B., Laboratory and controlled field experiments using potassium permanganate to remediate trichloroethylene and perchloroethylene DNAPLs in porous media. *Journal of Contaminant Hydrology* **1998,** 29, (3), 205-224.

6. Gardner, K. A.; Kuehnert, L. L.; Mayer, J. M., Hydrogen atom abstraction by permanganate: Oxidations of arylalkanes in organic solvents. *Inorganic Chemistry* **1997,** 36, (10), 2069-2078.

7. Strassner, T.; Houk, K. N., Mechanism of permanganate oxidation of alkanes: Hydrogen abstraction and oxygen "rebound". *Journal of the American Chemical Society* **2000,** 122, (32), 7821-7822.

8. Terry, P. H.; Borkovec, A. B., Insect chemosterilants. 4. Oxidation of hexamethylphosphoric triamide and synthesis of *N*-formylphosphoramides. *Journal of Medicinal Chemistry* **1968,** 11, (5), 958-961.

9. Fueno, H.; Tanaka, K.; Sugawa, S., Theoretical study of the dechlorination reaction pathways of octachlorodibenzo-p-dioxin. *Chemosphere* **2002,** 48, (8), 771-778.

10. Kilic, M.; Kocturk, G.; San, N.; Cinar, Z., A model for prediction of product distributions for the reactions of phenol derivatives with hydroxyl radicals. *Chemosphere* **2007,** 69, (9), 1396-1408.

11. Nonnenberg, C.; van der Donk, W. A.; Zipse, H., Reductive dechlorination of trichloroethylene: A computational study. *Journal of Physical Chemistry A* **2002,** 106, (37), 8708-8715.

12. Ozen, A. S.; Aviyente, V.; Klein, R. A., Modeling the oxidative degradation of azo dyes: A density functional theory study. *Journal of Physical Chemistry A* **2003,** 107, (24), 4898-4907.

13. Zhang, Q. Z.; Qu, X. H.; Wang, W. X., Mechanism of OH-initiated atmospheric photooxidation of dichlorvos: A quantum mechanical study. *Environmental Science & Technology* **2007,** 41, (17), 6109-6116.

14. Eykholt, G. R., Analytical solution for networks of irreversible first-order reactions. *Water Research* **1999,** 33, (3), 814-826.

15. Cances, E.; Mennucci, B.; Tomasi, J., A new integral equation formalism for the polarizable continuum model: Theoretical background and applications to isotropic and anisotropic dielectrics. *Journal of Chemical Physics* **1997,** 107, (8), 3032-3041.

16. Jaky, M.; Szammer, J., Oxidation of aldehydes with permanganate in acidic and alkaline media. *Journal of Physical Organic Chemistry* **1997,** 10, (6), 420-426.

17. Waters, W. A., Mechanisms of oxidation by compounds of chromium and manganese. *Quarterly Reviews* **1958,** 12, (4), 277-300.

18. Wiberg, K. B.; Stewart, R., The mechanisms of permanganate oxidation. I. The oxidation of some aromatic aldehydes. *Journal of the American Chemical Society* **1955,** 77, (7), 1786-1795.

19. Bakke, J. M.; Bethell, D., The mechanism of RuO_4-mediated oxidations of saturated hydrocarbons. Reactivity, kinetic isotope effect and activation parameters. *Acta Chemica Scandinavica* **1992,** 46, (7), 644-649.

20. Du, X. H.; Houk, K. N., Transition states for alkane oxidations by dioxiranes. *Journal of Organic Chemistry* **1998,** 63, (19), 6480-6483.

21. Glukhovtsev, M. N.; Canepa, C.; Bach, R. D., The nature of the transition structure for the oxidation of alkanes with dioxiranes. *Journal of the American Chemical Society* **1998,** 120, (40), 10528-10533.

22. Jones, A. R., Further metabolites of hexamethylphosphoramide. *Biochemical Pharmacology* **1970,** 19, (2), 603-604.

23. Zijlstra, J. A.; Brussee, J.; Vandergen, A.; Vogel, E. W., Importance of multiple hydroxylated metabolites in hexamethylphosphoramide (HMPA)-mediated mutagenesis in *Drosophila melanogaster*. *Mutation Research* **1989,** 212, (2), 193-211.

24. Ashby, J.; Lefevre, P. A., Formaldehyde Generators - Relationship between Stability, Lipophilicity and Carcinogenic Potency. *Carcinogenesis* **1982,** 3, (11), 1273-1276.

25. Noodleman, L.; Lovell, T.; Han, W. G.; Li, J.; Himo, F., Quantum chemical studies of intermediates and reaction pathways in selected enzymes and catalytic synthetic systems. *Chemical Reviews* **2004,** 104, (2), 459-508.

26. Niu, S. Q.; Hall, M. B., Comparison of Hartree-Fock, density functional, Moller-Plesset perturbation, coupled cluster, and configuration interaction methods for the migratory insertion of nitric oxide into a cobalt-carbon bond. *Journal of Physical Chemistry A* **1997,** 101, (7), 1360-1365.

27. Zhang, Q.; Bell, R.; Truong, T. N., *Ab initio* and density functional theory studies of proton transfer reactions in multiple hydrogen bond systems. *Journal of Physical Chemistry* **1995,** 99, (2), 592-599.

CHAPTER 5

DETERMINATION OF HMPA AND OTHER HIGHLY POLAR PHOSPHORAMIDES IN WATER SAMPLES USING REVERSED-PHASE LIQUID CHROMATOGRAPHY / ELECTROSPRAY IONIZATION TIME-OF-FLIGHT MASS SPECTROMETRY

Introduction

Hexamethylphosphoramide (HMPA) is a polar aprotic organophosphorus compound which is highly soluble in both aqueous and organic phases. These unique properties led to its extensive application as a solvent for gases, organic and organometallic compounds, as a polymerization catalyst, UV inhibitor in plastic, processing solvent for aromatic polyamide fiber, and for many other purposes (*1, 2*). The widespread use of HMPA has raised potential health concerns due to occupational exposure, for which skin absorption and inhalation are the major uptake mechanisms (*3*), as well as due to contaminated groundwater, which has been found in the U.S. (*4*). The acute toxicity of HMPA is low to moderate (*3*), but it has been classified as a possible human carcinogen (Group 2B) by IARC (*5*). Furthermore, HMPA and several of its oxidation products were shown to be mutagenic in *Drosophila*, which possesses metabolizing enzymes similar to those in mammals, such as cytochrome P-450 (*6*).

The oxidative metabolism of HMPA was proposed to proceed via sequential *N*-demethylation. Pentamethylphosphoramide (PMPA), tetramethylphosphoramide

(TetMPA), and trimethylphosphoramide (TriMPA) were detected in the excreta of mice, rats, and house flies through thin layer chromatography (TLC) coupled with infrared (IR) spectroscopy as well as gas chromatography in combination with a flame photometric detector (*3, 7, 8*). The generation of formaldehyde during demethylation led to the assumption that HMPA is initially oxidized to the mutagen hydroxymethyl-pentamethylphosphoramide (HM-PMPA), which then decomposes to produce formaldehyde and PMPA (*6, 8*). However, none of the applied analytical methods was capable of HM-PMPA detection. As minor metabolites, formylated oxidation products were detected in rat urine via TLC and IR spectroscopy (*9*).

Using gas-liquid partition chromatography coupled with IR and proton magnetic resonance spectroscopy as well as mass spectrometry, non-oxygenated and formylated reaction intermediates were identified from the abiotic oxidation of HMPA by permanganate (*10*), an oxidizing agent that is frequently used for drinking water, waste water, and groundwater treatment (*11*). Again, it was speculated that HM-PMPA was the precursor of formyl-pentamethylphosphoramide (formyl-PMPA). However, the applied methods were not capable of detecting any of the mutagenic hydroxymethylated reaction intermediates.

An analytical method based on liquid chromatography had not been developed, until it was shown for the first time in Chapter 2, using reversed-phase liquid chromatography (RPLC) in combination with electrospray ionization time-of-flight mass spectrometry (ESI-TOF-MS), that hydroxymethylated as well as minor amounts of carboxylated intermediates are formed from the oxidation of HMPA by aqueous permanganate (Figure 5.1). However, chromatographic separation was only performed for

the comparatively less polar products formed during the initial stage of the oxidation experiment.

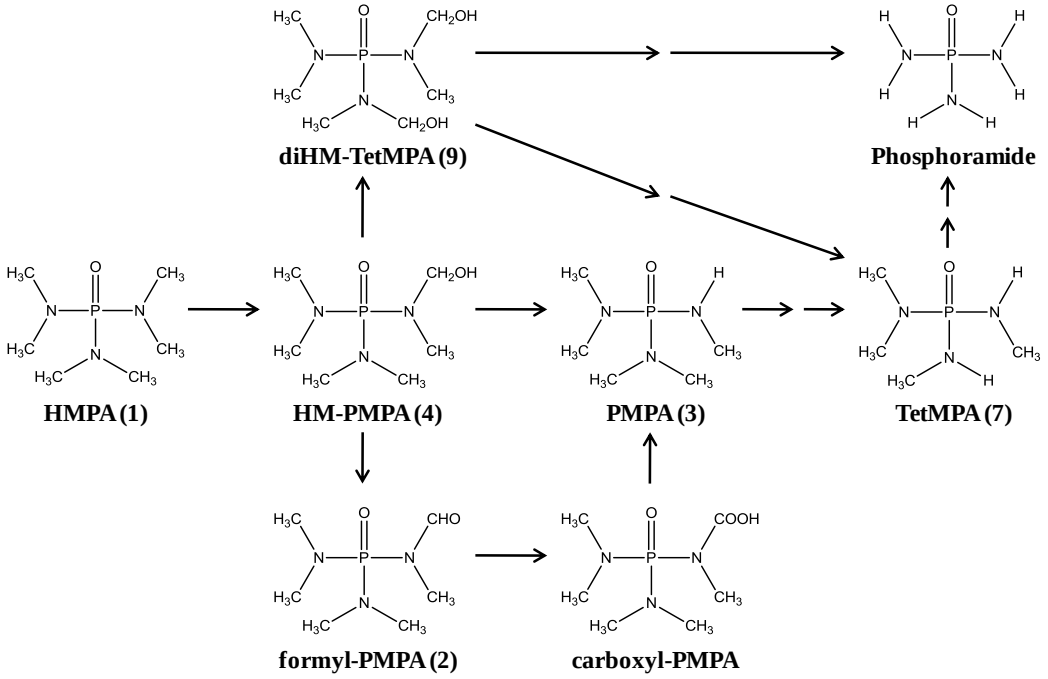

Figure 5.1: Degradation pathway for HMPA oxidation by aqueous permanganate. Numbers in parentheses refer to peak numbers in Table 5.1.

Thus, the objective of this Chapter was to develop an RPLC/ESI-TOF-MS method that is capable of separating and identifying all products of abiotic, as well as the proposed products of biotic HMPA oxidation. Furthermore, the impact of (forced) acid hydrolysis on separation characteristics is investigated. After testing several different RPLC columns, only two columns revealed satisfactory chromatographic separation: an XTerra Phenyl and an XBridge Phenyl column. The XTerra column is a first-generation organic-inorganic hybrid, produced from tetraethylsiloxane and methyltriethylsiloxane monomers, with a 2-phenylpropyl ligand bonded to the surface and a surface coverage of 2.47 μmol/m^2 (*12*, *13*). The XBridge column is a second-generation hybrid, based on

tetraethylsiloxane and bis(triethoxysilyl)ethane monomers, with a surface-bonded 1-phenylhexyl ligand and a surface coverage of 3.0 μmol/m^2 (*12*).

Experimental Section

Chemicals, Reagents and Materials

Hexamethylphosphoramide (99.1% purity) was purchased from MP Biomedicals (Solon, OH, USA). PMPA, TetMPA and TriMPA (each 97% purity) were custom synthesized and generously provided by E. I. du Pont de Nemours and Company (Wilmington, DE, USA). $KMnO_4$ (certified ACS), $Na_2S_2O_3$ (99.8% purity), and acetonitrile (99.9% purity) were purchased from Fisher Scientific (Fair Lawn, NJ, USA). Formic acid (98% purity) was purchased from Sigma-Aldrich (Steinheim, Germany). Puradisc 25 TF filters with a 0.25 μm pore size PTFE membrane were obtained from Whatman (Sanford, ME, USA). The water used in the preparation of standards, reaction media, and mobile phases was obtained from a Barnstead NANOpure system D8991 (Dubuque, IA, USA).

Sample Preparation

To synthesize the analytes that had previously been detected or suggested to be produced from both biotic and abiotic HMPA oxidation, HMPA was oxidized by aqueous permanganate, since this reaction was shown to lead to the formation of singly and multiply hydroxymethylated, formylated, and less methylated reaction intermediates (Chapter 2). In a 1-L Pyrex media glass bottle, an 800 mL solution containing 2.5 mM HMPA and 60 mM $KMnO_4$ in DI water was prepared. The bottle was sealed with a

PTFE-faced silicone septum and stored in the dark at 22 ºC without agitation. Samples were collected after 10 minutes, 6 hours, and 72 hours. For the early-stage oxidation (i.e., 10 minute) sample, 80 μL of the reaction solution were quenched by adding 7.92 mL of 6 mM $Na_2S_2O_3$ (1:100 dilution). For the mid- (i.e., 6 hour) and late-stage oxidation (i.e., 72 hour) samples, 800 μL of the reaction solution were quenched by adding 7.2 mL of 60 mM $Na_2S_2O_3$ (1:10 dilution). The lower dilution for the mid- and late-stage oxidation samples was applied due to decreased detector sensitivity for the more polar analytes. All quenched samples were vortexed until brown flocculates developed. Polytetrafluoroethylene (PTFE) filters were pre-flushed with 5 mL of quenched sample solution. Subsequently, 1.6 mL sample solution was filtered and analyzed immediately.

HPLC Chromatography

Analyses were performed on an Agilent 1100 Series liquid chromatograph (Agilent Technologies, Waldbronn, Germany) equipped with a vacuum degasser, a binary pump, an autosampler, and a temperature-controlled column compartment. Masshunter software (B.02.00) was used for instrument control, data acquisition, and analysis.

Initially, different columns were tested for chromatographic performance, however, with dissatisfactory results. A Supelcosil C_8 column (Supelco, 150 mm × 4.6 mm I.D., 5 μm), an Allure Biphenyl column (Restek, 150 mm × 3.2 mm I.D., 5 μm), and two Atlantis HILIC Silica columns (Waters, 100 mm × 4.6 mm I.D., 3 μm, and 50 mm × 4.6 mm I.D., 5 μm) showed peak broadening and poor separation performance. An XTerra Phenyl column (Waters, 250 mm × 4.6 mm I.D., 3.5 μm) revealed impractical (i.e., too long) retention times. Satisfactory chromatographic performance was achieved

using an XBridge Phenyl (Waters, 250 mm × 4.6 mm I.D., 3.5 μm) and an XTerra Phenyl column (Waters, 150 mm × 2.1 mm I.D., 5 μm), latter one, however, only after chemical modification as discussed below. These two columns were then used for method optimization.

Using the XBridge Phenyl column, separation for the early-stage oxidation sample was carried out isocratically with A (0.1% formic acid) and B (acetonitrile) at a ratio of 85:15 (XBridge method 1). While XBridge method 1 was capable of separating the early oxidation products HM-PMPA, formyl-PMPA, and PMPA, the separation performance for the higher oxidized products formed during the middle and late stage of HMPA oxidation was poor. Thus, for the mid- and late-stage oxidation samples, gradient elution was applied: 0-3 min, 0% B; 3-10 min, 0-15% B; 10-15 min, 15% B, 15-30 min, 0% B (XBridge method 2). For all samples, the injection volume was 5 μL, the flow rate was 1.2 mL/min, and the temperature was controlled at 30 °C.

Two pristine (150 and 250 mm long) XTerra Phenyl columns were initially tested under the same conditions as the XBridge Phenyl column. However, both columns revealed impractically long retention times, and substantially longer retention times than an aged, extensively-used 150 mm XTerra column that was tested previously (see Chapter 2). It was assumed that the stationary phase in the aged column had been altered due to hydrolysis reactions of siloxane bonds (for details, see the Results & Discussion section). Consequently, the pristine 150 mm XTerra Phenyl column was stored in 100% of 0.1% formic acid (pH 2.7) for two months, and six more months in 0.01% formic acid / acetonitrile (98:2, pH 3.1) to test this hypothesis. After storage of the 150 mm XTerra Phenyl column in acidic (formic acid) solution, separation of all samples was carried out

using gradient elution: 0-10 min, 0% B; 10-12 min, 0-5% B; 12-20 min, 5% B, 20-30 min, 0% B. The injection volume was 5 µL, the flow rate was 0.5 mL/min, and the temperature was controlled at 30 °C.

Mass Spectrometry

The HPLC was connected to an Agilent G3250AA MSD TOF system (Agilent Technologies, Wilmington, DE, USA) with an electrospray ionization (ESI) source (ESI-TOF-MS). The capillary, fragmentation, and skimmer voltages were 800 V, 130 V, and 60 V, respectively. The temperature of the drying gas (N_2) was 350 °C, the flow rate of the drying gas was 12 L/min, and the pressure of the nebulizer gas (N_2) was 50 psi. The mass analyzer was calibrated from *m/z* 90 to 600 in positive ionization mode.

Calibration, LOD, LOQ and Precision

Stock solutions containing the four available reference compounds (HMPA, PMPA, TetMPA, and TriMPA) were prepared and diluted to appropriate concentrations for the generation of ten-point calibration curves. Each concentration was injected in triplicates, using the XBridge Phenyl column and XBridge method 1. The limits of detection (LOD) and quantification (LOQ) were determined at a signal-to-noise ratio (S/N) of 3 and 10, respectively. The inter-day variability, expressed through the relative standard deviation (%RSD), was determined to assess the precision of the analytical method. For this purpose, one mixed standard solution was analyzed on six consecutive days.

Theoretical Calculations

Retention times (t_R), retention time factors (k'), and chromatographic resolution (R_S) were calculated for all compounds. k' was determined from $k' = (t_R - t_M) / t_M$, where t_M is the void time. R_S was calculated using the half-width method.

To determine analyte polarity, dipole moments were calculated using the Gaussian 03 software package. All molecular structures were initially optimized to a ground state (verified by absence of imaginary frequencies), and their dipole moments in aqueous phase were determined at the B3LYP/6-311++G(d,p) level of theory including the IEFPCM solvation model.

Results and Discussion

Reversed-Phase Liquid Chromatography

For the XBridge Phenyl column, it was generally observed that decreasing acetonitrile concentrations in the mobile phase led to increasing retention times. Three of the initial HMPA oxidation products, HM-PMPA, formyl-PMPA, and PMPA, were successfully separated (R_S > 1.5, Table 5.1) under isocratic conditions at 0.1% formic acid / acetonitrile (85:15) (Figure 5.2a). The fact that the retention time for PMPA was 0.22 min higher than for HM-PMPA and 0.22 min lower than for formyl-PMPA (Table 5.1) confirms that 15% acetonitrile was the optimal concentration in the mobile phase. At higher acetonitrile concentrations, PMPA and formyl-PMPA were not separated, at lower acetonitrile concentrations, PMPA and HM-PMPA were not separated. Also, an increase in temperature of up to 50 °C only led to poorer separation performance.

Table 5.1: TOF-MS characteristics, retention times (t_R), retention time factors (k'), and chromatographic resolution (R_S) for HMPA and its detected oxidation products. Relative standard deviation of t_R and k' < 1% (n = 5) for all compounds and all methods.

							XBridge method 1			XBridge method 2			XTerra		
Compound	Peak no.	Base peak	Base peak formula	Observed *m/z*	Theoretical *m/z*	Error (ppm)	t_R (min)	k'	R_S	t_R (min)	k'	R_S	t_R (min)	k'	R_S
HMPA	1	$[M+H]^+$	$C_6H_{19}N_3OP^+$	180.1261	180.1260	0.6	7.75	2.69	>1.5				17.43	19.50	>1.5
formyl-PMPA	2	$[M+H]^+$	$C_6H_{17}N_3O_2P^+$	194.1053	194.1053	0.0	4.38	1.09	>1.5	12.86	4.85	>1.5	9.42	10.08	1.00
PMPA	3	$[M+H]^+$	$C_5H_{17}N_3OP^+$	166.1110	166.1104	3.6	4.16	0.98	>1.5	12.40	4.64	>1.5	6.95	7.17	>1.5
HM-PMPA	4	$[M+H]^+$-H_2O	$C_6H_{17}N_3OP^+$	178.1106	178.1104	1.1	3.94	0.87	>1.5				8.71	9.24	>1.5
formyl-TetMPA	5	$[M+H]^+$	$C_5H_{15}N_3O_2P^+$	180.0899	180.0896	1.7	3.19	0.52	1.27	10.43	3.74	>1.5	2.95	2.47	0.37
formyl-HM-TetMPA	6	$[M+H]^+$-H_2O	$C_6H_{15}N_3O_2P^+$	192.0902	192.0896	3.1	3.07	0.46	0.48				2.95	2.47	0.00
TetMPA	7	$[M+H]^+$	$C_4H_{15}N_3OP^+$	152.0949	152.0947	1.3	3.02	0.44	1.01	9.81	3.46	>1.5	2.26	1.66	>1.5
HM-TetMPA	8	$[M+H]^+$-H_2O	$C_5H_{15}N_3OP^+$	164.0948	164.0947	0.6	2.90	0.38	0.23				2.45	1.88	0.94
diHM-TetMPA	9	$[M+H]^+$-H_2O	$C_6H_{17}N_3O_2P^+$	194.1052	194.1053	-0.5	2.86	0.36	>1.5				2.83	2.32	1.12
formyl-TriMPA	10	$[M+H]^+$	$C_4H_{13}N_3O_2P^+$	166.0739	166.0740	-0.6				6.41	1.91	>1.5	1.38	0.63	1.13
TriMPA	11	$[M+H]^+$	$C_3H_{13}N_3OP^+$	138.0794	138.0791	2.2				5.56	1.65	>1.5	1.24	0.46	1.45
formyl-DiMPA	12	$[M+H]^+$	$C_3H_{11}N_3O_2P^+$	152.0584	152.0583	0.7				3.93	0.79	>1.5	1.06	0.25	0.78
DiMPA	13	$[M+H]^+$	$C_2H_{11}N_3OP^+$	124.0635	124.0634	0.8				3.39	0.54	>1.5	0.98	0.15	1.49
formyl-MonoMPA	-	$[M+H]^+$	$C_2H_9N_3O_2P^+$	138.0423	138.0427	-2.9				2.75	0.25	>1.5	*non-retained*		
MonoMPA	-	$[M+H]^+$	$C_1H_9N_3OP^+$	110.0473	110.0478	-4.5				2.57	0.17	>1.5	*non-retained*		
Phosphoramide	-	$[M+H]^+$	$H_7N_3OP^+$	96.0319	96.0321	-2.1				2.34	0.06	1.45	*non-retained*		

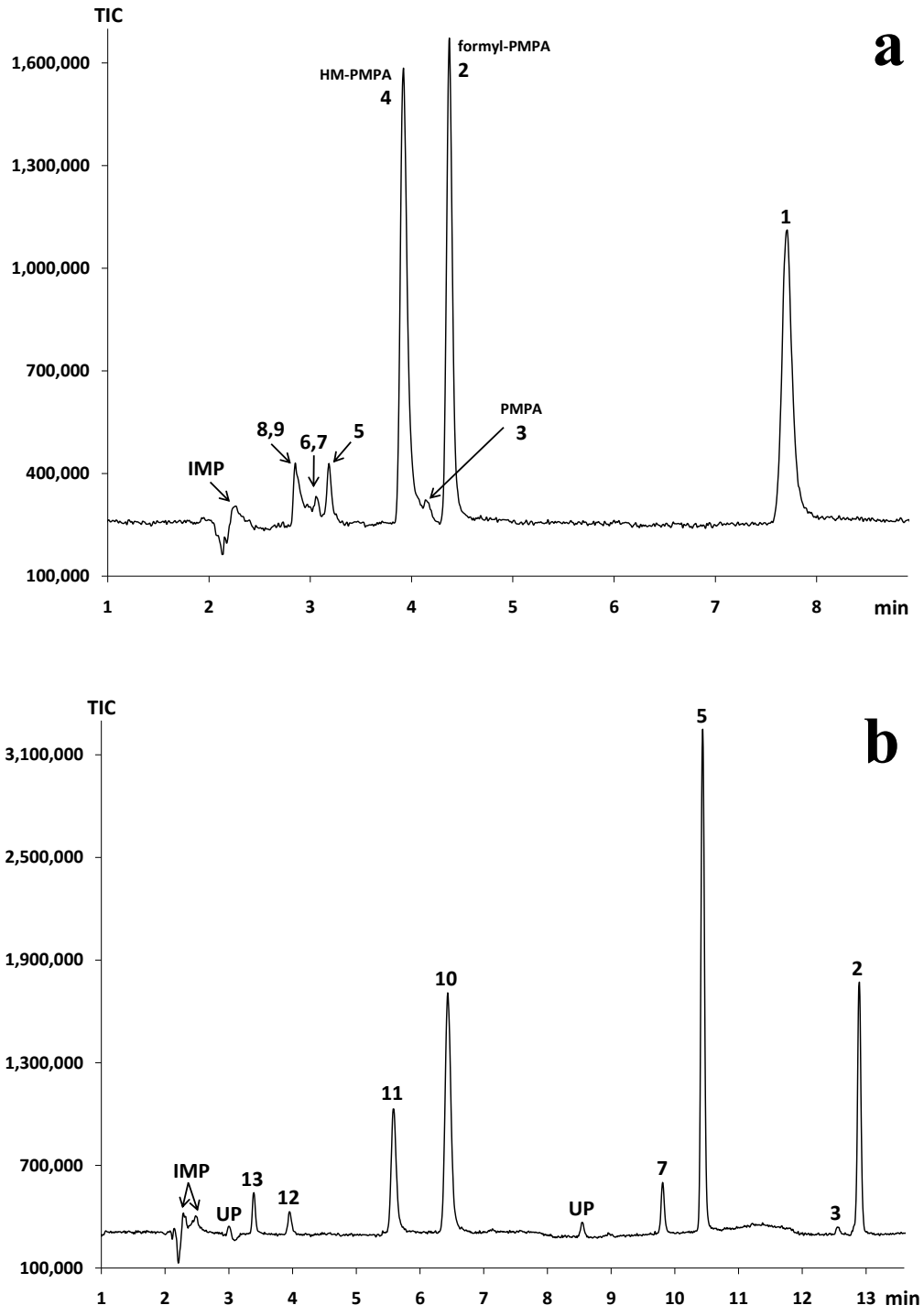

Figure 5.2: XBridge Phenyl chromatogram of (a) the early-stage oxidation sample using method 1 and (b) the mid-stage oxidation sample using method 2. The peak numbers are listed in Table 5.1 (IMP: impurity from Teflon filter; UP: unidentified peak).

The acetonitrile concentration of 15%, however, resulted in co-elution or poor separation of four of the more oxidized and polar tetramethylphosphoramide derivatives (peaks 6 - 9 in Figure 5.2a), as indicated by their low R_S values between 0.23 and 1.01 (Table 5.1). Thus, two methods were developed: the isocratic method 1 for the early-stage oxidation sample, where HM-PMPA, formyl-PMPA, and PMPA were all present, and the gradient method 2 with an initially lower acetonitrile concentration for the mid- and late-stage oxidation samples, where only non-oxygenated and formylated, but no hydroxymethylated reaction intermediates were present.

The chromatogram in Figure 5.2b reveals that, after 6 hours of reaction with permanganate (mid-stage oxidation), no hydroxymethylated intermediates are present, probably due to their faster oxidation or decomposition kinetics compared to the accumulating formylated and non-oxygenated compounds. Using method 2, baseline separation of all detected oxidation products was achieved (Table 5.1; Figure 5.2b). Phosphoramide, the end product of HMPA oxidation by permanganate (Figure 5.1), which was detected in the late-stage oxidation sample, was slightly retained with a retention time of 2.34 minutes compared to a void time of 2.1 minutes (R_S = 1.45). A stronger retention could not be achieved since, during the first three minutes of the chromatographic run, acetonitrile had to be absent in the mobile phase for optimal separation of the other analytes.

For column comparison, separation of the four phosphoramide-based reference compounds was initially attempted with an XTerra Phenyl column of the same dimensions as the XBridge Phenyl column (250 mm × 4.6 mm I.D., 3.5 μm), the differences only being a different structure of the surface-bonded phenylalkyl group and a

slightly lower surface coverage as noted in the Introduction. In contrast to the XBridge column, however, decreasing acetonitrile concentrations in the mobile phase led to decreasing retention times for the pristine XTerra Phenyl column, a behavior typical for normal phase chromatographic conditions. Furthermore, even under the fastest possible chromatographic conditions of 0% acetonitrile and a flow rate of 1.3 mL/min (which was not further increased due to a back pressure of 330 bar), retention times were impractically long, with 48 minutes for PMPA and 319 minutes for HMPA. A difference in the chromatographic performance between the XBridge Phenyl and the XTerra Phenyl columns can be expected since the different structure of the phenyl-containing ligands of the two columns may lead to differences in solvation and retention properties. However, the magnitude of the observed differences for the investigated phosphoramide-based compounds was substantially larger than the one reported by Kiridena and co-workers (*12*). They compared the separation characteristics of an XBridge Phenyl column and an XTerra Phenyl column using an acetonitrile-water mobile phase (acetonitrile ≥10%) for 70 analytes, including reduced and oxidized hydrocarbons as well as nitro, amino, and *N*-heterocyclic compounds, but no (highly polar) organophosphorus compounds. In their study, it was observed that the chromatographic performance of the two columns was quite similar under reversed-phase separation conditions.

A shorter, pristine XTerra Phenyl column was also used (150 mm × 2.1 mm I.D., 5 μm), which still resulted in impractically long retention times (HMPA 116 min at 0% acetonitrile, 0.5 mL/min, and 300 bar). Since the analytes had been successfully separated with an aged XTerra Phenyl column, it was hypothesized that the aged column had undergone severe ageing or hydrolysis, resulting in altered chromatographic behaviour.

Thus, the impact of column storage in acidic solution on chromatographic performance to simulate a potential ageing process was investigated by flushing with 100% of 0.1% formic acid (pH 2.7) followed by two months storage. Storage at low pH greatly decreased retention times (e.g., HMPA 11.3 min at 2% acetonitrile, 0.5 mL/min), and also reversed the effect of acetonitrile concentration in the mobile phase, with decreasing acetonitrile concentrations in the mobile phase now leading to increasing retention times, as observed for the XBridge Phenyl column. The chromatographic performance of the modified XTerra Phenyl column after two months of storage in acidic solution is reported in Chapter 2. It is suspected that hydrolysis of the stationary phase altered the surface composition, since it has been shown that acids can catalyze the hydrolysis of siloxane bonds (Si-O-Si) to produce surface silanol groups (Si-OH) (*14-16*) according to:

Substrate-Si-O-Si-R + *HCOOH* ↔ *Substrate-Si-OH* + *R-Si-COOH*

Collection of the hydrolysate from the column and analysis it via ESI-TOF-MS was attempted, however, without success.

The modified XTerra Phenyl column was then stored for six months in a slightly higher pH solution of 0.01% formic acid / acetonitrile (98:2, pH 3.1) and frequently used for HMPA analyses. During this time, the retention times continued to decrease (HMPA 11.3 min to 10.0 min at 2% acetonitrile, 0.5 mL/min), indicating further hydrolysis. At this point in time, the column was used for the method development reported here (Table 5.1, Figure 5.3a and b), and storage conditions were changed to DI water / acetonitrile (50:50) to minimize hydrolysis.

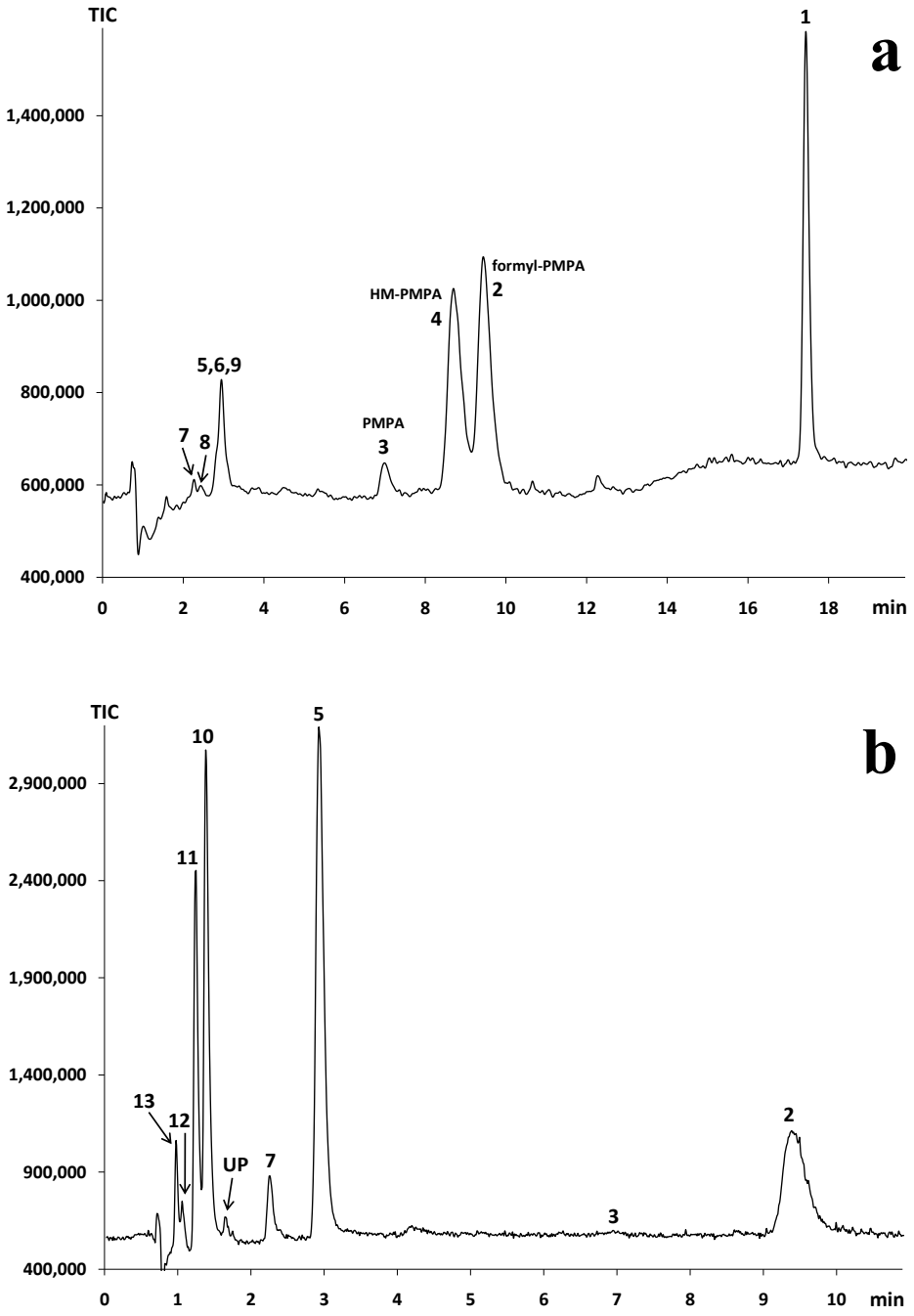

Figure 5.3: XTerra Phenyl chromatogram of (a) the early-stage oxidation sample and (b) the mid-stage oxidation sample. The peak numbers are listed in Table 5.1 (UP: unidentified peak).

For the modified XTerra Phenyl column, one gradient method was developed and applied to all samples. The initial HMPA oxidation products HM-PMPA and formyl-PMPA were not completely baseline-separated in the early-stage oxidation sample (R_S = 1.00, Figure 5.3a), but good separation was achieved for PMPA (R_S > 1.5). Poor separation, however, was observed for the tetramethylphosphoramides (peaks 5 - 9) when hydroxymethylated derivatives were present. Only in the mid-stage oxidation sample (Figure 5.3b), in which only non-oxygenated and formylated compounds were detected, the two present tetramethylphosphoramides (peaks 5 & 7) were completely baseline-separated. With increasing analyte polarity (decreasing number of methyl substituents), the chromatographic performance deteriorated. Both TriMPA (peak 11) and dimethylphosphoramide (DiMPA, peak 13) were not fully separated from their respective formylated derivative (peaks 10 or 12, R_S = 1.13 or 0.78, respectively). The very polar methylphosphoramide (MonoMPA), formyl-methylphosphoramide (formyl-MonoMPA), and phosphoramide were not retained on the modified XTerra Phenyl column, and stronger retention could not be achieved due to the absence of acetonitrile in the mobile phase (i.e., mobile phase composition 100% of 0.1% formic acid).

For the two XBridge methods as well as the XTerra method, it can be seen that the elution order was mainly determined by the number of methyl substituents, i.e., HMPA had the highest retention time, followed by the pentamethylphosphoramides, then the tetramethylphosphoramides, and so forth. This behavior indicates that hydrophobic interactions between the methyl groups and the surface-bonded alkylphenyl ligands were the major retention mechanism.

Within one group of phosphoramides with the same number of methyl substituents, however, differences in the elution order were observed as a function of mobile phase composition. When acetonitrile concentrations were ≤9% on the XBridge Phenyl column and ≤10% on the XTerra Phenyl column, the general elution order was -H, -CH_2OH, -CHO (for instance, PMPA, HM-PMPA, formyl-PMPA). At higher acetonitrile concentrations, the general elution order -CH_2OH, -H, -CHO was observed on both columns. Quantum chemical calculations of the dipole moments revealed that the order of polarity for the pentamethylphosphoramides is PMPA (6.2 Debye) > HM-PMPA (4.7 Debye) > formyl-PMPA (1.6 Debye). Thus, at low acetonitrile concentrations, the XBridge and XTerra Phenyl columns show the expected chromatographic performance under reversed-phase conditions, while at higher acetonitrile concentrations, the elution order of PMPA and HM-PMPA was inverted. This behavior can likely be explained by a collapse of the stationary phase. Stationary phase collapse in reversed-phase columns is believed to occur when the hydrophobic surface functional groups minimize their surface energy through self-association due to a highly aqueous and polar mobile phase (*17, 18*). Thus, at low acetonitrile concentrations, the collapse of the stationary may lead to a complete shielding of the underlying polar silicon-containing groups (*17*, *18*). The major retention mechanism is then governed by analyte sorption on top of the collapsed bonded layer based on hydrophobic interactions (*18*), in agreement with the observed elution order PMPA, HM-PMPA, which solely follows analyte polarity. A high acetonitrile concentration on the other hand allows the hydrophobic phenyl ligands to be solvated and extended away from the surface. The analytes may then partition into the stationary phase surface (i.e., in between the phenyl ligands) to also interact with siloxane and silanol

functional groups (*17*). This enables additional hydrophilic interactions and thus inverted elution orders with respect to reversed-phase chromatography (*19*), as observed here for PMPA and HM-PMPA.

Time-Of-Flight Mass Spectrometry

Capillary, fragmentation, and skimmer voltages as well as drying gas flow rate and nebulizer gas pressure were initially optimized to maximize detector sensitivity for the phosphoramide compounds. The calibration curves for the four available reference compounds HMPA, PMPA, TetMPA, and TriMPA (Table 5.2) were obtained by plotting total ion current (TIC) against concentration. The correlation coefficients revealed good linearity ($R^2 \geq 0.998$) over the linear range of less than two orders of magnitude for all reference compounds. The slopes of the linear regression equations revealed that the detector sensitivity decreased with increasing polarity of the analytes (i.e., decreasing degree of methylation). This is likely due to a decreased affinity of more polar compounds for the ESI droplet surface, where excess charge exists, and/or decreasing ion evaporation rates from the ESI droplets with increasing analyte polarity or solvation energy, respectively (*20*). Moreover, the linear range decreased with increasing analyte polarity, while LOD and LOQ (0.10 - 0.28 μM and 0.34 - 0.93 μM, respectively) increased with increasing analyte polarity. The inter-day variabilities for all four reference compounds showed an acceptable precision of the method (6.9 - 10.7 % RSD).

Identification of HMPA oxidation intermediates was performed via TOF-MS accurate mass measurement. Table 5.1 lists measured observed mass-to-charge ratios (*m/z*) and errors with respect to the theoretical masses for all detected compounds, including di- and monomethylated phosphoramides as well as phosphoramide, which

were detected in the late-stage oxidation sample. Fragmentation of all structures occurred at the P-N bond, in agreement with previous observations for cyclophosphamide, *N,N',N''*-triethylenephosphoramide, and *N,N',N''*-triethylenethiophosphoramide (*21*).

Table 5.2: Linear regression data, linear range, limit of detection (LOD), limit of quantification (LOQ), and inter-day variability for the reference compounds.

Analyte	HMPA	PMPA	TetMPA	TriMPA
Linear Regression Equation	y = 1,680,000x +66,000	y = 1,190,000x +196,000	y = 834,000x +194,000	y = 597,000x +244,000
R^2	0.9991	0.9980	0.9995	0.9988
Linear dynamic range [µM]	0.34 - 30	0.48 - 15	0.66 - 15	0.93 - 15
LOD [µM]	0.10	0.14	0.20	0.28
LOQ [µM]	0.34	0.48	0.66	0.93
Inter-day variability (% RSD, n=6)	7.0	6.9	8.6	10.7

Analyses for carboxylated oxidation products in negative ionization mode were not performed since these were shown to be produced in minor amounts only (Chapter 2).

Conclusion

A novel RPLC/ESI-TOF-MS method was developed, which is the first and currently only method that can be used to separate and detect HMPA and all of its biotic and abiotic oxidation products. Whereas the use of several different columns failed to achieve satisfactory chromatographic performance, only an XBridge Phenyl and an XTerra Phenyl column were capable of separating the majority of the phosphoramide-based analytes. The advantage of the XBridge Phenyl column is a better separation performance through the use of two elution methods, especially for the very polar mid-

and late-stage oxidation products with low degree of methylation, as well as for the early-stage oxidation products HM-PMPA and formyl-PMPA, which are the major initial products of abiotic oxidation by permanganate. Furthermore, the column can be used for separation of phosphoramide-based compound without previous modifications. The advantage of the formic acid-modified XTerra Phenyl column is that one elution method can be applied for all stages of oxidation, and that the early-stage oxidation product PMPA is baseline-separated from the oxygenated HM-PMPA and formyl-PMPA. This can be advantageous for biological systems, where formylated intermediates are only minor oxidation products (*6, 9*).

The pristine XTerra Phenyl column showed a substantially different chromatographic behavior from the XBridge Phenyl column, with acetonitrile concentrations in the mobile phase having an opposite effect on retention times as well as revealing impractically long retention times. Only after storage in low-pH formic acid solution, the chromatographic performance of the XTerra Phenyl column was altered in a way suitable for phosphoramide analysis, most likely due to hydrolysis of the siloxane bonds in the stationary phase.

References

1. Keller, D. A.; Marshall, C. E.; Lee, K. P., Subchronic nasal toxicity of hexamethylphosphoramide administered to rats orally for 90 days. *Fundamental and Applied Toxicology* **1997,** 40, (1), 15-29.

2. Normant, H., Hexamethylphosphoramide. *Angewandte Chemie - International Edition* **1967,** 6, (12), 1046-1067.

3. Mihal, C. P., The determination of parts-per-billion concentrations of hexamethylphosphoramide and its metabolite, pentamethylphosphoramide, in urine. *American Industrial Hygiene Association Journal* **1987,** 48, (12), 997-1000.

4. Campos, D., Field demonstration of UV/H_2O_2 on the treatment of groundwater contaminated with HMPA. In *Chemical Oxidation: Technologies for the Nineties.*, Eckenfelder, W. W.; Bowers, A. R.; Roth, J. A., Eds. Technomic Publishing Company: Lancaster, PA, 1997; Vol. 6, pp 19-26.

5. IARC, *Re-evaluation of Some Organic Chemicals, Hydrazine, and Hydrogen Peroxide. IARC Monographs on the Evaluation of Carcinogenic Risk of Chemicals to Humans, Vol. 71*; International Agency for Research on Cancer: Lyon, France, 1999; p 1589.

6. Zijlstra, J. A.; Brussee, J.; Vandergen, A.; Vogel, E. W., Importance of multiple hydroxylated metabolites in hexamethylphosphoramide (HMPA)-mediated mutagenesis in *Drosophila melanogaster*. *Mutation Research* **1989,** 212, (2), 193-211.

7. Chang, S. C.; Terry, P. H.; Woods, C. W.; Borkovec, A. B., Metabolism of Hempa uniformly labeled with C^{14} in male house flies. *Journal of Economic Entomology* **1967,** 60, (6), 1623-1631.

8. Jones, A. R.; Jackson, H., Metabolism of hexamethylphosphoramide and related compounds. *Biochemical Pharmacology* **1968,** 17, (11), 2247-2252.

9. Jones, A. R., Further metabolites of hexamethylphosphoramide. *Biochemical Pharmacology* **1970,** 19, (2), 603-604.

10. Terry, P. H.; Borkovec, A. B., Insect chemosterilants. 4. Oxidation of hexamethylphosphoric triamide and synthesis of *N*-formylphosphoramides. *Journal of Medicinal Chemistry* **1968,** 11, (5), 958-961.

11. Schnarr, M.; Truax, C.; Farquhar, G.; Hood, E.; Gonullu, T.; Stickney, B., Laboratory and controlled field experiments using potassium permanganate to remediate trichloroethylene and perchloroethylene DNAPLs in porous media. *Journal of Contaminant Hydrology* **1998,** 29, (3), 205-224.

12. Kiridena, W.; Atapattu, S. N.; Poole, C. F.; Koziol, W. W., Comparison of the separation characteristics of the organic-inorganic hybrid stationary phases XBridge C_8 and phenyl and XTerra phenyl in RP-LC. *Chromatographia* **2008,** 68, (7-8), 491-500.

13. Neue, U. D.; O'Gara, J. E.; Méndez, A., Selectivity in reversed-phase separations: Influence of the stationary phase. *Journal of Chromatography A* **2006,** 1127, (1-2), 161-174.

14. Fazio, S. D.; Tomellini, S. A.; Hsu, S. H.; Crowther, J. B.; Raglione, T. V.; Floyd, T. R.; Hartwick, R. A., Chemical characterization of bonded stationary phases for high-performance liquid-chromatography using hydrofluoric acid digestion and gas-chromatography. *Analytical Chemistry* **1985,** 57, (8), 1559-1564.

15. Haghedooren, E.; Farkas, E.; Kerner, A.; Dragovic, S.; Noszal, B.; Hoogmartens, J.; Adams, E., Effect of long-term storage and use on the properties of reversed-phase liquid chromatographic columns. *Talanta* **2008,** 76, (1), 172-182.

16. Trammell, B. C.; Boissel, C. A.; Carignan, C.; O'Shea, D. J.; Hudalla, C. J.; Neue, U. D.; Iraneta, P. C., Development of an accelerated low-pH reversed-phase liquid chromatography column stability test. *Journal of Chromatography A* **2004,** 1060, (1-2), 153-163.

17. Przybyciel, M.; Majors, R. E., Phase collapse in reversed-phase LC. *LC GC Europe* **2002,** 15, (10), 652-656.

18. Rustamov, I.; Farcas, T.; Ahmed, F.; Chan, F.; LoBrutto, R.; McNair, H. M.; Kazakevich, Y. V., Geometry of chemically modified silica. *Journal of Chromatography A* **2001,** 913, (1-2), 49-63.

19. Nguyen, H. P.; Schug, K. A., The advantages of ESI-MS detection in conjunction with HILIC mode separations: Fundamentals and applications. *Journal of Separation Science* **2008,** 31, (9), 1465-1480.

20. Cech, N. B.; Enke, C. G., Relating electrospray ionization response to nonpolar character of small peptides. *Analytical Chemistry* **2000,** 72, (13), 2717-2723.

21. de Jonge, M. E.; van Dam, S. M.; Hillebrand, M. J. X.; Rosing, H.; Huitema, A. D. R.; Rodenhuis, S.; Beijnen, J. H., Simultaneous quantification of cyclophosphamide, 4-hydroxycyclophosphamide, *N,N',N''*-triethylenethiophosphoramide (thiotepa) and *N,N',N''*-triethylenephosphoramide (tepa) in human plasma by high-performance liquid chromatography coupled with electrospray ionization tandem mass spectrometry. *Journal of Mass Spectrometry* **2004,** 39, (3), 262-271.

CHAPTER 6

SUMMARY

The research performed in this dissertation was designed to develop a method that can be used to predict the fate of any contaminant in both natural and engineered aqueous environments. Quantum chemical calculations based on density functional theory (DFT) were applied, since these do not require any previous knowledge about a compound of interest. The developed methodology comprises four elements: (1) the prediction of redox reactivity, (2) the prediction of potential degradation pathways, (3) the prediction of contaminant persistence, and (4) the prediction of the primary degradation pathway. Hexamethylphosphoramide (HMPA), a widely used solvent and potential groundwater contaminant, was used to develop and validate the predictive approach. This chapter summarizes the key findings and implications, and discusses model limitations.

For the first time, an approach was developed to estimate the redox reactivity of an aqueous contaminant, i.e., its degradability as a function of redox potential and pH (Chapter 2). Based on quantum chemically calculated Gibbs free energies of reaction, stability lines for a contaminant of interest and its potential oxidation or reduction product(s) are constructed. The subsequent superposition with documented stability lines of common electron acceptors or donors enables the identification of redox zones, in which degradation is favorable. For HMPA, it was estimated that its oxidation to

hydroxymethyl-PMPA is favorable under iron-reducing conditions at low to neutral pH, and nitrate-reducing conditions at high pH. Its oxidation to HMPA *N*-oxide, however, was predicted to be favorable only through the use of very strong oxidants, such as H_2O_2 or ozone, but not permanganate. Experimental validation confirmed that permanganate oxidizes HMPA at the methyl substituent, but not at the nitrogen.

Based on a hypothetical degradation pathway generated through expert knowledge, potential pathways for HMPA degradation in a permanganate-containing aqueous system were predicted (Chapter 2). Gibbs free energies of reaction were used to differentiate thermodynamically favorable and unfavorable transformations. Oxidation of HMPA by permanganate was predicted to proceed through sequential *N*-demethylation. Experimental validation based on LC/TOF-MS analyses confirmed the predicted pathways of HMPA oxidation to phosphoramide via the formation of less methylated as well as singly and multiply oxygenated reaction intermediates. Subsequently, phosphoramide hydrolyzes to ammonia and *o*-phosphate. Pathways predicted to be thermodynamically or kinetically unfavorable were similarly absent in the experimental studies. Thus, HMPA-contaminated water can be successfully remediated through the application of permanganate without accumulation of persistent reaction intermediates.

Hydrolysis of HMPA, however, which was predicted to be the only reaction that may lead to its degradation under strongly reducing conditions, was the only thermodynamically favorable reaction not observed in the permanganate-containing aqueous system. Thus, its persistence in the absence of suitable oxidants was estimated through identification of the kinetically most favorable hydrolysis mechanism and subsequent prediction of rate constants and half-lives (Chapter 3). It was predicted that

the P-N bond in HMPA hydrolyzes via a proton-activated mechanism at pH < 8.2, and a non-activated mechanism at pH 8.2 - 8.5. The estimated half-lives of thousands to hundreds of thousands of years over the groundwater-typical pH range of 6.0 to 8.5 imply that HMPA will be persistent under strongly reducing conditions. At pH 0, where the hydrolysis reaction was rapid enough to enable measurement, the experimentally determined rate constant and half-life were in excellent agreement with the predicted values.

Both quantum chemical and experimental investigations of the mechanism(s) of C-H bond oxidation in HMPA by aqueous permanganate, using ^{18}O-labeled water and ^{16}O-permanganate, revealed that the source of oxygen in the oxidation products is not only the solvent water, as suggested previously in the literature, but also permanganate (Chapter 4). A pseudo-first-order kinetic fit of the experimentally determined HMPA and oxidation product concentrations over time, in combination with theoretical transition state investigations, suggested that HMPA can be oxidized directly to its corresponding aldehyde, circumventing the formation of an alcoholic compound. This novel mechanism for C-H bond oxidation by aqueous permanganate is documented here for the first time.

The two simultaneously proceeding reactions of HMPA oxidation were observed experimentally, one leading to the formation of hydroxymethyl-PMPA and one leading to the formation of formyl-PMPA. These concurrent reactions were used as a proof-of-principle-type test case to conduct a primary degradation pathway prediction (Chapter 4). The general strategy is to determine the respective transition states and the related Gibbs free energy of activation in aqueous phase. It is then the reaction with the lower activation barrier that determines the primary degradation pathway. However, the

quantum chemical calculations were impeded by convergence problems with the IEFPCM solvation model in the applied software package, Gaussian 03. Furthermore, the Gibbs free energies of activation in aqueous phase for these two reactions, as determined by the kinetic model fit, revealed a difference of only 1.2 kJ/mol, thus within the expected error range of ca. 10 - 20 kJ/mol for the applied B3LYP level of theory. Consequently, for this specific test system of HMPA oxidation by aqueous permanganate, even the most accurate quantum chemical calculation can only predict that the two C-H bond oxidation reactions proceed at similar rates.

Finally, a new analytical method based on reverse-phase liquid chromatography / electrospray ionization time-of-flight mass spectrometry (RPLC/ESI-TOF-MS) was developed, which can be used to separate and detect HMPA and its biotic and abiotic oxidation products (Chapter 5). The chromatographic performance of two columns was compared, both of which possessed different advantages depending on the test system and focus of investigation. An XTerra Phenyl column showed better separation of the major metabolic early stage oxidation products PMPA and hydroxymethyl-PMPA, whereas an XBridge Phenyl column showed better separation for the major abiotic early stage oxidation products hydroxymethyl-PMPA and formyl-PMPA. Furthermore, the XBridge Phenyl column revealed a better chromatographic performance for the very polar middle and late stage oxidation products. The pristine XTerra Phenyl column showed very long retention times, which were substantially shortened to practical times after storage in low-pH solution, most likely due to hydrolysis of the siloxane bonds in the stationary phase. The analytical method using the (hydrolyzed) XTerra Phenyl column was applied in all model validation experiments, and enabled the detection of

multiple hydroxymethylated and carboxylated oxidation products of HMPA for the first time.

In theory, the methodology developed here, which is based on the principles of chemical thermodynamics and kinetics, can be applied to any system of interest. However, due to the nature of quantum chemical calculations and due to the complexity of aqueous environments, there are limitations to this approach. These limitations will have to be addressed by future research.

An apparent limitation is computer speed. Depending on system size and level of theory, a single quantum chemical calculation can take several days, weeks, months, and theoretically even longer, even when parallelized over several processors on high performance computer clusters. This compares to a few seconds or less for QSAR-based calculations, however, under the condition that an appropriate QSAR has been developed for the compound of interest, which is often not given for new and emerging contaminants. Thus, although highly accurate quantum chemical models are available (e.g., full configuration interaction (*1*)), practicality usually demands the application of lower level of theories that are associated with a higher error in the predictions.

For some predictions, such as redox potentials and thermodynamic favorability of degradation reactions, an error of ≤0.1 V or ≤20 kJ/mol, respectively, as estimated for the level of theory used in this dissertation, will be accurate enough for most environmental assessments. However, some parameters are highly sensitive to errors in the estimated free energies, such as reaction rates, equilibrium constants, and ionization constants, for which a deviation of only 5.7 kJ/mol from the experimental value results in an error of one order of magnitude under standard conditions. In his Nobel Lecture (*2*), John A.

Pople, one of the pioneers of *ab initio* quantum chemical methods, suggested a general target of ≤ 1 kcal/mol (≤ 4.184 kJ/mol) in error for energy predictions. This is still challenging even with high-level post-Hartree-Fock methods, given that computational capacities allow for their application.

Clearly, the applicability of high levels of theory and consequently the accuracy of quantum chemical calculations will increase over time as a result of continuously increasing computer performance. The development of computer speed thus far has followed Moore's law, which predicted some 40 years ago that computer performance will double every two years (*3*). The example in Figure 6.1 illustrates that the impact of this predicted development over the next 20 years is a decrease in computing time of ca. three orders of magnitude.

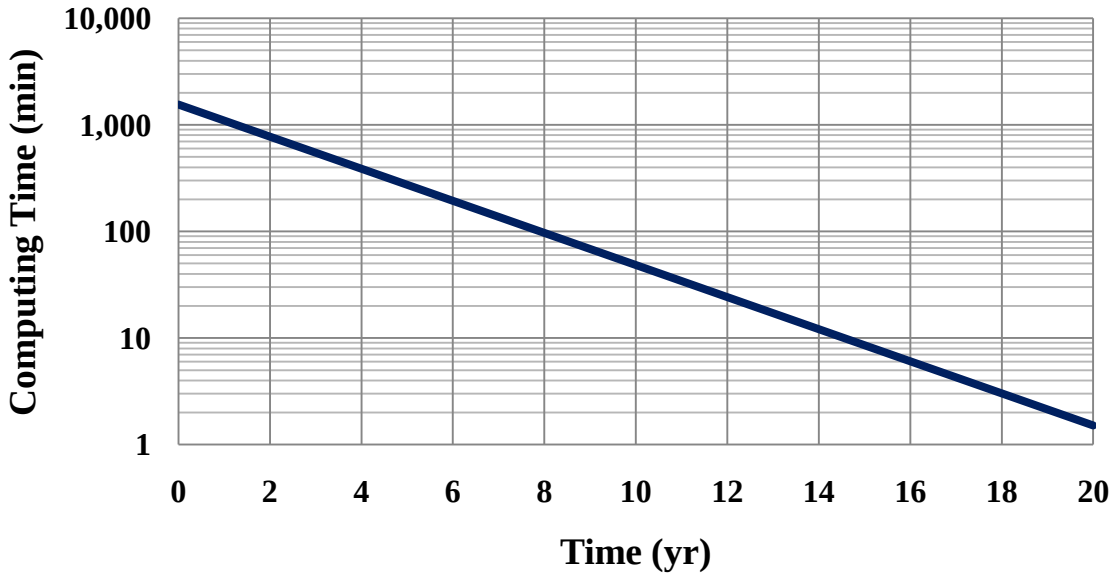

Figure 6.1: Predicted development of computational speed over the next 20 years according to Moore's law. The initial time of 1,548 minutes refers to the time consumed to perform a geometry optimization and frequency analysis for HMPA at the B3LYP/6-311++G(d,p) level of theory including IEFPCM as used for the calculations in Chapter 2. This calculation was performed on an Apple G5 cluster, parallelized over 6 Xserve G5 nodes (12 CPUs).

Another limitation of the developed methodology is the accurate description of solvation effects. While an explicit treatment using several complete solvent shells around the molecule(s) of interest is desirable, it is also currently not practical due to limited computational capacities. Thus, as discussed previously in this dissertation (Chapter 3), the use of mixed cluster/continuum approaches will remain the one of the most appropriate alternatives for many years. The application of continuum solvation models in Gaussian 03, however, is associated with their notorious convergence problems (*4, 5*), as encountered here in several computations (Chapters 3 & 4). Gaussian, Inc. claims that in the new version Gaussian 09, geometry optimizations with PCM converge at the same rate as the corresponding gas-phase optimizations. Initial test calculations conducted here (Chapters 3 & 4) thus far support this statement.

Neither explicit nor implicit solvation models, however, can take into account the multitude of dissolved organic and inorganic species in natural waters, which may interact with a contaminant or with a remediation agent through a multitude of processes, such as complexation, hydrogen bonding, redox and non-redox reactions. Also, they may alter the activity of a solute, which is used in Gibbs free energy calculations rather than the molar concentration of a solute (*6*). One way to account for the actual activity is through the dielectric constant of the solvent, which depends on the nature and concentration of the dissolved species (*7, 8*), and - if known - can be adjusted accordingly in implicit continuum solvation models (*1*).

The model predictions were experimentally validated here in a simplified aqueous system, using a soluble contaminant and remediation agent only, to mimic the quantum chemical model system. However, many environmental contaminants are present in the

solid phase, as non-aqueous phase liquid, or sorbed to the complex soil matrix, where accessibility and mass transfer limitations may limit their degradation kinetics (*9, 10*). These conditions can hardly be modeled quantum chemically, except as idealized systems where reaction occurs at the contaminant/particle and contaminant/solvent interfaces. This entails the investigation of very large systems, which again is limited by computational capacities. Consequently, non-quantum chemical methods such as classical molecular dynamics are currently most often used for their investigation (*11*).

Moreover, many solid phases in the environment are often hard to define due to their complex nature, such as amorphous minerals (e.g., ferrihydrite) or oxide coatings of aged zero-valent metals (*12*). In addition, the structure or reactivity of most soil minerals can be heavily influenced by surface-sorbed species (e.g., organic matter, silicate and phosphate), co-precipitated metals/organics, and isomorphic substitution (*13-16*). Yet, solid phases play an important role in determining the fate of a contaminant as they may influence sorption behavior, perform or catalyze the oxidation or reduction of a contaminant, and deplete remediation agents that have been injected into the groundwater to enhance contaminant degradation. However, systems for quantum chemical calculations have to be defined on an atomic scale, which is only possible through the use of highly idealized systems that will not adequately represent the complex composition of these phases or, even more so, the entire soil matrix at a given site. The same is valid for autochthonous bacteria, which can catalyze the degradation of a contaminant. Here, an entire enzyme, or at least its active site, would have to be defined through its elementary composition in a theoretical calculation, not taking into account contaminant bioavailability and bacterial population density or activity. Thus, in these cases, quantum

chemical calculations may be used for qualitative, but rarely for quantitative investigations.

Nevertheless, the quantum chemical methodology developed in this dissertation is a valuable tool for scientists, regulators and engineers to predict the favorability of contaminant degradation at a specific field site, suitable approaches to enhance degradation, degradation products, and the persistence of a contaminant and/or its reaction intermediates. This novel approach overcomes many limitations of standard QSAR-based models, which rely on experimental data of structurally similar compounds and do not cover the widely varying redox settings of natural and engineered environments.

References

1. Foresman, J. B.; Frisch, Æ., *Exploring Chemistry with Electronic Structure Methods*. 2nd ed.; Gaussian: Pittsburgh, PA, 1996; p 302.

2. Pople, J. A., Nobel Lecture: Quantum chemical models. *Reviews of Modern Physics* **1999,** 71, (5), 1267-1274.

3. Thompson, S. E.; Parthasarathy, S., Moore's law: the future of Si microelectronics. *Materials Today* **2006,** 9, (6), 20-25.

4. Barone, V.; Cossi, M.; Tomasi, J., A new definition of cavities for the computation of solvation free energies by the polarizable continuum model. *Journal of Chemical Physics* **1997,** 107, (8), 3210-3221.

5. Stare, J.; Henson, N. J.; Eckert, J., Mechanistic aspects of propene epoxidation by hydrogen peroxide. Catalytic role of water molecules, external electric field, and zeolite framework of TS-1. *Journal of Chemical Information and Modeling* **2009,** 49, (4), 833-846.

6. Stumm, W.; Morgan, J. J., *Aquatic Chemistry: Chemical Equilibria and Rates in Natural Waters*. 2nd ed.; John Wiley & Sons, Inc.: New York, NY, 1996; p 1022.

7. Kalcher, I.; Dzubiella, J., Structure-thermodynamics relation of electrolyte solutions. *Journal of Chemical Physics* **2009,** 130, (13).

8. Lyashchenko, A. K.; Karataeva, I. M., Relation of water activity to the static dielectric constant of concentrated electrolyte solutions. *Doklady Physical Chemistry* **2007,** 414, 120-122.

9. Quinn, J.; Geiger, C.; Clausen, C.; Brooks, K.; Coon, C.; O'Hara, S.; Krug, T.; Major, D.; Yoon, W. S.; Gavaskar, A.; Holdsworth, T., Field demonstration of DNAPL dehalogenation using emulsified zero-valent iron. *Environmental Science & Technology* **2005,** 39, (5), 1309-1318.

10. Yu, X. Y.; Amrhein, C.; Zhang, Y. Q.; Matsumoto, M. R., Factors influencing arsenite removal by zero-valent iron. *Journal of Environmental Engineering-Asce* **2006,** 132, (11), 1459-1469.

11. Aryanpour, M.; van Duin, A. C. T.; Kubicki, J. D., Development of a reactive force field for iron-oxyhydroxide systems. *Journal of Physical Chemistry A* **2010,** 114, (21), 6298-6307.

12. Sohn, K.; Kang, S. W.; Ahn, S.; Woo, M.; Yang, S. K., Fe(0) nanoparticles for nitrate reduction: Stability, reactivity, and transformation. *Environmental Science & Technology* **2006,** 40, (17), 5514-5519.

13. Borch, T.; Masue, Y.; Kukkadapu, R. K.; Fendorf, S., Phosphate imposed limitations on biological reduction and alteration of ferrihydrite. *Environmental Science & Technology* **2007,** 41, (1), 166-172.

14. Jones, A. M.; Collins, R. N.; Rose, J.; Waite, T. D., The effect of silica and natural organic matter on the Fe(II)-catalysed transformation and reactivity of Fe(III) minerals. *Geochimica Et Cosmochimica Acta* **2009,** 73, (15), 4409-4422.

15. Masue, Y.; Loeppert, R. H.; Kramer, T. A., Arsenate and arsenite adsorption and desorption behavior on coprecipitated aluminum: iron hydroxides. *Environmental Science & Technology* **2007,** 41, (3), 837-842.

16. Weissmahr, K. W.; Hildenbrand, M.; Schwarzenbach, R. P.; Haderlein, S. B., Laboratory and field scale evaluation of geochemical controls on groundwater transport of nitroaromatic ammunition residues. *Environmental Science & Technology* **1999,** 33, (15), 2593-2600.